



The
University
Of
Sheffield.

Exploring adaptations and integration in the zebrafish visual and olfactory systems.

Elliot William Birkett

A thesis submitted in partial fulfilment of the requirements for the degree of Doctor of Philosophy.

Supervisors:

Dr. Anton Nikolaev

Prof. Suresh Jesuthasan

Advisors:

Prof. Carl Smythe

Dr. Stuart Johnson

September 2022

Abstract

Sensory integration is fundamental to survival. Each of our sensory systems function to perform three essential tasks – firstly, they must detect changes in the surrounding environment. Secondly, they must also understand the meaning behind this change, for example, comprehend whether it possesses a threat to its survival or the possibility that food is nearby. Thirdly, each sensory system must also be able to localise where the change is occurring. Each sensory system can encode different elements of the stimulus with varying speed and accuracy (Angelaki *et al.*, 2009). With the increased complexity of behavioural and motor control throughout evolution, it has become increasingly vital for organisms to interrelate sensory cues and also process these alongside the internal state of the organism (Mausfeld, 2013). (Angelaki *et al.*, 2009). Resultantly, the integration of information from each sensory system is essential for optimising the behavioural responses and therefore the fundamental survival of an organism. How both visual/olfactory systems function has been researched intensely in the past, thus these processes are well understood. However, it is not well understood how these two systems integrate their sensory information and what effect, if any, the sensory integration has.

In this thesis, I display evidence of olfactory stimulation being able to alter how visual stimuli are perceived by fish, with the same visual stimulus being perceived as aversive or a potential source of food with just a change of olfactory cue. Mechanistically, we have shown that olfactory stimuli may be able to influence predictions in the main visual processing centre, the optic tectum through altering both the quantity and spatiotemporal patterning of spontaneous activity. Additionally, visual stimulation can be seen to evoke responses in olfactory cells in the olfactory bulbs and olfactory epithelium. Further experimentation will be required to understand what effect this sensory integration has on perception.

Acknowledgements

This work was sponsored by the A*STAR ARAP studentship and the Royal Society Seed Award. I am thankful to Dr. Sandra Toledo Rivera and Alexander Staruschenko from the Nikolaev lab, Sheffield, for helpful discussions and support of this work. I am thankful to Dr. Federico Ciriani and Dr. Francesca de Faveri as well as the rest of the Marcotti lab for the use of and training provided for 2-photon microscopy system at the University of Sheffield and for the helpful discussions throughout. I would also like to acknowledge members of the Jesuthasan and Wee labs, Singapore, for helpful discussions and support of this work.

I am also thankful to the Monk lab for providing the *slc1a3b* promoter for use in our astrocyte imaging work. Finally, I would like to thank members of Bateson Centre aquarium, Sheffield and both Nanyang Technological University aquarium staff and Institute of Molecular and Cellular Biology aquarium staff in Singapore for help with animal husbandry throughout my project.

Declaration

I, Elliot Birkett, confirm that the Thesis is my own work. I am aware of the University's Guidance on the Use of Unfair Means (www.sheffield.ac.uk/ssid/unfair-means). This work has not previously been presented for an award at this, or any other university.

Table of Contents

ABSTRACT	2
ACKNOWLEDGEMENTS	3
DECLARATION	4
LIST OF FIGURES	6
LIST OF TABLES	9
INTRODUCTION	10
BACKGROUND INFORMATION	10
THE VISUAL SYSTEM.	13
<i>The Retinal Transduction Cascade</i>	13
<i>Visual Processing in Humans and Teleosts</i>	18
<i>Centrifugal Feedback to the Retina</i>	23
THE OLFACTORY SYSTEM.....	24
<i>The Zebrafish Olfactory System</i>	24
<i>Similarities Between the Human and Zebrafish Olfactory Systems</i>	28
EVIDENCE FOR VISUAL-OLFACTORY INTEGRATION	30
<i>Can Vision Influence Olfactory Perception?</i>	30
<i>Can Olfaction Influence Visual Perception?</i>	31
MECHANISMS OF SENSORY INTEGRATION	33
PREDICTIVE CODING FRAMEWORK FOR SENSORY INTEGRATION.	39
SHORT-TERM SENSORY PLASTICITY.....	41
RESEARCH GOALS AND OBJECTIVES	43
MATERIALS AND METHODS	44
3.1 ANIMALS AND HUSBANDRY.....	44
<i>Zebrafish Lines</i>	45
3.2 BEHAVIOUR EXPERIMENTS	45
3.3 NEURONAL TRACING	47
3.4 2-PHOTON IMAGING.....	48
<i>Spontaneous Activity Recordings (A*STAR Singapore):</i>	49
<i>Olfactory Adaptation Recordings (The University of Sheffield):</i>	50
<i>Effect of Olfaction on Visual Adaptation (The University of Sheffield):</i>	53
<i>Visual Responses in the Olfactory Bulbs</i>	55
<i>Imaging of Astrocyte-Neuron Interactions</i>	56
RESULTS	64
4.1 BEHAVIOUR ASSAY	64
4.2 OLFACTO-VISUAL NEURONAL TRACING.	70
4.3 PREDICTIVE CODING AND SENSORY INTEGRATION.....	72
4.4 OLFACTORY ADAPTATION	81
<i>Diversity of Olfactory Adaptations</i>	83
<i>Diversity of Adaptations is not Reflected in the Brain Structure</i>	88
<i>The Alarm Substance Evokes Different Olfactory Adaptations Compared to Food Odour</i>	89
<i>Mechanisms of Olfactory Sensitisation</i>	94
4.5 EFFECT OF OLFACTORY INPUT ON TECTAL PROCESSING	97
4.6 VISUAL RESPONSES IN THE OLFACTORY BULBS	103
4.7 REGULATION OF CHANGES IN SPONTANEOUS ACTIVITY	108
DISCUSSION	112
CHALLENGES FACED	120
CONCLUSIONS	122
REFERENCES	123

List of Figures

Figure 1.1: Calcium Imaging of the Zebrafish Optic Tectum

Figure 1.2: The Zebrafish Retina

Figure 1.3: Retinal Layers and Structure

Figure 1.4: Human Visual Processing

Figure 1.5: Retinal Projections of the Zebrafish

Figure 1.6: The Diverse Morphology of Neurons in the Multi-Layered Optic Tectum

Figure 1.7: Avian Retinal Negative Feedback Loop

Figure 1.8: Anatomy of the Zebrafish Olfactory System

Figure 1.9: Mitral Cell Outputs to the Zebrafish Brain.

Figure 1.10: Comparing the Zebrafish and Human Olfactory System

Figure 1.11: Projections of Terminal Nerve Fibres

Figure 1.12: The Zebrafish Habenula

Figure 3.4.1: jRGECO1a attb High Fidelity PCR

Figure 3.4.2: Colony PCR Identified Multiple jRGECO1a positive colonies.

Figure 3.4.3: LR Reaction Colony PCR Identified 2 positive colonies for slc1a3b;jRGECO1a.

Figure 3.4.4: Restriction Digest Gel Confirmation for slc1a3b;jRGECO1a

Figure 3.4.5: Slc1a3b;jRGECO1a Plasmid Map

Figure 4.1.1: Experimental Design for Visual Perception Behaviour Test

Figure 4.1.2: Fish Exposed to Alarm Substance and Food Odour Showed No Difference in Freezing Behaviour.

Figure 4.1.3: Fish Exposed to Food Odorant Showed More Exploration Towards the Visual Stimulus.

Figure 4.1.4: Fish Exposed to Different Odourants Demonstrated No Significant Change in Eye Convergence.

Figure 4.1.5: Treatment of Food Odour or Alarm Substance Had No Effect on the Number of High-Angle Turns Made.

Figure 4.2.1: The Terminal Nerve Projects from the Olfactory Bulbs to the Retina and Optic Tectum

Figure 4.3.1: Spontaneous Activity Profiles for Cells Across the Optic Tectum and Habenula.

Figure 4.3.2: Application of Alarm Substance Alters Spontaneous Activity in the Optic Tectum

Figure 4.3.3: Application of Food Odour Alters Spontaneous Activity in the Optic Tectum

Figure 4.3.4: Visualisation of Responding Clusters Demonstrated Cells Were Located in the Optic Tectum and Habenula

Figure 4.3.5: Laplacian Eigenmaps for Control Fish Demonstrates the System Resided in a Similar State Before and After the Stimulus was Applied.

Figure 4.3.6: Laplacian Eigenmaps for Fish Exposed to Olfactory Stimulus Demonstrates the System Resided in a Different State Before and After the Stimulus was Applied.

Figure 4.4.1: Application of Olfactory Stimuli

Figure 4.4.2: Application of Food Odorant Evoked Olfactory Responses.

Figure 4.4.3: The Zebrafish Olfactory System Displays a Diversity of Adaptations.

Figure 4.4.4: Manual and Automated Analysis Display the Same Diversity of Adaptations.

Figure 4.4.5: Distribution of Adaptation Indices in the Zebrafish Olfactory System.

Figure 4.4.6: Diversity of Olfactory Adaptations Persists in Older Larval Zebrafish.

Figure 4.4.7: Diversity of Adaptations is not Reflected in the Brain Structure.

Figure 4.4.8: Olfactory Neurons Display Facilitation to Repeated Presentations of Alarm Substance.

Figure 4.4.9: Diversity of Adaptations to the Alarm Substance in Olfactory Bulbs.

Figure 4.4.10: Diversity of Adaptations to the Alarm Substance in Olfactory Epithelium.

Figure 4.4.11: The Olfactory System Remains Sensitive After Alarm Substance Exposure.

Figure 4.4.12: The Effect of Alarm Substance on Food Odour Responses

Figure 4.4.13: The Effect of PTZ on Responses to Food Odour Application

Figure 4.4.14: PTZ exposure decreased the number and increased the adaptation index of facilitating voxels.

Figure 4.4.15: The Effect of PTZ on Olfactory Sensitisation.

Figure 4.5.1: Imaging Chamber for Application of Olfactory and Visual Stimuli

Figure 4.5.2: Tectal Responses to a Moving Ball Visual Stimulus Adapt Over Time.

Figure 4.5.3: Different Layers of the Optic Tectum Display Differing Levels of Adaptation

Figure 4.5.4: Effect of Olfaction on Visual Processing in the Optic Tectum

Figure 4.5.6: Effect of Olfaction on Adaptation to Visual Stimulation Across Different Layers of the Optic Tectum

Figure 4.6.1: Visually Responsive Cells Are Present in the Olfactory Bulbs

Figure 4.6.2: Visual Responses to a Moving Ball Visual Stimulus Within the Olfactory Bulbs.

Figure 4.6.3: Visual Responses are also seen in the Olfactory Epithelium.

Figure 4.6.4: Olfaction Enhances Olfactory Bulbs Visual Responses

Figure 4.6.5: Individual Cell Responses to a Moving Ball Visual Stimulus Within the Olfactory Bulbs Display Diversity.

Figure 4.7.1: Expression of *slc1a3b*:jRGECO1a Across the Zebrafish Brain.

Figure 4.7.2: Tectal Astrocytes Display Responses to Food Odour Delivery.

Figure 4.7.3: Spiking Between Tectal Neurons and Astrocytes Are in Anti-Phase After Olfaction.

List of Tables

Table 3.4.1: jRGECO1a attb High Fidelity PCR

Table 3.4.2: BP Reaction

Table 3.4.3: BP Reaction Colony PCR

Table 3.4.4: LR Reaction

Table 3.4.5: LR Reaction Colony PCR.

Table 4.3.1: Diversity of Changes in Spontaneous Activity Profiles in the Optic Tectum to Olfactory Stimuli

Introduction

Background Information

Each of our sensory systems primary function is to detect changes in the external environment. It is then the function of higher brain centres to process this information and thus intervene between sensory input and behavioural output. Integration occurs across the sensory modalities of all forms of life (Vanwalleghem *et al.*, 2015). This allows for inputs from one modality to modify the responses of another modality to stimuli in the environment. In addition to this, integration can also improve the speed of processing and reduce the amount of lag or error in stimulus detection (Mu *et al.*, 2012). With the increased complexity of behavioural and motor control throughout evolution, it has become increasingly vital for organisms to interrelate sensory cues and also process these alongside the internal state of the organism (Angelaki *et al.*, 2009, Mausfeld, 2013). Thus, the integration of information from each sensory system is essential for optimising the behavioural responses and therefore the fundamental survival of an organism.

In this thesis, my focus will primarily be on integration between two sensory systems: vision and olfaction. How both the visual and olfactory systems function has been researched intensely in the past, thus these processes are well understood (Easter and Nicola, 1996, Shapley and Enroth-Cugell, 1984, Northcutt and Wullimann, 1988, Bilotta and Saszik, 2001, Byrd and Brunjes, 1995, Sarafoleanu *et al.*, 2009b). There is now also evidence supporting interactions between both systems; it has been shown that olfactory input can aid with visual object recognition as well modulating the OFF pathway in the retina (Esposti *et al.*, 2013, Seigneuric *et al.*, 2010b, Zhou *et al.*, 2010). In addition, fibres from the *nervus terminalis*, also known as the terminal nerve, originate in the olfactory bulbs and have been seen to project to both the optic tectum and retina in zebrafish. Furthermore, olfaction has also been shown to modulate ambiguous visual motion perception (Dowling, 2013, Kuang and Zhang, 2014). However, the mechanisms behind how this integration occurs and the full extent to which these interactions can influence behaviour are still poorly understood. I therefore aimed to investigate if olfaction can influence how objects are perceived and the neuronal mechanisms through which this integration of sensory information may occur.

To conduct this research, I have used the zebrafish as my model organism of choice. Over 70% of human genes have orthologues in the zebrafish genome (Howe *et al.*, 2013). Zebrafish are frequently used in functional and developmental research due to the ease with which they can be genetically modified alongside the transparent nature of their larvae during development. These factors allow for sophisticated molecular and genetic analysis and the ability to record functional measurements of neuronal activity in live fish (Miyasaka *et al.*, 2013, Denk *et al.*, 1996, Yasuda *et al.*, 2004, Burgoyne, 2007, Akerboom *et al.*, 2012, Akerboom. *et al.*, 2013, Kim *et al.*, 2017, Dana *et al.*, 2019, Li and Saha, 2021).

Zebrafish are also an appealing animal model because the breeding process is highly efficient, with the female fish laying around 200 eggs per breeding session (Wyatt *et al.*, 2015). The developmental process is also very rapid, with larvae swimming just 48 hours post-fertilisation (Kimmel *et al.*, 1995). The visual system develops rapidly with the extraocular muscles achieving adult structure by 66 hours post fertilisation. This timing coincides with the fish being able to detect dramatic changes in light intensity at 68 hours post-fertilisation and showing optokinetic responses by 73 hours post-fertilisation (Easter and Nicola, 1996). Odour responses have been detected in the olfactory bulb before the fish have hatched between 2-3 days post fertilisation (Li *et al.*, 2005). Shortly after hatching, zebrafish are seen to increase their swimming activity when exposed to amino acid stimuli (Lindsey and Vogt, 2004) and can show aversive responses to certain nucleotides (Vitebsky *et al.*, 2005). This indicates the olfactory system is functional at an early stage in development, like the visual system.

With this being said, the number of neurons in the olfactory bulb at the time of hatching is only about 5% of that seen in adult (Miyasaka *et al.*, 2013) but are still able to respond to chemo-signals triggering the alarm response by 5 days post-fertilisation (Jesuthasan *et al.*, 2020). The exact time course for which the olfactory system becomes fully developed is currently unknown (Mack-Bucher *et al.*, 2007).

The transparent nature of zebrafish larvae allows for the neuronal activity of single cells to be measured across almost the entire brain (Timothy W Dunn, 2016). Calcium ions are present within all neurons and glia across the brain (Burgoyne, 2007) and pass into the cell during neuronal action potential firing and through synaptic input (Denk *et al.*, 1996, Jaffe *et al.*,

1992). In glia, calcium signals are also propagated in response to various types of stimulation and the spreading intercellular calcium wave allows for information exchanges across the glial network (Deitmer *et al.*, 1998). Measuring the changes of intracellular calcium ion concentrations therefore provides quantification for frequency and timing of spiking as well as levels of synaptic input (Akerboom. *et al.*, 2013, Yasuda *et al.*, 2004).

GCaMPs are a genetically engineered calcium indicator (GECI) which enable non-invasive mass imaging of defined cells across the zebrafish brain (Akerboom *et al.*, 2012, Dunn *et al.*, 2016). GECI's are encoded genetically into the living model through translation of DNA, meaning no lesion or chemical injection is required in the developed animal (Li and Saha, 2021). One of the most common of these, GCaMP3, also used in our experiments, functions by undergoing a conformational change transduced by the M13 peptide when calcium binds to calmodulin, allowing for fluorescence of its circularly permuted GFP molecule (Akerboom *et al.*, 2012). More recent advances have led to brighter and more sensitive GCaMP sensors such as GCaMP6 (Chen *et al.*, 2013) and GCaMP7 (Dana *et al.*, 2019). Frequently used common pan-neuronal *elavl-3* promoters only allowed visualisation of neuronal activity up until day 6-7 days post-fertilisation before the visualisation of the activity would decrease (Bergmann *et al.*, 2018).

Previous work in the Nikolaev lab demonstrated a model to study neuronal activity in the optic tectum of zebrafish larvae up to at least 21 days post-fertilisation using the *tg(Xla.Tubb:GCaMP3)* line (Bergmann *et al.*, 2018). This new zebrafish line allows for prolonged visualisation of neuronal activity in the optic tectum (see figure 1.1), which has been shown to receive input from both the retina (Bodick and Levinthal, 1980) and olfactory bulbs (Esposti *et al.*, 2013, Dowling, 2013, Koide *et al.*, 2018).

Figure 1.1: Calcium Imaging of the Zebrafish Optic Tectum



Figure 1.1: The Optic Tectum. 2-photon microscopy image of a Tg(NBT:GCaMP3) 4 days post-fertilisation zebrafish larva. The image focuses on the optic tectum and shows calcium activity can be monitored in both individual cell bodies and in the neuropil where cells from the retina and other parts of the brain synapse and converge. Scale bar = 50 μm.

The Visual System.

The Retinal Transduction Cascade.

The vertebrate visual systems neuronal architecture has been highly conserved throughout evolution (Ramón and Cajal, 1893). It is known that vision occurs through light interacting with our eyes however converting this information into neural signals is a complex process, and further processing for how this information is perceived by the brain is even more complex. Light can behave as both waveforms at particles or photons, with humans being able to visualise wavelengths of light approximately in the range of 400nm to 830nm (Sloney, 2016). Zebrafish contain four types of cone photoreceptors which allow them to visualise wavelengths of light ranging from ultraviolet (360nm) to red (650nm) (Wan and Goldman,

2016, Meier *et al.*, 2018). Zebrafish have also been shown to display negative phototactic responses to near infrared wavelengths (860nm) (Hartmann *et al.*, 2018).

Light passes through the pupil of the eye which can constrict and dilate to alter the quantity of light entering the eye, the light then hits the lens which focuses incoming wavelengths onto the photoreceptors of the eye. In the mammalian and zebrafish retina, there are five different groups of neurons which are involved in the phototransduction cascade: photoreceptors, bipolar cells, horizontal cells, amacrine cells and the retinal ganglion cells (Baden *et al.*, 2020). Zebrafish and humans display the same major cell types in the retina and share the same layered structure. This pattern is such that the light-sensing photoreceptors are located on the outer-most layer, coined the outer nuclear layer and the cells responsible for the output of the retina, the ganglion cells are in the innermost layer (Figure 1.2(A)). As the photoreceptors are in the deepest of these layers, light must travel through all other layers to activate a photoreceptor. There are two different classes of photoreceptors, rods and cones which display different morphologies (Baden *et al.*, 2020). Photoreceptors of the zebrafish retina, specifically the cones, are organised in a regular pattern known as photoreceptor mosaic (Avanesov and Malicki, 2010). The cones form regular rows, within which double cones are separated by alternating short/long single cones. Adjacent rows of cones are then staggered in such a way that a short cone in one row will align with a long cone in the next (see Figure 1.2 (B)). Between each row of cones lies the rods, however no obvious pattern can be seen from their arrangement (Fadool, 2003).

Figure 1.2: The Zebrafish Retina

A. Retinal Anatomy

B. Zebrafish Photoreceptor Mosaic

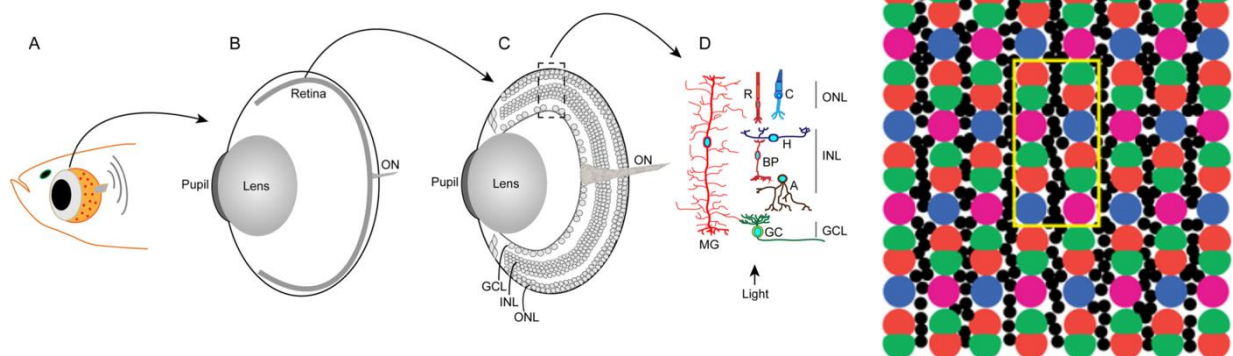


Figure 1.2: The Zebrafish Retina. (A) The anatomy and structure of the zebrafish eye. The retina is composed of multiple layers, the outer nuclear layer (ONL) containing the photoreceptor cells, the inner nuclear layer (INL) containing the retinal interneurons and the ganglion cell layer. Between these are the outer and inner plexiform layers (OPL/IPL) where the cells synapse. Muller glial cells span all three layers of the retina and function to maintain retinal homeostasis and provide neural protection. Figure adapted from Wan and Goldman, 2016. (B) The adult zebrafish retinal photoreceptor mosaic arrangement. The yellow box identifies the 12-cone repeating motif. This is composed of four types of cones: red, green, blue and ultraviolet which are stimulated by long, medium, and short wavelengths of light respectively. In between each column of cone photoreceptors are the rods, represented as smaller black circles on the schematic. Figure adapted from (Salbreux et al., 2012).

The number of rod cells in the retina is about 20-fold higher than the number of cone cells in the majority of mammalian retinas (Masland, 2012). The rod cell structure is composed of hundreds of membranous disks, which each contain thousands of rhodopsin molecules (Nakai *et al.*, 2001). Rhodopsin is a photosensitive pigment which can undergo a transformational change in the presence of dim light resulting in hyperpolarisation of the cell (Kolb, 1995). In dark conditions, this allows us to see differing shades of grey but images will lack specific details including defined borders and colour (Richardson *et al.*, 2017). In contrast to rods, the cone photoreceptors are responsible for mediating vision when light is highly available (Tong *et al.*, 2020) and perform much more effectively at colour identification and edge detection (Kolb, 1995).

The photoreceptors transduce their electrical information onto bipolar cells which are the primary excitatory synapse to the output neurons of the retina, retinal ganglion cells. The cell body of the bipolar cell sits in the inner nuclear layer with dendrites extending to the photoreceptor terminals in the outer plexiform layer and an axon extending to the retinal ganglion cell dendrites in the inner plexiform layer (Kolb, 1995). There are multiple different subtypes of bipolar cell (Masland, 2012) including ON and OFF cells which can be depolarised or hyperpolarised by the same stimulus respectively to provide more accurate receptive fields (Connaughton, 1995).

Regulating the photoreceptor, bipolar cell and retinal ganglion cell activity are the amacrine and horizontal cells. The horizontal cells are located in the outer plexiform layer and are

mainly GABAergic inhibitory neurons (Filippo Del Bene *et al.*, 2010). The horizontal cell receives glutamatergic input from the photoreceptor. It then provides its own GABA feedback to the photoreceptors by projecting laterally across the outer plexiform layer to inhibit their activity, providing a control mechanism for the system which is particularly useful when undergoing light/dark condition changes (Masland, 2012). Similar to horizontal cells, amacrine cells also lay between two cell types in the phototransduction cascade, but instead this time within the inner plexiform layer between bipolar cells and retinal ganglion cells (Kaneko, 1970). The amacrine cells are again mainly GABAergic but can also release dopamine and acetylcholine in order to finely tune the action potentials leaving the bipolar to the retinal ganglion cells. (Masland, 2012). It has also been shown that amacrine cells can contact the synaptic boutons of rod cells in order to provide feedback/regulation of information along the transduction cascade in dark conditions (Meier *et al.*, 2018). The final retinal cell-type is the müller glia. The müller glia span across the entire width of the retina and have the capability to regenerate into retinal cells to replace those which have become damaged, as well as provide structural support (Wan and Goldman, 2016).

The retinal ganglion cells are the only retinal neurons projecting out of the retina and are therefore responsible for transducing visual information onto the rest of the brain (Northcutt and Wullimann, 1988). Retinal ganglion cells have dendritic extension into the inner plexiform layer where they synapse with bipolar cells axons, while their own axons project laterally and converge to form the optic nerve at the optic disk (Kolb, 1995). Retinal ganglion cells have different tuning properties therefore different cells will be activated by shape, colour, angles, and movement of stimuli (Antinucci and Hindges, 2018). This collective individual specificity helps to regulate how different stimuli are perceived by the fish. For example, midget cells, a morphologically small class of retinal ganglion cell, receive input from just a single photoreceptor meaning it can retain and transduce whether the photoreceptor is stimulated by red, green, blue or ultraviolet light onto the rest of the brain. This makes this class of retinal ganglion cell important for discrimination of colour (Patterson *et al.*, 2019). It has been identified that there are over 20 different classes of retinal ganglion cell with studies ongoing into determining more about their structure and function. The layers and structure of the retina is summarised in figure 1.3 below.

Figure 1.3: Retinal Layers and Structure.

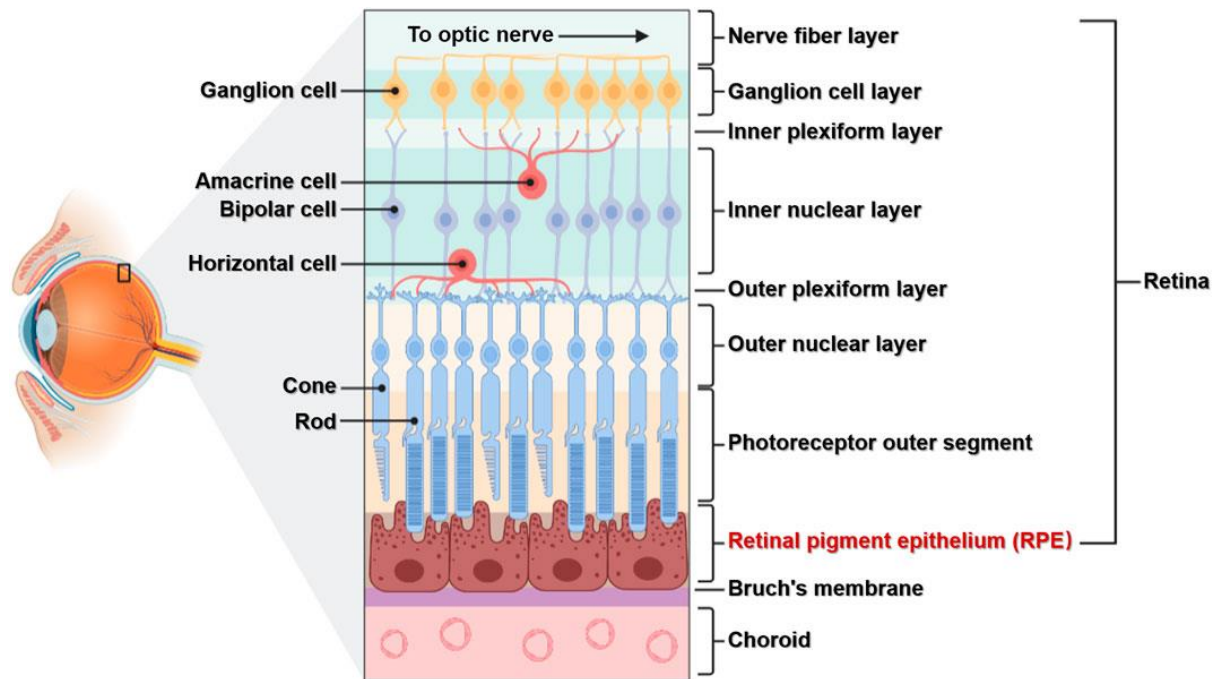


Figure 1.3: Retinal Layers and Structure. The cell types and layers of the retina. Light travels through to the retinal pigment epithelium before the phototransduction cascade convey information from the photoreceptor layer to the outer plexiform layer to bipolar cells in the inner nuclear layer. These synapse with ganglion cells in the inner plexiform layer and convey retinal output to higher centres along the nerve fibre layer. (Figure adapted from (Yang *et al.*, 2021).

The neuronal network of the retina is largely self-contained, with most regulation occurring inside the retina (Antinucci and Hindges, 2018). Exceptions to this have however been discovered where modulation of retinal ganglion cells activity can occur. One example of this regards olfacto-retinal centrifugal input, providing early evidence of visual-olfactory integration (Huang *et al.*, 2005, Esposti *et al.*, 2013). Despite this, as most of the neuronal architecture is self-contained, we hypothesise that further integration and modulation will occur in higher visual processing centres.

Visual Processing in Humans and Teleosts

The visual transduction cascade is a complex process but understanding how this information is then perceived by the brain is even more so. In the human brain, visual information must travel along way from the retina to reach its primary cortical processing centre, the occipital cortex at the posterior of the brain (Krubitzer, 2009). When light enters into the eye, the lens flips the visual information, meaning that photons entering from the temporal fields will activate RGCs in the nasal portion of the retina and vice versa (Helmbrecht *et al.*, 2018). The world-renowned drawings of Ramon y Cajal from the later 19th century demonstrates that fibres coming from the nasal retina decussate at the optic chiasm while temporal fibres continue to project to the ipsilateral portion of the brain. This process realigns the visual information and corrects for the changes due to the lens (see figure 1.4 below).

After the chiasm, around 90% of the visual neurons will project to the lateral geniculate nucleus. The lateral geniculate nucleus also contains a high number of GABAergic interneurons suggesting there is some refinement and processing of visual information here (Sherman and Koch 1986). As well as temporal and nasal information being retained by retinal projections, dorsal/ventral organisation must also be conveyed. From the lateral geniculate nucleus, information from the upper visual fields is conveyed to the visual cortex via the temporal loop whereas lower visual fields project along the superior loop. This allows for precise visual maps to be retained in the visual processing centres of V1 and V2 in the occipital cortex.

The other 10% of these fibres project to the superior colliculi (Wullimann, 1998). The superior colliculi are a small thalamic structure involved in visual reflexes; fast-moving objects across the visual field will result in a reflex action causing a head turn towards the object – this is orchestrated by the superior colliculi (Moini *et al.*, 2021). This extrageniculate pathway projects to a group of caudal thalamic nuclei which relay sensory information onto V2-V4, the other visual cortical regions and also the lateral amygdala (Doron and Ledoux, 2000).

Figure 1.4: Human Visual Processing

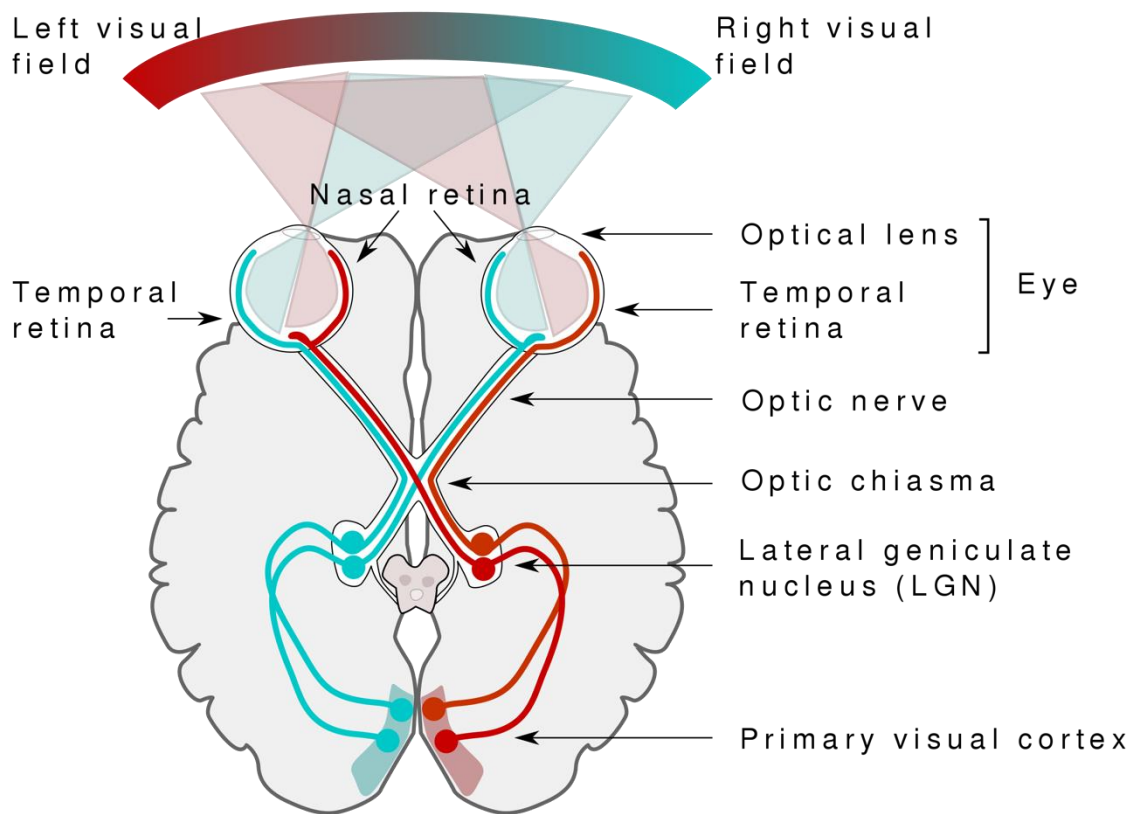


Figure 1.4: Human visual processing. Visual information entering the eyes is inverted by the lens and processed into neuronal signals via the phototransduction cascade. Retinal ganglion cells project the output information to the optic chiasma where cells from the nasal retina decussate and cross the midline to the contralateral side of the brain. Projections pass through the superior colliculi and lateral geniculate nucleus before terminating in the primary visual cortex. Figure created by Miquel Perello Nieto, 2015.

As mentioned, the main features of the retina have been highly conserved throughout evolution meaning the zebrafish and mammalian retina display a high degree of similarity (Chhetri *et al.*, 2014). However, differences in higher visual processing are present due to the lack of visual cortex (or any other cortex) in the zebrafish (Friedrich *et al.*, 2010). Zebrafish retinal ganglion cells project to at least ten target areas but the largest and most prevalent of these is the optic tectum. The optic tectum is the main visual processing centre in zebrafish as well as in other teleost species (Northmore, 2009), receiving more than 97% of retinal ganglion cell input in the zebrafish (Robles *et al.*, 2014) (see figure 1.5 below). It is homologous to the superior colliculus in the mammalian brain. Retinal ganglion cell projections navigate largely through the midline of the ventral diencephalon to the contralateral tecti (Bodick and Levinthal, 1980). The spatial arrangement of the retinal ganglion cells is precisely reproduced

by their projections in the tectum in reverse. This means the ventral-nasal retinal ganglion cells project to the dorsal-posterior region of the optic tectum compared to the dorsal temporal retinal ganglion cells projecting to the ventral-anterior region of the optic tectum (R O Karlstrom *et al.*, 1996). By just three days post-fertilisation, these topographic maps will have begun to be established in zebrafish (Avanesov and Malicki, 2010, Easter and Nicola, 1996). The optic tectum is much more complex than the superior colliculi and this has been hypothesised to be due to the optic tectum performing vision-related functions that would be performed by the cortex in the mammalian brain as well as the extrageniculate pathway in mammals (Filippo Del Bene *et al.*, 2010). Only one thalamic nucleus has been found to function in visual processing in teleosts and this is the anterior thalamic nucleus. Because of this it had been considered to be either a homologue to the dorsal lateral geniculate nucleus (Butler and Hodos, 2005) or part of the geniculate pathway (Wullimann, 1998). However, the anterior thalamic nucleus is mainly GABAergic whereas the dorsal lateral geniculate nucleus in mammals is glutamatergic so this is unlikely to be true, thus a dorsal lateral geniculate nucleus homologue may be absent in teleosts (Mueller, 2012).

Figure 1.5: Retinal Projections of the Zebrafish

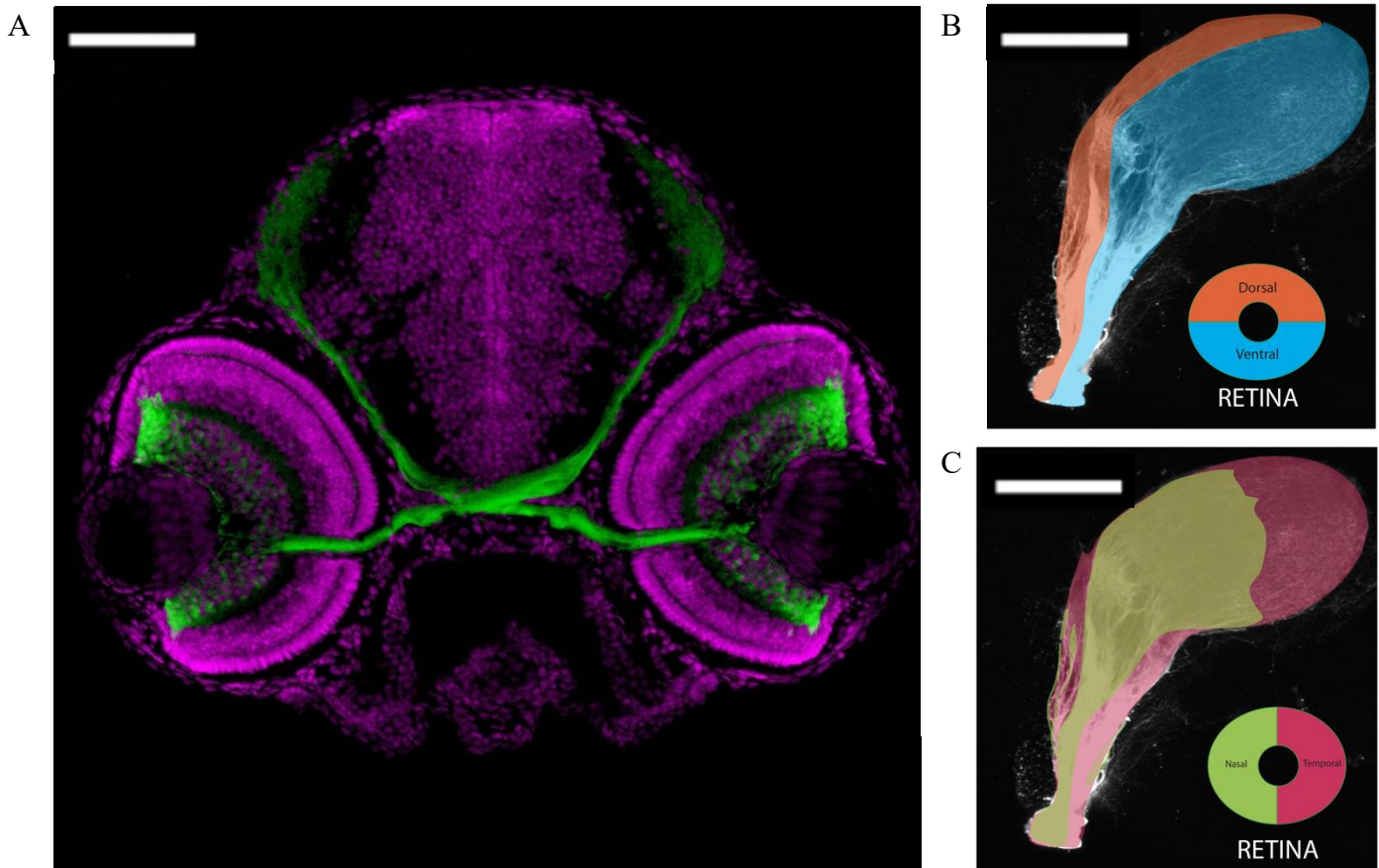


Figure 1.5: Retinal projections of the zebrafish. (A) RGCs from the zebrafish eye project largely to the optic tectum. (B-C) Projections maintain dorsal ventral and nasal temporal patterning in order to form precise retinotopic maps in the optic tectum. Figure adapted from (Robles et al., 2014, UCL, 2022) Scale Bar = 100 μ m for A and 65 μ m for B and C.

The optic tectum is located in the zebrafish dorsal midbrain and is composed of six well-defined layers: stratum marginale, stratum opticum, stratum fibrosum et griseum superficiale, stratum griseum centrale, stratum album centrale and the stratum periventriculare (see figure 1.6 below) (Nevin *et al.*, 2010). The tectal neurons can also be classified into three major classes according to where their projections terminate – these are periventricular projection neurons, periventricular interneurons, and superficial interneurons. Many of the retinal projections terminate in the layers of the stratum opticum and stratum fibrosum et griseum superficiale. Information is then processed in the other layers and the majority of tectal outputs project out from the stratum album centrale and stratum griseum centrale to the hindbrain where they can help regulate the behavioural output of the fish (Nevin *et al.*, 2010, Bollmann, 2019). This makes both the retinal ganglion cells and optic tectum essential in visual perception.

Different layers also receive input from other brain areas. For example, the stratum griseum centrale receives projections from torus longitudinalis (processing response to the overall change in light intensity) and the nucleus isthmi (regulating hunting behaviour), while the stratum album centrale receives projections from torus semicircularis, responsible for processing auditory information. It has been demonstrated that cells in the optic tectum responded to visual, auditory and mechanosensory stimuli (Thompson *et al.*, 2016). Furthermore, it was shown that visual responses could be inhibited in the optic tectum when multi-modal stimulation was applied (Thompson *et al.*, 2016). Collectively, these features make the optic tectum a highly complex neural network and a hub for sensory integration in the zebrafish brain. Resultingly, this is an area that we hypothesised would likely be involved in visual olfactory integration.

Figure 1.6: The Diverse Morphology of Neurons in the Multi-Layered Optic Tectum.

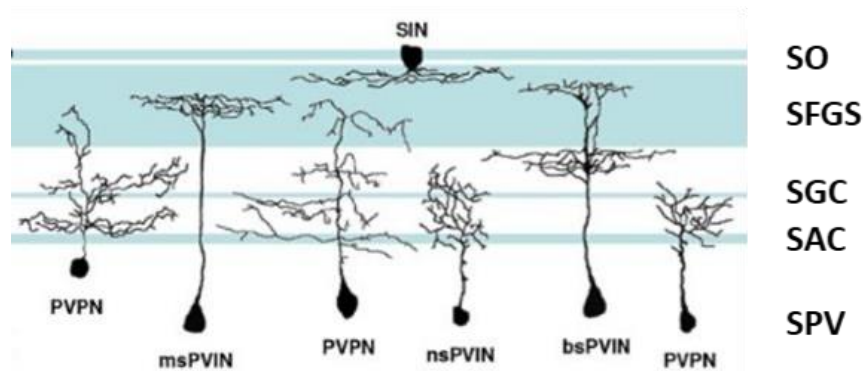


Figure 1.6: The diverse morphology of zebrafish tectal neurons in the multi-layered optic tectum. The different subtypes of neurons can be seen to terminate across the multiple layers of the tectum. PVPN - periventricular projecting neurons, msPVIN, bsPVIN and nsPVIN – mono- stratified, bi-stratified and non-stratified periventricular neurons; SIN – superficial inhibitory neurons. SO - stratum opticum, SFGS - stratum fibrosum et griseum superficiale, SGC - stratum griseum centrale, SAC - stratum album centrale and SPV - stratum periventriculare. Sixth layer (stratum marginale) not shown. (Figure adapted from (Nevin *et al.*, 2010))

One of the functions of the optic tectum is to filter visual information in zebrafish in order to improve the ability of the fish to capture prey (Filippo Del Bene *et al.*, 2010). The neuronal activity recorded in the layers of the neuropil containing terminals from the retinal ganglion cells will not be equal to that in the deeper lying output layers of the stratum album/griseum centrale. Neurons in the deeper layers are preferentially activated by smaller stimuli and some larger stimuli are often filtered out and not processed onto higher centres as a result of activation of GABAergic interneurons which are stimulated by these larger visual stimuli (Filippo Del Bene *et al.*, 2010). Conversely, the opposite process can also occur. Different rows of cells focus on different shape/size stimuli, with some cells being stimulated by larger, looming stimuli. Activation of these can lead to the escape response as these forms of stimuli often represent danger (Temizer *et al.*, 2015). Previous work from the Nikolaev lab has also investigated this phenomenon, where a *tg(Xla.Tubb:GCaMP3)* fish was immobilised in agar gel and bars of light passed across the visual field of the fish. Simultaneously, recordings of the neuronal activity in the optic tectum were taken using 2-photon microscopy and analysed. The analysis showed large calcium fluctuations in response to the stimulus in the stratum opticum but there was little activity seen in the stratum album/griseum centrale.

Centrifugal Feedback to the Retina

After more than a century of work, it has now been established that centrifugal fibres from the brain terminate can be seen projecting to the retina of all classes of vertebrates. While the mammalian retina possesses just a few fibres, the bird retina's descending input is the most highly elaborated (Cajal, 1889). Soon after their discovery, these fibres were shown to project from a region in the caudal midbrain known as isthmo-optic nucleus (Wallenberg, 1898). Input to the isthmo-optic nucleus comes from the ipsilateral tecti (Woodson *et al.*, 1991). The isthmo-optic nucleus itself is composed of just two cell types, inhibitory GABAergic interneurons and the output neurons, known as IO-neurons (Dom Miceli, 1995). Each IO-neuron gives rise to a single axon which projects to the contralateral retina and terminates in a single efferent terminal (Wilson and Lindstrom, 2011). This resultant negative feedback loop is summarised in figure 1.7 below.

Figure 1.7: Avian Retinal Negative Feedback Loop.

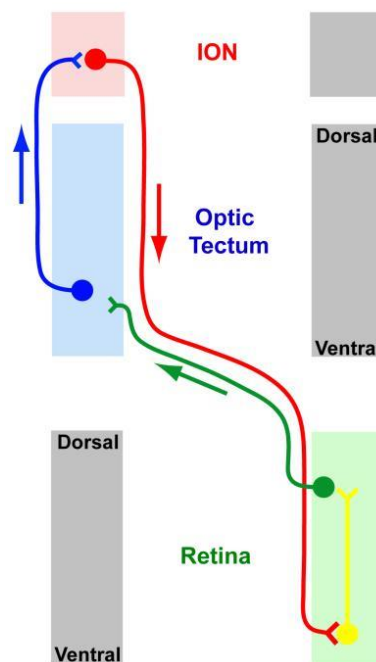


Figure 1.7: The negative feedback system between the retina, optic tectum and isthmo-optic nucleus in birds. This loop has been found to be present across many different species of birds but has not yet been identified in zebrafish. The main source of input to the optic tectum comes from the retina. A subset of tectal neurons (tecto-IO neurons) then project from the tectum to the isthmo-optic nucleus which is then able to inhibit activity of some of the retinal interneurons. Figure adapted from Wilson and Lindstrom, 2011.

Research into the tecto-IO neurons has shown these are predominantly located in the ventral region of the tectum in birds (Wilson and Lindstrom, 2011). In zebrafish, GnRH3 neurons from the *nervus terminalis* and also auditory responses have been shown to act on cell bodies in the deeper layers of the tectum (Umatani *et al.*, 2015, Thompson *et al.*, 2016). If a similar negative feedback loop is also present in the zebrafish, this may potentiate a mechanism through which multi-sensory integration can regulate visual perception in the zebrafish.

The Olfactory System

Much like the visual system, the olfactory system is also fundamental to both human and animal's responses to stimuli in the external environment. The process involves the detection of a huge diversity of chemical odorants and converting this information into electrical signals to send to the brain and influence the resulting behaviour. Ultimately, olfaction enables the detection of food and mates as well as danger, with further implications linked to emotion and memory formation (Axel, 1995, Buchanan *et al.*, 2003). It is therefore fair to conclude that olfaction is a vastly important sensory modality.

The Zebrafish Olfactory System

Odour responses have been detected in the olfactory bulbs before the fish have hatched between 2-3 days post fertilisation Li *et al.* (2005). As in higher vertebrates, odours are detected in the zebrafish olfactory system by olfactory sensory neurons in the olfactory epithelium. The adult zebrafish olfactory organs carry a distinctive rosette shape and are composed of 3 types of cells, olfactory sensory neurons, supporting cells and basal cells (Axel, 1995, Shipley and Ennis, 1996, Ahuja *et al.*, 2015). The olfactory sensory neurons can then be further subdivided into five established classes. The first of these are ciliated neurons which can be found deep within the olfactory epithelium and express long cilia. Secondly, there are microvillous neurons which lay in the intermediary portion of the olfactory epithelium with microvilli on their apical surface. Thirdly are the crypt neurons which contain both cilia and microvilli and can be found close to the microvillous neurons. The fourth class are kappe neurons, these are microvillous cells and are found in the most superficial layer of the olfactory epithelium. The final class are the pear neurons which display short apical dendrites (Ahuja *et al.*, 2015, Bannister, 1965, Cheung *et al.*, 2021). Motile cilia are located on the

surface of many epithelia and are once again found on the surface of epithelial cells in the olfactory system (Reiten *et al.*, 2017). Olfactory cilia project out into the water anterior to the nose of the fish and beat asymmetrically to generate a robust flow around the nose of the fish. The flow pattern generated draws odours towards the nose pit and thus facilitates odour detection (Reiten *et al.*, 2017). Each olfactory sensory neuron expresses just one form of G-protein coupled odorant receptor out of an array of several hundred in the zebrafish, with each being encoded by a specific odorant receptor gene (Miyasaka *et al.*, 2013). Each odorant receptor will have the capacity to bind specific odorants such as amino acids or pheromones (Axel, 1995). The axonal projections of the olfactory sensory neurons traverse from the basal side of the olfactory epithelium within the olfactory nerve fascicle to the olfactory bulbs where olfactory sensory neurons expressing the same receptor type converge to form spherical neuropil complexes called glomeruli (Miyasaka *et al.*, 2013). Different classes of olfactory sensory neurons will project to different areas of the olfactory bulb, creating a topographic map; for example, microvillous olfactory sensory neurons expressing amino acid receptors will project specifically to the lateral olfactory bulb where they will be able to effectively stimulate feeding behaviours (Axel, 1995, Koide *et al.*, 2009).

Figure 1.8: Anatomy of the Zebrafish Olfactory System

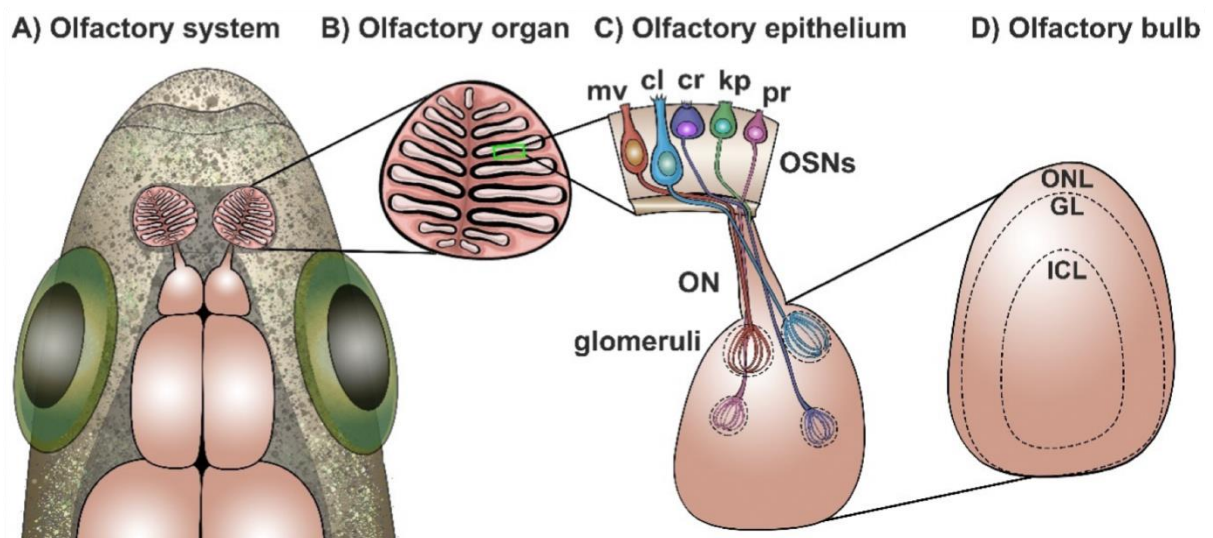


Figure 1.8: Anatomy of the olfactory epithelium and olfactory bulb. (A) The location of the zebrafish olfactory rosette on the adult fish. Posterior to the rosette-shaped olfactory epithelium is the olfactory nerve connecting the epithelium and olfactory bulbs. (B) Enhanced view of the olfactory rosette. The epithelium is organised along the lamellar structures extending out from a non-sensory central raphe. (C) Axonal

projections of the different olfactory sensory neurons along the olfactory nerve to the olfactory bulbs. (D) Enhanced view of the 3 layered olfactory bulb, the olfactory nerve layer (ONL), glomerular layer (GL), and intracellular layer (ICL), containing the cell bodies of mitral cells and granule cells (figure adapted from (Calvo-Ochoa and Byrd-Jacobs, 2019)).

The olfactory bulb is composed of 3 layers, the most superficial of these is the olfactory nerve layer, the second is the glomerular layer, and the deepest of the three, the intracellular layer which contains the cell bodies for the mitral cells and inhibitory granule cells (see figure 1.8 (Calvo-Ochoa and Byrd-Jacobs, 2019)). The olfactory nerve layer is formed from the axonal endings of the olfactory sensory neurons which then form glomeruli in the glomerular layer. Here, these form glutamatergic synapses with the dendritic projections of mitral cells, the output neurons of the olfactory bulb (Olivares and Schmachtenberg, 2019). The glomerular layer also contains nerve endings from higher telencephalic centres and GABAergic granule cells, which project onto the mitral cell dendrites in the glomerular layer (Satou, 1990).

An olfactory sensory neuron conveys its sensory information onto its corresponding mitral cell, the principal cell of the olfactory bulb. The mitral cells, also known as olfactory projection neurons, relay olfactory information from the olfactory bulb onto higher brain regions, with different sensory information being sent to different regions of the brain (see figure 1.9 below). The main target of these secondary olfactory neurons is the telencephalic dorsal posterior nucleus, comparable to the primary olfactory cortex in the mammalian brain (Kermen *et al.*, 2013), whilst the ventral ventral nucleus receives olfactory information regarding reward (Biechl *et al.*, 2017) and the habenula and interpeduncular nucleus receive information regarding aversive olfactory cues which may in turn result in fearful behaviour (Choi *et al.*, 2021, Krishnan *et al.*, 2014).

Figure 1.9: Mitral Cell Outputs to the Zebrafish Brain.

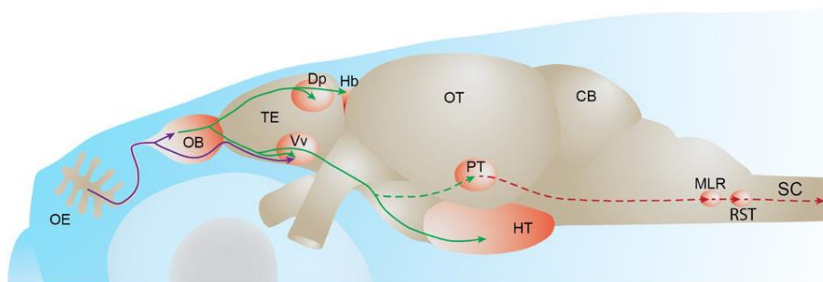


Figure 1.9: Mitral Cell Outputs to the Zebrafish Brain. Olfactory information is detected by olfactory sensory neurons in the olfactory epithelium which project along the olfactory nerve to form glomeruli in the olfactory bulb. Mitral cells form dendrodendritic glutamatergic synapses with olfactory sensory neurons and relay the information onto higher brain regions, primarily the dorsal posterior and ventral ventral nuclei but also to the habenula and posterior tuberculum. Figure adapted from (Kermen et al., 2013).

Some odorants have the capacity to activate just a single glomerulus, meaning information about that odorant is encoded by just a single output. This is coined non-combinatorial input. More frequently, a single odorant will activate multiple glomeruli meaning information regarding the odorant is encoded broadly in the locations of activated glomeruli but more finely in the specific activation pattern (Friedrich and Korsching, 1998). Evidence of these combinatorial activation patterns comes from experiments which show that glomeruli can respond to multiple odours and that single odorants can activate multiple glomeruli (Levetau and MacLeod, 1966). Through these patterns of activation, the olfactory bulb has been compartmentalised into functional sub-regions. The anterior lateral sub-region has been shown to respond to amino acid stimuli whilst the posterior lateral sub-region better responds to nucleotides stimuli. The medial sub-region is activated by bile acids and the ventral sub-region is only activated by pheromones. (Friedrich and Korsching, 1998). A finer chemotopy is then likely to be present, at least for the detection of amino acids which will provide information on the properties of the amino acid side chains (Friedrich and Korsching, 1998).

It is one of the jobs of the mitral cells to adapt the sensory input from the olfactory sensory neurons in order to convey the necessary and accurate output onto higher brain centres (Friedrich *et al.*, 2004). Their activity is finely regulated by GABA inhibition via two types of interneuron – granule cells and periglomerular cells (Tabor *et al.*, 2008). Initially, mitral cells are driven by their sensory inputs with odours evoking asynchronous spikes of activity in olfactory sensory neurons which are conveyed onto the mitral cells. Over the first second of an odour response, mitral cells responses adapt. It is thought that GABA_A interactions shape the olfactory bulbs' output activity by mutual inhibition of mitral cells with overlapping tuning ranges and also by synchronising the oscillatory activity of the mitral cells to a common level across the bulb. (Shepherd, 2004). Periglomerular cells receive glutamatergic input from

mitral cells and feedback inhibitory GABAergic output by activating nearby mitral cells' GABA_A receptors. GABA can also inhibit olfactory sensory neurons through paracrine activation of GABA_B, inhibiting the release of neurotransmitter at the olfactory sensory neuron synapse (Vucinic *et al.*, 2006). Granule cells, found in the deeper layers of the bulb are activated in a similar manner to periglomerular cells, inhibiting mitral cells through the release of GABA onto mitral cell dendrites (Shepherd, 2004, Tabor *et al.*, 2008). These adaptations may be necessary to keep the level of activity in a range that is appropriate for optimal functionality of the higher centres (Friedrich *et al.*, 2004). This adaptation is not seen in the olfactory sensory neurons and persists when output to the higher brain centres is ablated, suggesting interneurons are responsible (Tabor *et al.*, 2008).

Similarities Between the Human and Zebrafish Olfactory Systems

The basic organisation of the olfactory sensory system has been highly conserved across vertebrates, meaning many similarities exist between the human and zebrafish olfactory networks. The human olfactory organ contains approximately 50 million olfactory sensory neurons, each expressing one of the 350 different odorant receptor genes. Olfactory sensory neurons project apical dendrites into a mucus layer produced by Bowman's glands in the olfactory epithelium meaning only substances which are soluble in mucus can activate the olfactory sensory neurons (Sarafoleanu *et al.*, 2009a, Elsaesser and Paysan, 2007). Aside from olfactory sensory neurons, like in zebrafish the olfactory epithelium also contains basal cells which can give rise to mature receptor neurons when these become damaged. Olfactory sensory neurons cross the cribriform plate of the ethmoid bone and project into the olfactory bulbs where they converge to form glomeruli. Each glomerulus will be formed of approximately 1000 olfactory sensory neurons expressing the same receptor and form a topographic map in the olfactory bulbs (Sarafoleanu, 1999, Sarafoleanu *et al.*, 2009a). Again, similarly to teleosts, here mitral cells will also converge with the glomerulus and convey the olfactory information to higher brain centres. The olfactory tract projects out to the olfactory cortex and the amygdala, the homologues for which exist in the zebrafish and receive olfactory input (Kermen *et al.*, 2013, Whitlock and Palominos, 2022).

Figure 1.10: Comparing the Zebrafish and Human Olfactory System

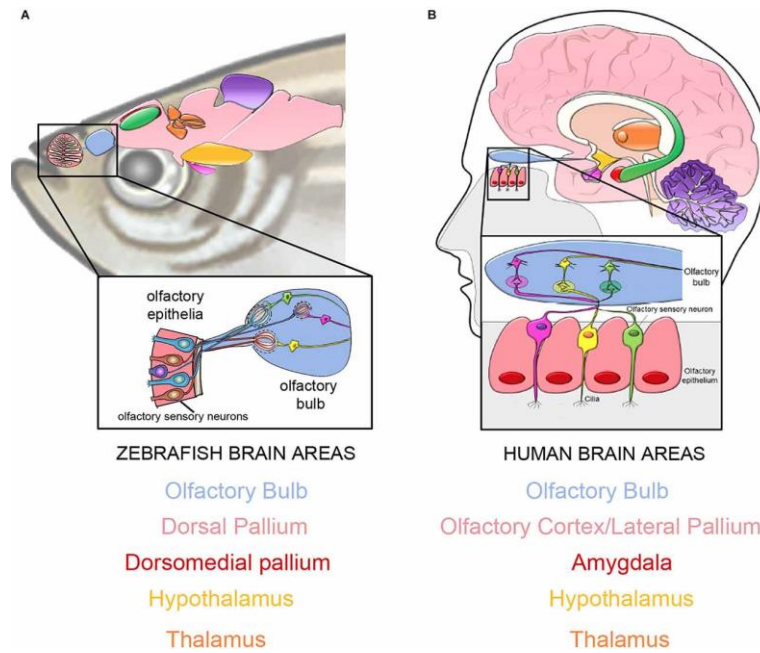


Figure 1.10: Comparing the Zebrafish and Human Olfactory System. The projections from the olfactory epithelium to the olfactory bulb and onto higher brain centres are highly conserved across evolution as demonstrated by the comparison between the olfactory network in zebrafish (A) and the human brain (B). olfactory sensory neurons detect odours in the external environment and relay this information to the olfactory bulbs (blue). Olfactory sensory neurons converge to form glomeruli in both systems in the olfactory bulbs and output neurons project to the olfactory cortex (pink) and its homologous structure in the zebrafish, dorsal pallium. Both species also show olfactory input to the amygdala/its proposed homologue in the zebrafish, the dorsomedial pallium (red). Figure adapted from (Whitlock and Palominos, 2022).

The human sense of smell serves equally important functions as it does in zebrafish. It provides us with the ability to monitor the safety of the inhaled air (Zhou *et al.*, 2019, Pence *et al.*, 2014), the safety of the food we are about to eat (Yeomans, 2006) and also has implications on our emotions and social lives (Zhou *et al.*, 2019). These functions are likely carried out by the olfactory cortex and amygdala away from the nose. The Zhou lab attempted to summarise and illustrate the potential roles of different olfactory subregions in the primary olfactory cortex by recording fMRI images of the human brain during olfaction. They suggested that the anterior olfactory nucleus may aid in forming olfactory object representations, whilst the olfactory tubercle may extract social and emotional information from olfactory cues. The frontal piriform cortex may function to plan olfactory-related

movements whilst the temporal piriform cortex could be responsible for respiratory modulations and verbal communication regarding olfactory stimulation (Zhou *et al.*, 2019).

Although differences particular in the higher processing of olfaction may exist, the numerous similarities present between the human and zebrafish olfactory system have made it a suitable model organism for studies of anosmia and olfaction.

Evidence for Visual-Olfactory Integration

Can Vision Influence Olfactory Perception?

Interest in visual and olfactory integration began in the early 2000s. Some of the first major evidence of integration between the two modalities was published in 2003 in a paper by Morrot *et al.* Here a panel of 54 wine tasters described the odours of two wines, one red wine and one white wine. The words used to describe the wine were then cross-referenced against standard wine-tasting descriptive words for each type of wine and plotted for each taster. In a second experiment, the tasters were presented with two glasses of the same white wine, but the second had been artificially coloured to appear like a red wine. Here they noted that the visual system was able to evoke a perceptual illusion, where the tasters would smell the coloured white wine and detect odours which are characteristic of red wine. This enabled the authors to conclude that the colour of wine dictated odour identification and thus is an example where a change in visual perception was able to evoke a change in olfaction (Morrot *et al.*, 2001).

A study 2 years later by Gottfried *et al.* used fMRI studies to investigate the underlying mechanisms of olfactory and visual integration. To do this, pictures of various visual stimuli were presented to subjects, alongside congruent odorants, incongruent odorants, or no odorant. Analysis of the fMRI data aimed to identify areas of the brain where bimodal activity would exceed the sum of the unimodal responses from the olfactory and visual systems (Gottfried and Dolan, 2003). This identified two areas of interest. The first was the left rostromedial orbitofrontal cortex which had previously been shown to receive innervation from both visual and olfactory systems in nonhuman primates (Rolls *et al.*, 1996). The second

region was the posterior intraparietal sulcus, which is a section of the brain that becomes active during visual stimulation. Additionally, in these experiments, it was noted that simultaneous olfactory and visual stimulation enhanced neuronal activity in this region. The paper also reported that olfactory detection was facilitated in the presence of congruent visual-olfactory cues, and incongruent cues would lead to poorer olfactory detection. When congruent conditions were present, fMRI images detected significant activation of the left anterior hippocampus and the amygdala (Gottfried and Dolan, 2003). Cumulatively, this data provides evidence to support the presence of sensory integration through differences in neuronal activity within the human brain in response to unimodal and bimodal stimulation.

It was later shown that colour wasn't the only mechanism through which the visual system can alter olfactory perception. Work conducted by Demattè et al. looked to understand if shape also contributed to olfactory perception. Subjects were presented with two odours, strawberry or lemon, and asked to identify the odorant in the presence of red or yellow visual distractors shaped like either fruit. They concluded that both shape and colour were able to influence speeded olfactory discrimination, which hinted at the presence of higher level cross-modal interactions taking place between the visual and olfactory systems (Demattè *et al.*, 2009).

Can Olfaction Influence Visual Perception?

As summarised above, it has been well documented that vision can drive olfactory perception. More recent evidence has shown that olfactory stimulation is also capable of altering visual perception. The first evidence for this arose in 1988 when it was shown that olfactory input was able to evoke an electrophysiological response in the zebrafish retina (Weiss and Meyer, 1988). In 2010, a paper by Zhou et al. investigated the effect olfactory modulation has on binocular rivalry. Here, two different visual images were presented to subjects, one to each eye, thus creating binocular rivalry. The first of these images was a rose and the second a marker pen. Presentation of the congruent odorant (phenyl-ethyl alcohol for the rose and butanol for ink) was shown to prolong the dominance period during which the subject could see the respective image throughout the experiment. This was the first time that an olfactory stimulus was shown to be able to modulate visual perception (Zhou *et al.*, 2010). In a second experiment, either image was presented to one eye as was done previously, but this time it

was paired with white noise in the second eye. Over time, the white noise would increase in contrast causing suppression of the visual cue. Application of the congruent olfactory cue was shown to reduce the suppression time caused by the white noise (Zhou *et al.*, 2010). Further evidence of olfaction being able to modulate visual perception came through a study conducted by Seigneuric *et al.* A photograph containing a range of visual stimuli was presented to the subjects. An olfactory cue congruent to one of the images was then presented unknowingly whilst the eye movements were tracked to analyse changes in object recognition within the photo. Analysis identified that the congruent visual cue was explored much faster, which was likely to be an effort made by the brain to identify the source of the olfactory cue. This in turn facilitates the identification of the congruent image (Seigneuric *et al.*, 2010a).

The data described above discusses ways in which olfactory stimulation was able to modulate the visual ventral pathway in the brain, the primary function of which is object and shape recognition. Work conducted by Kuang and Zhang in 2014 was able to conclude that olfactory cues can also implement a bias on ambiguous visual motion perception. This demonstrated that there is also an integratory link between olfaction and the visual dorsal pathway as well as the ventral pathway (Kuang and Zhang, 2014), suggesting more complex integratory mechanisms may exist. To summarise, these early experiments showed that both visual and olfactory cues can alter the processing of the other sensory modality. What remained unanswered was how this process occurs within the brain.

Evidence from behavioural studies in guppies has displayed further evidence of visual olfactory integration. Raising the fish in either normal or low-light conditions can result in a sensory compensation. After exposure to either normal or dark conditions for 4 weeks, guppies better-located food cues in the environment in which they were raised. Furthermore, in both conditions, it was concluded that guppies preferred food cues which stimulated both the visual and olfactory systems rather than unimodal stimuli. This suggests the behavioural outcome was most successful when the visual and olfactory systems could work together (Kimbell *et al.*, 2019).

Perhaps most convincingly of all was a study conducted in 2012 by Jessica Stephenson et al., where they were analysing the optomotor response in the zebrafish. The optomotor response is an innate orienting behaviour which is commonly studied in both fish and insects and is evoked by whole-field visual motion. They showed that in low light conditions, fish responded better to the visual stimulus in the presence of both food odorants and the alarm substance (Stephenson *et al.*, 2012). More recently, it has also been highlighted that cadaverine, formed by the decay of animal proteins after death, may trigger aversive responses in the zebrafish and halt the optomotor response, providing evidence that olfaction can override visually directed behaviour.

Mechanisms of Sensory Integration

It is evident from the current literature that integration is occurring between the visual and olfactory systems, in turn aiding organisms to optimise their behaviour. What is not evident is how this integration occurs.

Nervus terminalis, or the terminal nerve, has been brought to the forefront as a potential mechanism through which the two modalities can interact. The terminal nerve is considered by many as cranial nerve zero due to its location rostral to the other cranial nerves (Sonne *et al.*, 2017). It was first identified in the brain of a shark in 1878 by Gustav Fritsch. The terminal nerve is located very closely anatomically to the olfactory nerve but experiments by Sonne et al, 2018 have shown the two arise at different stages in development and therefore are distinct.

Terminal nerve neurons express two types of peptides, gonadotropin-releasing hormone 3 (GnRH3) and molluscan cardio-excitatory peptide (FMRFamide) (Dowling, 2013). NT originates by the cribriform plate in the olfactory bulbs and has been shown to project directly to the retina and optic tectum (Dowling, 2013). This olfacto-retinal centrifugal pathway has been identified in all fish species analysed to date, including zebrafish (Maaswinkel and Li, 2003b). Terminal nerve fibres have been noted in the human brain from as early as 1914 (Vrapciu and Popescu, 2016) however their function is still unclear and has been long overlooked across the fields of anatomy and neuroscience.

Given their anatomical projections seen in teleosts (Esposti *et al.*, 2013, Koide *et al.*, 2018), it is possible that the terminal nerve may act as a neuronal link between the sensory systems. Within the retina, terminal nerve projections terminate in the inner plexiform layer and synapse onto perikarya and proximal dendrites of dopaminergic inter plexiform cells (Behrens and Wagner, 2004). The normal function of these cells is to inhibit retinal ganglion cell activity through the release of dopamine. However when the terminal nerve was activated through olfactory stimulation, dopamine release was inhibited, thus RGCs became active (Huang *et al.*, 2005).

Other experiments have shown changes in visual sensitivity of zebrafish, measured both behaviourally and through using an electroretinogram, when the olfactory system is activated by various amino acid stimuli. This process again was mediated by the terminal nerve modulating dopamine release from inter plexiform cells, this time functioning to increase the sensitivity of OFF bipolar cells. Work conducted by the Lagnado lab in 2013 described a mechanism through which olfactory stimulation can selectively modulate OFF bipolar cells in the retina of teleosts. Methionine, a food-related amino acid, was shown to be able to reduce the gain of response to both luminance and contrast through OFF bipolar cells. Furthermore, it was also shown to increase the sensitivity of responses in these cells through pre-synaptic calcium release regulated by dopamine (Esposti *et al.*, 2013). A subsequent review by John Dowling then explored the literature for further evidence of integration and physiological interactions between these two sensory modalities, centrifugal input to the retina, and possible effects of the circadian clock on visual-olfactory integration. Dowling also posed the question of whether the terminal nerve may have a role in visual/olfactory sensory integration given its anatomical prominence in both sensory systems (Dowling, 2013).

Since then, further studies have begun to research the role the terminal nerve plays in visual-olfactory integration. The Oka lab used fluorescently labelled GnRH3 peptides, the neurotransmitter secreted by terminal nerve fibres, to show that GnRH receptors are localised around the cell bodies of postsynaptic neurons in the optic tectum (Umatani *et al.*, 2015). Electrophysiology recordings then demonstrated that activation of the GnRH receptors leads to activation of large-conductance calcium-activated potassium channels and therefore

suppression of membrane excitability. These results suggest that the terminal nerve acts to suppress the excitability of projection neurons in the tectum (Umatani *et al.*, 2015) and therefore may prove to be a means through which olfaction can regulate the visual pathway. Work conducted in 2018 once again showed terminal nerve projections originating in the olfactory bulbs and projecting to the retina and optic tectum in zebrafish (Koide *et al.*, 2018). In this paper, Koide *et al.* described a functional role for the terminal nerve as a carbon dioxide sensor however, they also hypothesised that it may have a wider olfactory function. If this is indeed the case, the research conducted in these experiments would provide evidence for a neuronal mechanism through which the visual system is being regulated by olfaction.

Figure 1.11: Projections of Terminal Nerve Fibres.

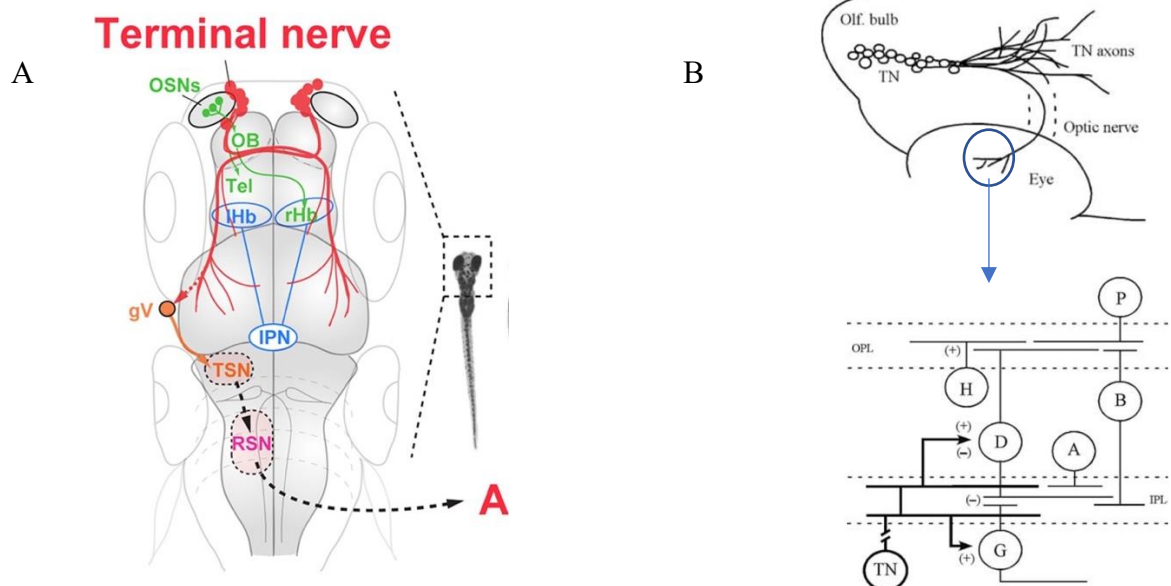


Figure 1.11: Projections of Terminal Nerve Fibres: (A) The trajectory of terminal nerve axons in Zebrafish. The terminal nerve originates at the cribriform plate and the anterior end of the fish. The fibres pass through each olfactory bulbs and then cross the midline to project to the contralateral tecti. Figure adapted from (Koide *et al.*, 2018). (B) Projections of the terminal nerve axons highlighting their regulatory effect in the retina. The cell bodies of terminal nerve axons are located in the olfactory bulb and ventral region of the telencephalon. Most terminal nerve fibres project to either the forebrain or the midbrain but some fibres project to either the optic tectum or the retina. In the retina, the terminal nerve fibres branch in the inner plexiform layer to synapse on either dopaminergic inner-plexiform cells or directly on retinal ganglion cells where they can have a stimulatory effect. The effect terminal nerve fibres have on the dopaminergic retinal cells depends on the neuropeptide released: GnRH stimulates dopamine release whereas FMRFamide inhibits its release. Figures adapted from (Esposti *et al.*, 2013, Koide *et al.*, 2018).

Another notable region of interest is the habenula. The habenula are a set of diencephalic asymmetric nuclei, evolutionarily conserved across vertebrates. The mammalian habenula consists of at least two functionally different subnuclei – the left and right medial and lateral habenula. In zebrafish, the structural arrangement of the nuclei differs slightly compared to the mammalian system, with zebrafish demonstrating a dorsal/ventral arrangement as opposed to medial/lateral (Jesuthasan, 2018). An increasing amount of evidence over recent years has suggested the habenula could play a role in sensory processing (Fore *et al.*, 2017).

Recent discoveries suggest that the habenula plays a role in behavioural choice through the regulation of the dopamine and serotonin systems (Hikosaka, 2010). It is believed to be responsible for value-based decision making and behavioural responses to pain, stress, sleep, reward and anxiety. To accurately make these decisions, it would be logical that the habenula receives input from multiple sensory systems. The olfactory nerve has been shown to send some neuronal projections specifically to the right dorsal habenula from the olfactory bulb and these projections can be stimulated by a broad range of different odorants (Fore *et al.*, 2017, deCarvalho *et al.*, 2013). Projections from the retina via the thalamus can be found to the left dorsal nuclei in the habenula. This therefore means the habenula receive input from the olfactory and visual systems but not to the same nuclei (Dreosti *et al.*, 2014).

The intrinsic circuitry of the habenula is poorly understood but both the left and right dorsal habenula project out to the interpeduncular nuclei (McLaughlin *et al.*, 2017). The interpeduncular nuclei projects some of its efferent neurons to the tegmental system in zebrafish which as previously stated can act as an input to the optic tectum. In summary, the habenula may also act as a source of integration for the sensory modalities but more experimentation is needed to identify the extent of communication between the left/right sides.

Figure 1.12: The Zebrafish Habenula

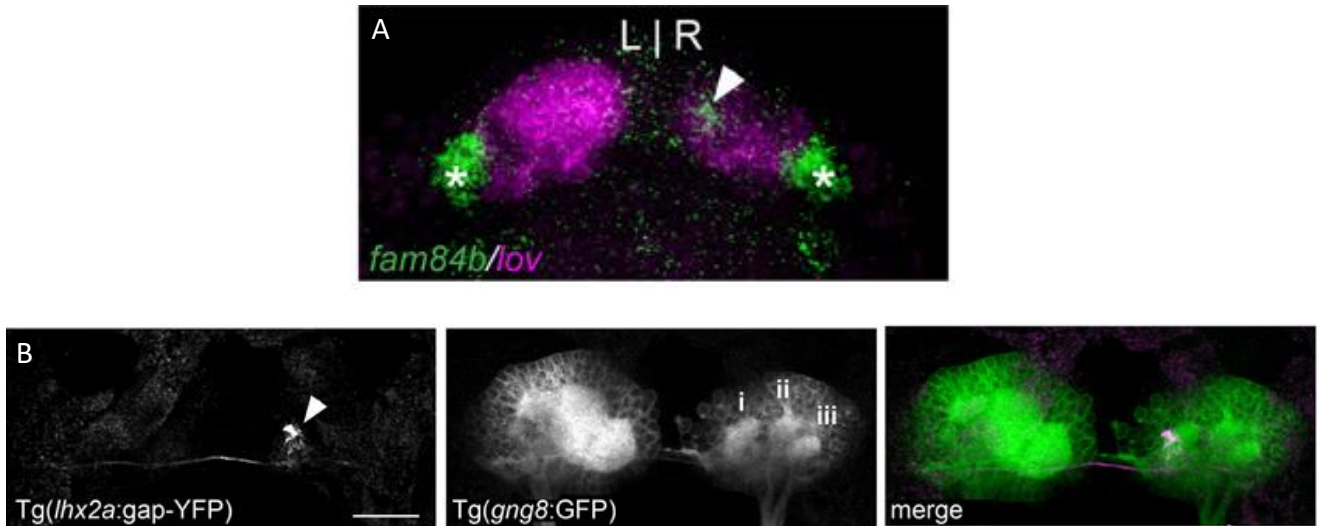


Figure 1.12: The Zebrafish Habenula: A. Dorsal and ventral labelling of both the left and right zebrafish habenula. B. Olfactory axons labelled with *lhx2a:gap-YFP* (white arrow) can be seen to innervate the medial neuropil of the right habenula (i). Figure adapted from (deCarvalho *et al.*, 2013) Scale bar = 30 μ m.

Although the neuronal mechanisms linking both vision and olfaction may remain unclear, evidence from further behavioural studies has displayed more conclusive results. A study conducted using both guppies and zebrafish analysed the behaviour to both visual and olfactory social cues. A custom-built tank was used where on one half fish would see conspecifics but not be able to smell them, and on the other half a conspecific odorant was added to the chamber but no conspecifics could be seen. The data showed that guppies spent a larger amount of time in the tank with the visual cue whereas zebrafish spent more time around the olfactory cue. This suggests that different species of fish will rely more on either their visual or olfactory system and that there is versatility and trade-offs between the two modalities (Santaca *et al.*, 2021). With this being said, as there is not a huge difference between the results for each dataset, Santaca *et al.* (2012), concluded that both species likely rely on integration of multiple sensory modalities, in this case vision and olfaction, to locate nearby shoals.

The olfactory bulbs in zebrafish receive centrifugal input from two brain regions – the first of which is the raphe nuclei. Dorsal raphe neurons and the medial raphe neurons have both been shown to densely innervate the olfactory bulbs with dorsal raphe neurons projecting to

the granule cell layer and medial raphe neurons projecting the glomerular layer (Steinfeld *et al.*, 2015). It was already known that the raphe receive innervation from periventricular projection neurons of the optic tectum (Nevin *et al.*, 2010) so this may act as an integratory mechanism for both the visual and olfactory systems. A study which analysed fMRI data on application of both visual, olfactory, and bimodal stimulation in humans noted that all bimodal visual-olfactory networks studied consistently revealed a negative neural network. This suggests that sensory interactions here may be dominantly driven by inhibitory interactions (Ripp *et al.*, 2018) and could be further supported by the dorsal raphe fibres terminating in the granule cell layer of the olfactory bulbs in the zebrafish. The second structure providing centrifugal input to the olfactory bulbs is the terminal nerve but given its anatomical origins, it is unlikely that this will provide visual input to the olfactory bulbs. Further experimentation will be required to understand the mechanistic nature of how responses to visual stimuli can be found within the olfactory system and what effect these may have on olfactory processing.

Further studies have been conducted in human subjects using various visual and olfactory stimuli whilst conducting fMRI scans to analyse which areas of the brain are active during unimodal and bimodal stimulation. Work by Stickel *et al.* (2019), identified that the inferior parietal sulcus becomes activated during bimodal stimulation. Additionally, the study noted that during bimodal stimulation, there is an increase in activity of visual processing areas, with these becoming more engaged during simultaneous olfactory stimulation (Stickel *et al.*, 2019). Experiments conducted by Amsellem *et al.* (2018), involving the presentation of further congruent and incongruent visual-olfactory stimuli to further human subjects led the authors to conclude that bimodal connections were able to influence both odour identity and the pleasantness of odorants. This suggests interactions between the two modalities may take place in different stages of sensory processing (Amsellem *et al.*, 2018). A further study later by Gottfried *et al.* used fMRI studies to investigate the underlying mechanisms of olfactory and visual integration. To do this, pictures of various visual stimuli were presented to subjects, alongside congruent odorants, incongruent odorants, or no odorant. Analysis of the fMRI data sought to find areas of the brain where bimodal activity would exceed the sum of the unimodal responses from the olfactory and visual systems (Gottfried and Dolan, 2003). This identified two areas of interest, the first was the left rostro-medial orbitofrontal cortex

which had previously been shown to receive innervation from both visual and olfactory systems in nonhuman primates (Rolls and Baylis, 1994). The second region was the posterior intraparietal sulcus – this section of the brain becomes active during visual stimulation but in these experiments, it was noted that when simultaneous olfactory stimulation was paired with the visual stimulus, activity was enhanced. The paper also noted that olfactory detection was facilitated in the presence of congruent olfacto-visual cues and incongruent cues would lead to poorer olfactory detection. When congruent conditions were present, fMRI images detected significant activation of the left anterior hippocampus and the amygdala. Homologues for both of these structures can be found within the zebrafish forebrain (Cheng *et al.*, 2014).

Predictive Coding Framework for Sensory Integration.

Another angle through which sensory integration needs to be further investigated further is through predictive coding. Each sensory system can detect stimuli in the external environment at differing speeds and accuracies. The predictive coding framework explains that each sensory system creates estimates or priors of the environment (Friston, 2010). It was previously thought that these priors had a degree of rigidity but it is now thought that multimodal signals can provide continual updating of priors to provide better fine tuning and adaptation to multimodal signalling (Altieri, 2014). This mechanism provides sensory areas at the initial stages of sensory processing with predictions which can in turn be used to alter their sensitivity to ongoing sensory input. (Talsma, 2015). This was evidenced when a comparison between visual and auditory responses in speech processing noted that the visual signal precedes the auditory cue by tens or even hundreds of milliseconds (V van Wassenhove *et al.*, 2005). The authors were then able to evidence that the preceding visual cue was able to speed up auditory processing through reductions in residual error in the auditory signal (V van Wassenhove *et al.*, 2005). Internal comparison of these sensory predictions against actual sensory input will sometimes lead to large mismatches in information. This would result in a major update in the internal prediction model and several studies have provided evidence whereby this classic example of bottom-up processing in one sensory modality is able to adjust the internal representation of a stimulus in another (L Busse *et al.*, 2005, Burg *et al.*, 2008, Burg *et al.*, 2011, Talsma, 2015).

As well as bottom-up processing, situations will arise where complex environments can provide the brain with an overload of sensory information. In these conditions, many stimuli will be competing for processing capacity within the brain and the most relevant stimuli will require prioritisation. It was hypothesised that this may be achieved through higher-order brain areas providing feedback connections to lower-order perceptual regions to provide a selective bias. This type of sensory processing is known as top-down and has similarities to selective attention (Corbetta and Shulman, 2002). In this way, it is thought that the feedback projections can alter sensitivity in neurons responsive to the prioritised attended feature and decrease the responsiveness of the features not selected for (Motter, 1994, LaBerge, 1995, Corbetta and Shulman, 2002). This cross-modal processing would work alongside bottom-up processing to continually update predictions and processing across each sensory modality by combining and comparing the information received from each system.

In the brain of behaving animals, neuronal activity can be seen in populations when driven by sensory stimuli and in the absence of those. These spontaneous bursts of activity are commonly seen across the brain and appear to oscillate with up and down states (Koren and Denève, 2017). This activity has also been shown to exhibit levels of spatial precision so is therefore not considered to be random. It has been hypothesised that it has functions in guiding development through establishing appropriate connectivity in neural circuits (Wosniack *et al.*, 2021), error correction in the quiescent state (Koren and Denève, 2017) and perhaps also in updating sensory priors and optimizing generative models for future interactions (Pezzulo *et al.*, 2021).

Further experimental evidence is needed to identify if and how input from one sensory modality, in this case the visual or olfactory system, may be able to regulate sensitivity and stimulus detection in the other. Astrocytes have been shown to be responsive to a range of neuromodulators, with noradrenaline being shown to have the capacity to evoke robust calcium transients in astrocytes across the brain (Wahis and Holt, 2021). A single astrocyte can on average maintain and regulate neurotransmitter levels at 140,000 synapses where the astrocyte can ensheath the neuron and modulate synaptic activity. Furthermore, astrocytes can also form a network and affect distant cells through the release of their own

gliotransmitters such as ATP or glutamate (Pacholko *et al.*, 2020). This enable an astrocyte to be primed to relay or amplify the effects of neurotransmitters onto neurons (Wahis and Holt, 2021). In the zebrafish, radial astrocytes have been demonstrated to accumulate noradrenaline released from neurons in response to swim failures. The astrocytes can then trigger behavioural suppression through activation of GABAergic neurons and prevent further futile behaviours (Mu *et al.*, 2019). Work conducted by the Monk lab has also identified a potential *bona fide* astrocyte in the zebrafish (Chen *et al.*, 2020). They demonstrated that the cell type integrates into neural circuits and can exhibit both microdomain and whole cell calcium transients. Extensive astrocyte-neuron interactions may present a way in which multi-sensory integration can occur across the brain without direct neuron-neuron contacts being in place. The function of astrocytes has been overlooked in sensory neuroscience for many years meaning their complete functions are still not fully understood and should therefore be better investigated.

Short-Term Sensory Plasticity.

An alternate route through which sensory integration may be evident is through changes in short term plasticity. Short term adaptations happen in the range of milliseconds to seconds and may help to fine-tune the transduction process or synaptic activity, in contrast, long term adaptation responds to background levels of stimuli and largely functions to suppress transduction (Katherine Nagel and Wilson., 2011, Jafari and Alenius, 2021). To provide efficient transfer of sensory information to the brain, neurons can show short term plasticity and adapt their response to persistent or prolonged stimulation.

Adaptation is a feature shown by some cells where they have the capability to reduce the gain of response to persistent features from the input. This phenomenon allows for the prevention of saturation to prolonged or repetitive stimulation and continued futures signalling upon increases in stimulus strength. However, these cells will not be able to accurately transfer information regarding future decreases in stimulus strength. To combat this, a second subset of cells can be found that gradually increase the gain of response to prolonged stimulation, this feature is coined sensitisation. These cells will therefore efficiently respond to future

decreases in stimulus strength. Together, adaptation and sensitisation allow for the efficient transfer of sensory information over the course of time.

Thus far, both forms of sensory plasticity have been identified in the visual system (Nikolaev *et al.*, 2013), the lateral line (Pichler and Lagnado, 2019) and the auditory system in the zebrafish (Echeverry *et al.*, 2022). Although it is not clear if these features are present in the olfactory system of zebrafish, both slow and fast adaptations have been described in the drosophila olfactory system, in particular in the OSNs (Jafari and Alenius, 2021). One working theory exists that short-term sensory plasticity is versatile. Depending on the current state of the fish and the effect the stimulus will have on the fish may alter the levels of short-term plasticity seen. Neuromodulators are able to adapt sensory circuits to a constantly updating environment. It has been shown that different levels of information are transmitted across synapses across the morning and afternoon (Moya-Diaz *et al.*, 2022). As a result, we hypothesise that neuronal circuits may also be modulated and show differing adaptations to unimodal stimulation vs bi-modal stimulation. These changes may result in a shift in information transfer which may be visible through changes in the short term plasticity to our visual/olfactory stimuli.

Research Goals and Objectives

Experiments conducted by Gil Morrot et al. (2001), provided strong evidence that visual information was able to change olfactory perception. In contrast, behaviour experiments such as those conducted by Demattè et al. (2009), Jessica Stephenson et al. (2012), and Zhou et al. (2010), all displayed evidence of olfaction aiding visual function but did not confirm if olfactory input was able to change the way we perceive objects. As a result, it was my goal to investigate if the olfactory system was able to change visual perception, not just aid visual function.

In addition to this, it has been demonstrated that centrifugal olfactory input to the retina has the capacity to modulate retinal ganglion cells. Overall, however, the neuronal architecture is fairly self-contained and little evidence exists of any visual-olfactory integration elsewhere in the brain. The optic tectum receives input from multiple sensory modalities and has already been hypothesised to function as an integratory hub. In addition, the habenula has been seen to receive input from both the visual and olfactory systems and plays a key role in regulation of behaviour. Consequently, I also aimed to investigate their role in visual-olfactory integration by testing to see if multi-modal input could alter the neuronal responses in either of these brain areas. We hypothesised that this may be in the form of influencing predictions through changes in spontaneous activity and additionally through alterations in short-term plasticity and sensory adaptations.

Modulation of synaptic activity is essential for sensory circuits to adapt to a constantly updating external environment. Sensory plasticity and adaptation are one way in which this is done which can be regulated through neuromodulator release. As a result, we intend on also investigating to see how changes in neuronal short-term plasticity may change during multimodal sensory stimulation to see if modulation at the synapses could act as a method of sensory integration.

Only recently have potential *bona fide* astrocytes been described in zebrafish (Chen *et al.*, 2020, Tan *et al.*, 2021). These cells have been shown to be remarkably similar to mammalian astrocytes and derive from radial glia. These cells associate closely with neuronal synapses

and also exhibit both whole cell and microdomain calcium transients. We therefore hypothesise that astrocytes may be able to regulate this modulation across sensory modalities due to their extensive projections across the brain and pre-existing known role in modulating neuronal responses.

In summary, in this PhD thesis, it was my aim to identify how and where visual and olfactory information integrates within the zebrafish brain and to better understand what effect this integration can have on behaviour.

Materials and Methods

3.1 Animals and Husbandry

The animal studies throughout were reviewed and approved by ethics committees in Sheffield and Singapore. All zebrafish work in Sheffield was completed under license from the Home Office and additionally reviewed by the Project Applications and Amendments Committee of the Animal Welfare and Ethical Review Body (AWERB). All work was conducted according to recommended standard husbandry conditions (Aleström *et al.*, 2020). Fish were housed in a Tecniplast system (Tecniplast S.p.A., Buguggiate, Italy) and fed twice a day. No more than 20 fish were housed per tank. All experiments in Singapore were performed under guidelines approved by the Institutional Animal Care and Use Committee of Biopolis (#181408) and Nanyang Technological University.

Adult zebrafish in all facilities were kept in a 10 h dark/14 h light cycle at 28.5°C and progeny spawned by pair-mating or marbling (Aleström *et al.*, 2020). Eggs were collected and staged according to standard protocols (Nüsslein-Volhard and Dahm, 2002, Kimmel *et al.*, 1995) and raised in E3 medium (5 mM NaCl, 0.17 mM KCl, 0.33 mM CaCl₂, 0.33 mM MgSO₄, with 0.0001% methylene blue at early stages) at 28.5°C.

Zebrafish Lines

For all listed experiments, 2-photon calcium imaging of zebrafish neurons was conducted using the pan-neuronal *tg(Xla.Tubb:GCaMP3)* (Bergmann *et al.*, 2018), *tg(elavl3:H2B-GCaMP6s)* (Dunn *et al.*, 2016) and *tg(Xla.Tubb:jGCaMP7f)* (Chia *et al.*, 2019) zebrafish lines whilst behaviour experiments were conducted on wild type (AB strain—ZFIN) or nacre fish (Lister *et al.*, 1999).

Imaging of astrocytic calcium activity was conducted on *slc1a3b:jRGECO* larvae. The construct was made within the lab using gateway cloning protocol (Katzen, 2007) and injected into 1 cell stage nacre or *tg(elavl3:H2B-GCaMP6s)* embryos.

3.2 Behaviour Experiments

For behaviour experimentation 10 days post-fertilisation AB wildtype fish were used throughout to match the age of fish used in our calcium imaging described in section 3.4. Two fish were placed into a 3cm diameter Nunc™ Cell Culture Petri Dish (150318, Thermo Scientific) simultaneously for 10 minutes to allow for acclimatisation. The area of the culture dish was slightly reduced using low melting point agarose to aid with analysis further down the line as reflections on the wall of the dish hindered animal tracking. Experiments were recorded using a Basler USB3 acA1440-220um camera with culture dishes containing each fish placed onto an iPad screen. Visual stimuli were created using PsychoPy (Pierce, 2009) and consisted of a small black dot which would pass along the iPad screen underneath the imaging chamber. The dot used for experimentation has a diameter of approximately 390µm. The experiment consisted of 6 passes in total, in passes 1 and 4 the dot would move from left to right across the centre of the dish while passes 2 and 5 the dot moved from right to left. In passes 3 and 6 a dot would move in each direction simultaneously. Presentations lasted approximately 4 minutes in total. After the experiment, a 10-minute waiting period began to try to minimise effects of habituation. After this, an olfactory stimulus was added to the chamber and the experiment repeated. Stimuli consisted of either food odorant or the alarm substance, schreckstoff and were obtained as described by Kermen *et al.* (2019), and Jesuthasan *et al.* (2020), respectively. 1g of Zebrafeed (Sparos) powdered fish food was

incubated in 50ml of E3 medium for 30 minutes. The solution was centrifuged to remove physical contaminants from the odourant. Stock solution was then diluted 1 in 10 for working concentration. For extraction of alarm substance, adult zebrafish were euthanised by immersion in tricaine MS-222. Fish were dried and shallow lesions made along the body of the fish using a microsurgical knife, ensuring no blood was drawn. Each fish was immersed into an Eppendorf tube with E3 solution. Tubes were shaken on an orbital shaker for 30 minutes, before fish were removed and the extracts combined. Extract was centrifuged at 13,000 RPM for 2 minutes and filtered. Stock solution was then diluted to 1:10 for working concentrations and aliquoted. Experiments were conducted separately on different fish for each odorant, meaning each dataset had its own pre-stimulus control/baseline recording taken before addition of 500 μ l of either olfactory stimulus. In order to allow for comparison of effects of food odour vs alarm substance, we first ensured no significant differences were present between the control recordings of both datasets in all analyses. No statistical analyses were conducted between the baseline recordings and the olfactory datasets as the stimulus was no longer novel when the olfactory stimulus was applied, meaning two experimental conditions had been changed.

The saved TIF files were converted into movies using ImageJ. Real time tracking of the fish was achieved through use of a custom written Python code using the OpenCV library on each movie file. Each recording lasted up to 12,000 frames with recordings imaged at 30fps. Real time tracking allowed for selection of a small rectangular ROI around each of the two fish and the rest of the field of view was excluded from further analysis. Each of these subsequent movies was uploaded into the DeepLabCut (Lauer *et al.*, 2022) pose estimation software for Python. A network was trained to identify 4 markers on each of the eyes of the zebrafish and 8 markers along the tail. This would allow for pose estimation throughout each experiment to analyse hunting and avoidance behaviour. Pose estimation was then mapped back onto the full-scale original movie and X-Y coordinates of the fish were exported into Microsoft Excel for further processing.

In Microsoft Excel 360, Visual Basic Application codes were custom-written to handle the X-Y coordinates data. It was hypothesised that the fish treated with food odour will be more attracted to the visual stimulus whilst, the fish in the alarm substance condition will find the

stimulus more aversive. To test this, a battery of behavioural variables was measured to compare the differences between food-treated and alarm substance-treated fish. The distance travelled was calculated frame by frame to calculate the swimming speed of each larva during the visual stimulus time windows. An episode of escape response was determined by any successive 4 frames of accumulated distance travelled totalling at least 140 pixels (avg. 35 per frame). In contrast, freezing was represented as a ratio of time fish spent motionless (or near motionless) through movement of 2 pixels or less per frame during each passing of the visual stimulus. The distance between each fish and the moving dots was also calculated and averaged across the entire duration of each time window. Finally, the ratio of time each fish spent in the centre area of the well was calculated during each episode of visual stimulation. The centre area of the well is determined by the trajectory band of the 2 moving dots, which spans about 20 % of the well diameter plus another 10 % above and below the trajectory of the moving dots. This band is thus defined as the centre area of the well, which is about 40 % of the well diameter.

Statistical analyses, in the form of repeated measures two-way ANOVA were conducted to identify any significance for the interaction statistic which would signify affects from addition of our olfactory odourants on the behaviours in question. A secondary analysis was also conducted whereby the control responses were used as a baseline and subtracted from the behaviours quantified for each olfactory test condition. The difference between the two olfactory groups was then compared via t-test. All statistics were conducted in either Microsoft Excel or Prism 9.

3.3 Neuronal Tracing

Around 20-24 hours post fertilisation, *tg(Xla.Tubb:GCaMP3)* zebrafish larvae were placed into 75 μ M 1-phenyl 2-thiourea (PTU) in E3 solution in order to inhibit pigmentation. At 3 days post-fertilisation, larvae were immobilised in 1% agarose (made with 75 μ M PTU in E3). Microinjection of 6% Tetramethylrhodamine dextran, 10,000 MW, Lysine fixable – Fluoro Ruby (ThermoFisher) was achieved in both the eye and the optic tectum using microcapillary injection needles (Harvard Apparatus, 300038, 1 mm O.D. \times 0.78 mm I.D) with a 5-10 μ m injection tip. Larvae were subsequently removed from the agarose and returned to 75 μ M PTU

in E3 for a further 24 hours. 2-photon microscopy was then used to image expression of tetramethylrhodamine dextran across the brain.

Imaging of the expression was conducted using 2-photon microscopy on the Bergamo II system. Z-stacks were taken from the dorsal most border of the optic tectum to the ventral border of the olfactory bulbs at a resolution of 1024x1024 pixels, with slices approximately 1µm apart and 10-20 frames per slice.

Images were processed in ImageJ where all frames at the same z-plane were averaged together. Regions of interest were identified, and maximum intensity projections were calculated to show neuronal projections visualised by the injections.

3.4 2-Photon Imaging.

2-Photon microscopy was carried out across multiple experiments in both Sheffield and Singapore using 1 of the 3 following systems:

Nikon System: A*STAR Singapore.

A commercially available Nikon A1RMP upright two-photon system with a 25x water immersion objective (CFI75 Apochromat 25XC W, Nikon). Time-lapse images were collected with no delay between frames, using a resonant scanner. A single plane was recorded at 30 Hz and a resolution of 256 x 256 pixels with excitation being provided by 920 nm infrared light.

Bergamo II System, Thorlabs Inc: University of Sheffield.

Commercially available two-photon laser-scanning microscope (Bergamo II System, Thorlabs Inc., USA) based on a mode-locked laser system operating at 925 nm, 80-MHz pulse repetition rate, < 100-fs pulse width (Mai Tai HP DeepSee, Spectra-Physics, USA). Images were captured using a 60x objective, 1.1 NA (LUMFLN60XW, Olympus, Japan) using a GaAsP PMT (Hamamatsu) coupled with a 525/40 bandpass filter (FF02-525/40-25, Semrock) as described in (Faveri *et al.*, 2021). Single plane responses were recorded at 15 frames per second at a resolution of 512 x 512 pixels.

NOBIC System: Nanyang Technological University, Singapore.

A bespoke custom built 2-photon microscope (NOBIC). The system contained a 920nm and 1064nm laser (ALCOR 920-1 and ALCOR 1064-2, Spark Lasers), both used for illumination. The output beam was expanded 2-fold by a reflective beam expander (#37-193, Canopus Reflective Beam Expanders, Edmund Optics, NJ, USA). The beam was then directed into a scan engine module, which consisted of an 8-Khz resonant galvanometer scanner mirror (CRS 8 KHz, Cambridge Technology) and a galvanometer scanner (6215H, Cambridge Technology). The scanned laser beam is further expanded before passing through a long-pass dichroic mirror (BLP01-785R-35x50, Semrock) and reaching the objective lens (Zeiss objective W "Plan-Apochromat" 20x/1.0, Jena, Germany). Excited fluorescent light is collected by the same objective lens. In order to separate the two-photon emission from excitation, collected light is reflected by the long pass-dichroic mirror previously mentioned. Collected light is then separated into a two-channel, green and red, detection arrangement by a second dichroic mirror (FF562-Di03-38x45, Semrock). Light passes onto the light sensitive area of two photomultiplier tubes (PMT, H7422-20, Hamamatsu, Japan), cooled to a constant temperature of 20°C. The current signal generated by the PMTs is amplified by a variable gain transimpedance amplifier (DHPCA-100, FEMTO) and subsequently sent to a data acquisition device (vDAQ, ScanImage, Vidrio Technologies). Image acquisition was controlled by ScanImage software (Vidrio Technologies).

Spontaneous Activity Recordings (A*STAR Singapore):

10 days post-fertilisation stage *tg(elavl3:H2B-GCaMP6s)* larvae were anaesthetised with mivacurium (1.25mg/ml in E3) Fish were mounted dorsal side up in 2% low melting point agarose prepared in standard E3 solution (5 mM NaCl, 0.17 mM KCl, 0.33 mM CaCl₂, 0.33 mM MgSO₄) into a series 20 chamber (Warner Instruments). The agarose surrounding the nose of the fish was carefully removed to allow the fish to detect olfactory stimuli. Olfactory stimuli were applied using a perfusion system. Perfusion was applied throughout and switched from an E3 control to olfactory stimuli during desired periods. The stimuli presented consisted of a food-based stimulus, and the alarm substance, schreckstoff. The food-based stimulus and alarm substance were obtained as described by Kermen *et al.* (2020), and Jesuthasan *et al.* (2020), respectively. Control experiments switched from one solution of E3 to a second E3 solution. All solutions were filtered to remove all physical contaminants. Changes in the

neuronal activity in the olfactory bulbs, optic tectum and habenula were recorded using 2-photon microscopy.

2-photon imaging was carried out on the Nikon system. Each experiment began with a 10-minute period of recording spontaneous activity before the perfusion system switched from E3 to the odorant for 5 minutes. After this time, perfusion returned to E3 for a further 10 minutes of spontaneous activity recordings.

Data Analysis.

All processing steps for the recordings, including motion correction and detection of regions-of-interest (ROIs), were done using suite2p (Pachitariu *et al.*, 2017) with the ROIs subsequently manually curated to exclude neurons outside the region of the habenula. From the fluorescence signals obtained via suite2p, the corresponding $\Delta F/F$ traces were then computed (Jia *et al.*, 2011), following which discrete spikes were inferred using the MATLAB package MLspike with gCaMP6s parameters given in the paper (Denuex *et al.*, 2016). K-means clustering was conducted to identify clusters of neurons which displayed either increases or decreases in spiking activity in response to the application of our olfactory stimulus. Clusters displaying similar response profiles were concatenated across fish for each individual experimental condition (control, alarm substance and food odour). Four main clusters were identified, 1. Consistent spiking, 2. Decreased Spiking, 3. Increased Spiking, 4. Mechanosensory Responses.

For each fish, the obtained $\Delta F/F$ traces for all neurons were then averaged by three, in order to reduce the number of timepoints from approximately 45,000 to 15,000 for handling purposes. Laplacian Eigenmaps were calculated for each $\Delta F/F$ as described in (Rubin *et al.*, 2019) to provide a collective comparison of changes in neuronal activity.

Olfactory Adaptation Recordings (The University of Sheffield):

Non-anaesthetized *tg(Xla.Tubb:GCaMP3)* 4-5 days post-fertilisation stage larvae were immobilised in 3.5% low melting point agarose prepared in standard E3 solution (5 mM NaCl, 0.17 mM KCl, 0.33 mM CaCl₂, 0.33 mM MgSO₄) and mounted dorsal side up on a custom-built chamber. Fish aged 10-17 days post-fertilisation were immobilised in 3.5% low melting point

agarose prepared in oxygenated E3 solution (Bergmann *et al.*, 2018). The agarose surrounding the nose of the fish was carefully removed to allow the fish to detect olfactory stimuli. Olfactory stimuli were applied using a picospritzer set to 3psi for a duration of 3 seconds. Application was achieved through a 10 μ m diameter glass pipette. The stimuli presented consisted of an E3 control, a food-based stimulus, and the alarm substance, schreckstoff. The food-based stimulus and alarm substance were obtained as described in Kermen *et al.* (2020), and Jesuthasan *et al.* (2020), respectively. The chamber also contained a metal inlet pipe which was utilised for application of 2ml 5mM pentylenetetrazol (Sun *et al.*, 2019) using a syringe pump. All solutions were filtered to remove all physical contaminants and applied anterior to the nose of the fish to minimise mechanosensory stimulation. Changes in the neuronal activity in the olfactory bulbs and telencephalon were recorded using 2-photon microscopy.

2-photon imaging of olfactory responses was conducted using the Bergamo II system. Single plane responses were recorded at 15 frames per second at a resolution of 512 x 512 pixels. Each experiment began with a 30-second base line fluorescence recording before the first presentation of the odorant was applied with a further 30 seconds interval between subsequent presentations.

Data Analysis.

Raw data files obtained from 2-photon imaging were analysed using SARFIA (Dorostkar *et al.*, 2010) and custom-written scripts for Igor Pro (WaveMetrics, Lake Oswego, OR, USA) as described in (Bergmann *et al.*, 2018). Before the analysis, images were registered using TurboReg (Thévanaz *et al.*, 1998) for ImageJ to remove motion artefacts and every 5 frames were averaged to reduce noise artefacts. The forebrain was then split through the midline so analysis could be conducted separately for the left and right side of the brain and improve ease of data handling. Analysis was performed on a voxel-wise basis, with response dynamics of individual voxels being normalised and olfactory responsive traces selected by calculating the skewness of the distribution curve. Traces with a skewness > 1.0 were regarded as responding based on work described in (Bergmann *et al.*, 2018). To categorise the different response types, all responding traces were re-organised based on their similarity to one

another based on the similarity index (Pearson coefficient) and then every 5-10th trace was manually sorted into categories based on their response shape.

To avoid bias resulting from manual sorting, registered files were also analysed using an advanced region of interest (ROI) detection plugin (Johnston *et al.*, 2019) for Igor Pro (WaveMetrics, Lake Oswego, OR, USA), code and manual available at <https://github.com/JohnstonLab/Igor-ROI-tools>. The script identified ROIs which showed similar patterns of calcium activity across neighbouring voxels. The response traces for voxels within each region were averaged to create a response trace for that ROI. All ROIs were then manually sorted based on the form of short-term sensory plasticity they exhibited or sorted via adaptation index. The amplitude of responses was defined by calculating the difference between the baseline and highest peak of each response. Adaptation index (AI), defined via the below equation:

$$AI = \frac{\text{Amplitude of Response 1} - \text{Amplitude of Response 5}}{\text{Amplitude of Response 1} + \text{Amplitude of Response 5}}$$

was then calculated to give a resultant value between -1 and 1. All traces with an AI between 0.2 and -0.2 were classified as non-adapting, greater than 0.2 were classified as depressing and those lower than -0.2 were classified as sensitising.

Statistical Analysis.

Statistical analysis was performed using IgorPro version 6.3. All average traces are shown as mean \pm S.E.M. Differences in adaptation index between response types and before and after PTZ application were analysed using two-tailed Wilcoxon rank-sum test. Data before and after drug application were considered independent. The non-normal distribution of adaptation indices is shown and validated through the Jarque-Bera test. Data collection was not performed blind to the conditions of the experiment, but the analysis was performed automatically using a set of custom-made scripts for IgorPro to remove potential human bias at all necessary stages. As well as full datasets, we performed analysis on subsets of data

through which every 'nth' trace was selected from across all fish to reduce the sample size and make datasets more manageable.

Effect of Olfaction on Visual Adaptation (The University of Sheffield):

Non-anaesthetized 8-13 days post-fertilisation stage *tg(Xla.Tubb:GCaMP3)* larvae were immobilised in 3.5% low melting point agarose prepared in oxygenated E3 solution (Bergmann *et al.*, 2018) and mounted dorsal side up on a custom built chamber. The agarose surrounding the nose of the fish was carefully removed to allow the fish to detect olfactory stimuli. Olfactory stimuli were applied using a picospritzer set to 3psi for a duration of 3 seconds. Application was achieved through a 10 μ m diameter glass pipette. The stimuli presented was a food-based stimulus, obtained as described in (Kermen *et al.*, 2020). All solutions were filtered to remove all physical contaminants and applied anterior to the nose of the fish to minimise mechanosensory stimulation. Visual stimuli were generated using custom-written code for MATLAB (MathWorks, Natick, MA, USA) with the Psychophysics Toolbox [33–35] using an Optoma PK320 projector connected to a Linux laptop. Projections were made onto the side of the imaging chamber across the visual field of the left eye (dimensions restricted to - 90 mm (W) \times 15 mm (H) due to working distance of the objective). The eye-to-screen distance was 1.3cm.

Imaging of neuronal responses was conducted using a two-photon laser-scanning microscope (Bergamo II System, Thorlabs Inc., USA) based on a mode-locked laser system operating at 925 nm, 80-MHz pulse repetition rate, < 100-fs pulse width (Mai Tai HP DeepSee, Spectra-Physics, USA). Images were captured using a 60 \times objective, 1.1 NA (LUMFLN60XW, Olympus, Japan) using a GaAsp PMT (Hamamatsu) coupled with a 525/40 bandpass filter (FF02-525/40-25, Semrock) as described in (Faveri *et al.*, 2021). Single plane responses were recorded at 15 frames per second at a resolution of 512 x 512 pixels. Each experiment began with a 30-second baseline fluorescence recording before the first presentation of the moving ball began. One single pass of the moving ball lasted 7 seconds, equating to 28 seconds per set of repeats. A 30-second stimulus free gap was present between each set of repeats. No olfactory stimulation was applied in control experiments. In test experiments, food odour was applied anterior to the nose of the fish at the start of repeats 6 through 10.

Data Analysis.

Raw data files obtained from 2-photon imaging were analysed using SARFIA (Dorostkar *et al.*, 2010) and custom written scripts for Igor Pro (WaveMetrics, Lake Oswego, OR, USA) as described in (Bergmann *et al.*, 2018). Before the analysis, images were registered using TurboReg (Thévanaz *et al.*, 1998) for ImageJ to remove motion artefacts and every 5 frames were averaged to reduce noise artefacts. The forebrain was then split through the midline so analysis could be conducted separately for the left and right sides of the brain and improve the ease of data handling. Analysis was performed on a voxel-wise basis, with response dynamics of individual voxels being normalised and olfactory responsive traces selected by calculating the skewness of the distribution curve. Traces with a skewness > 1.0 were regarded as responding based on work conducted previously in the lab demonstrated in (Bergmann *et al.*, 2018). Responding traces were concatenated into one dataset for control and one dataset for test fish. The same was conducted for positional information.

Responses for repeats 4 + 5 and repeats 6 + 7 were combined and averaged to calculate the overall response in this epoch. The amplitude of responses was defined by calculating the difference between the baseline and highest peak of each pass of the visual stimulus. Adaptation index (AI), defined via the below equation, was then calculated to give a resultant value between -1 and 1 for each epoch.

$$AI = \frac{\textit{Amplitude of Pass 1 Response} - \textit{Amplitude of Pass 4 Response}}{\textit{Amplitude of Pass 1 Response} + \textit{Amplitude of Pass 4 Response}}$$

Responses located within the first third, middle third and final third of the Y axis were separated and analysed separately to further identify positional variation amongst our data.

Statistical Analysis.

Statistical analysis was performed using IgorPro version 6.3. All average traces are shown as mean \pm SEM. Differences in adaptation index between response types before and after PTZ application were analysed using a two-tailed Wilcoxon rank-sum test. Data before and after drug application were considered independent. The non-normal distribution of adaptation index is shown and validated through the Jarque-Bera test. Data collection was not

performed blind to the conditions of the experiment, but the analysis was performed automatically using a set of custom-made scripts for IgorPro to remove potential human bias at all necessary stages. As well as full datasets, we performed analysis on subsets of data through which every 'nth' trace was selected from across all fish to reduce the sample size and make datasets more manageable.

Visual Responses in the Olfactory Bulbs.

Non-anaesthetized *tg(Xla.Tubb:GCaMP3)* 8-13days post-fertilisation larvae were immobilised in 3.5% low melting point agarose prepared in oxygenated E3 solution (Bergmann *et al.*, 2018) and mounted dorsal side up on a custom built chamber. The agarose surrounding the nose of the fish was carefully removed to allow the fish to detect olfactory stimuli. Olfactory stimuli were applied using a picospritzer set to 3Psi for a duration of 3 seconds. Application was achieved through a 10 μ m diameter glass pipette. The stimuli presented was a food-based stimulus, obtained as described in Kermen *et al.* (2020). All solutions were filtered to remove all physical contaminants and applied anterior to the nose of the fish to minimise mechanosensory stimulation. Visual stimuli were generated using custom-written code for MATLAB (MathWorks, Natick, MA, USA) with the Psychophysics Toolbox [33–35] using an Optoma PK320 projector connected to a Linux laptop. Projections were made onto the side of the imaging chamber across the visual field of the left eye (dimensions restricted to - 90 mm (W) \times 15 mm (H) due to working distance of the objective). The eye to screen distance was 1.3cm.

2-photon imaging of neuronal responses was conducted using the Bergamo II system. Each experiment began with a 30-second baseline fluorescence recording before the first presentation of the moving ball began. One single pass of the moving ball lasted 7 seconds, equating to 28 seconds per set of repeats. A 30-second stimulus free gap was present between each set of repeats. In test experiments where food odour was applied anterior to the nose of the fish, an additional 30 second gap was inserted between repeats 5 and 6 of the moving ball during which odour was applied.

Data Analysis.

Raw data files obtained from 2-photon imaging were analysed using SARFIA (Dorostkar *et al.*, 2010) and custom-written scripts for Igor Pro (WaveMetrics, Lake Oswego, OR, USA) as described in (Bergmann *et al.*, 2018). Before the analysis, images were registered using TurboReg (Thévanaz *et al.*, 1998) for ImageJ to remove motion artefacts and averaged by 5 to reduce noise artefacts. To avoid bias resulting from manual sorting, registered files were also analysed using the advanced ROI detection plugin (Johnston *et al.*, 2019) for Igor Pro (WaveMetrics, Lake Oswego, OR, USA), code and manual available at <https://github.com/JohnstonLab/Igor-ROI-tools>. The script identified ROIs which showed similar patterns of calcium activity across neighbouring voxels. The response traces for voxels within each region were averaged to create a response trace for that ROI. All subsequent ROIs were concatenated into a single dataset and averaged to create average response traces used in figures.

Statistical Analysis.

Statistical analysis was performed using IgorPro version 6.3. All average traces are shown as mean \pm SEM. Data collection was not performed blind to the conditions of the experiment, but analysis was performed automatically using a set of custom-made scripts for IgorPro to remove potential human bias at all necessary stages.

Imaging of Astrocyte-Neuron Interactions

Creation of *tq(slca1a3b:jRGECO1a)*.

The *slca1a3b:jRGECO* plasmid was made following standard gateway cloning protocol (Katzen, 2007). Previous reactions in the lab had already formed p3e polyA tail and p5e *slca1a3b*. This meant it was just required to construct our pMe *jRGECO1a* and conduct the LR reaction to combine the constituents into a single pDONR.

To begin formation of pMe *jRGECO1a*, high-fidelity PCR was run using the reagents shown in table 1 below, one reaction Phusion high fidelity PCR kit (E0553, New England Biolabs) and the other containing the ThermoFisher equivalent (F531L, Thermo Scientific). 35 PCR cycles were completed at annealing temperatures of 56°C.

Table 3.1: *jRGECO1a* attb High Fidelity PCR

Buffer	5 μ l (NEB)	5 μ l (Thermo)
Forward Primer	0.5 μ l	0.5 μ l
Reverse Primer	0.5 μ l	0.5 μ l
dNTPs	0.5 μ l	0.5 μ l
Phusion HF DNA Polymerase	0.25 μ l	0.25 μ l
Template (25ng/ μ l)	1 μ l	1 μ l
MilliQ	17.25 μ l	17.25 μ l

The jRGECO1a attb construct is 1479bp in size. I then used gel electrophoresis to confirm our PCR product was the same size as the expected jRGECO1a attb construct. The sample was run for 25 minutes at 150V in a 1% LMP agarose gel made with 50ml TAE Buffer (Cat#B49, Thermo Scientific), containing 1ul GelStar(Cat#50535, Lonza).

Figure 3.1: jRGECO1a attb High Fidelity PCR

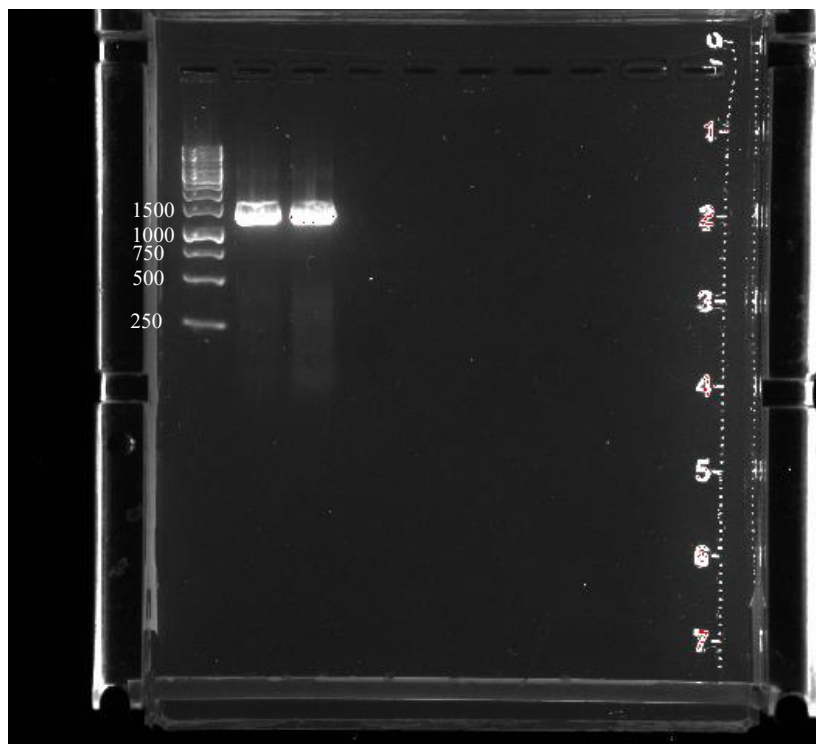
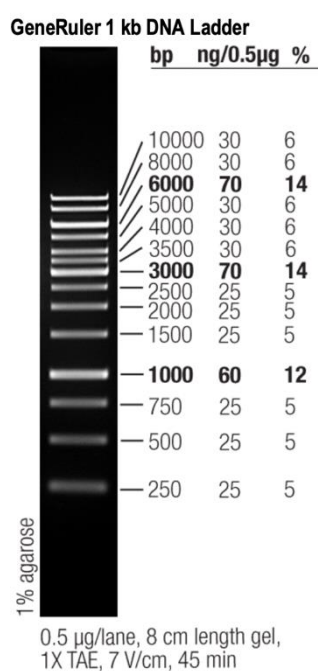


Figure 3.1: *jRGECO1a attb* high fidelity PCR results. (A) GeneRuler 1kb DNA Ladder band sizes when run in 1% agarose. (B) High fidelity PCR result for detection of *jRGECO1a attb* construct. Lane 1 contained GeneRuler 1kb ladder. The construct is 1479bp in length and we detected bands just below 1500bp on the gel in both lanes 2 and 3 where the sample was loaded.

The bands in both lanes 2 and 3 were the correct size for our construct so I proceeded with DNA purification (28104, QIAGEN) and obtained a concentration of 46.5ng/μl. To now finalise the pME *jRGECO1a*, the BP reaction had to now be conducted whereby the *jRGECO1a attb* PCR product was inserted into a donor vector containing the bacterial resistance gene kanamycin. The reagents described in table 2 were added to a PCR tube, mixed, and left at room temperature for 15 hours.

Table 3.2: BP Reaction

Attb-PCR product (50fmol)	1.06μl
pDONR vector (50fmol)	1μl
5x BP clonase enzyme mix	2μl
TE Buffer, pH 8.0	5.94μl

After 15 hours, 1μl of proteinase K was added and incubated for 10 minutes at 37 degrees to end the reaction. The BP reaction product could then be transformed into chemically competent DH5 alpha cells. 1μl of the BP product was added to 50μl of cells, with some gentle mixing and placed on ice for 30 minutes. The cells were then heat shocked at 42°C in a water bath for exactly 30 seconds and returned to the ice for a final 5 minutes. 950μl of SOC medium (15544034, Invitrogen) was added to the cells, and these were then incubated on a shaker at 37 degrees for 2 hours. Cells were then spread on an LB broth agar plate containing kanamycin and incubated overnight to allow colonies which had successfully transformed to grow. The next day, 8 isolated colonies were selected from the agar plate and added to the PCR reagents listed below in table 3 to identify pDONR *jRGECO1a* positive colonies.

Table 3.3: BP Reaction Colony PCR

10x Taq Buffer	2μl
dNTPs	0.5μl
Forward Primer	1μl
Reverse Primer	1μl
MgCl ₂	2μl

DNA Pol	0.1 μ l
Template (colony)	1 μ l
MilliQ	12.4 μ l

The PCR ran for 34 cycles with annealing temperature of 55°C after completion, gel electrophoresis was again conducted on the PCR products. The construct tested for was a 250bp region that span across pDONR and jRGECO1a and all 8 samples were positive for this band size as shown in the gel below.

Figure 3.2: Colony PCR Identified Multiple jRGECO1a positive colonies.

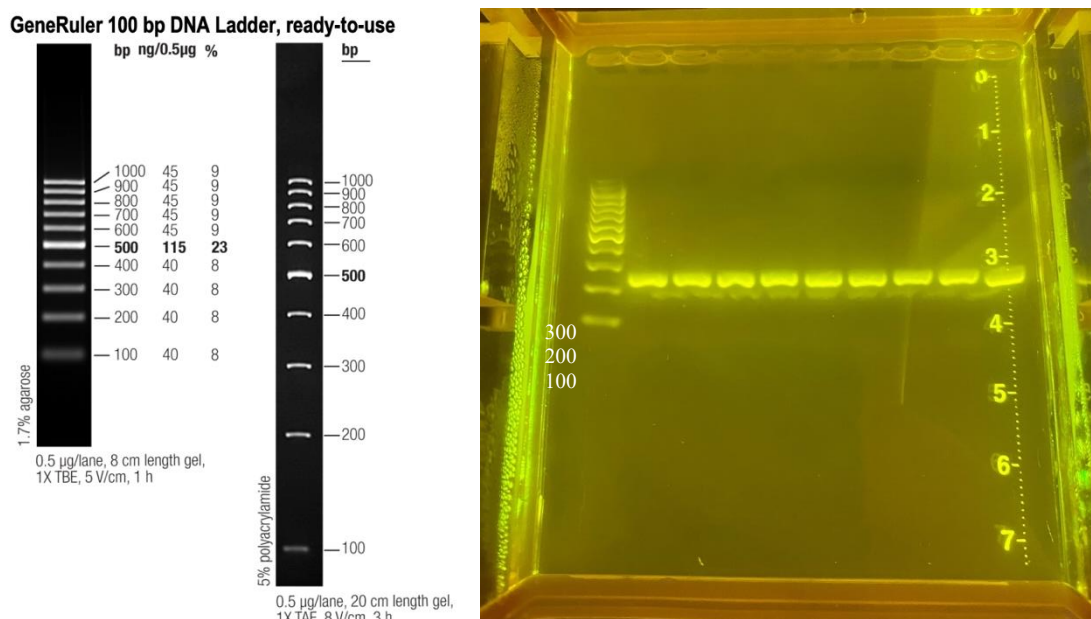


Figure 3.2: Colony PCR Identified Multiple jRGECO1a positive colonies. (A) GeneRuler 100bp DNA Ladder band sizes when run in 1.7% agarose and 5% polyacrylamide. (B) PCR results testing for presence of 250bp region which span across the junction of pDONR and jRGECO1a. 9 colonies were selected and ran through the PCR. All 9 returned positive bands around 250bp (lanes 2-10).

Once again, the DNA in the positive lanes was purified following the Qiagen DNA purification protocol and sent for sequencing to confirm jRGECO1a was present. The final step was to now conduct the LR reaction and combine the 3' entry, middle entry and 5' entry plasmids in a new destination vector. As the size of the LR reaction product will be greater than 10kb, it was essential to linearise the destination vector before conducting the LR reaction. This was done by using EcoRI as it had a single cut site, thus linearising the plasmid to aid with

integration. The LR reaction reagents (shown in table 4 below) were added to PCR tubes, mixed well, and left at room temperature for 15 hours. Like with the BP reaction, proteinase K was added and incubated at 37 degrees for 10 minutes to end the reaction.

Table 3.4: LR Reaction

$$\frac{(\text{concentration in ng}/\mu\text{l})}{(660 \text{ g/mol} \times \text{average library size in bp})} \times 10^6 = \text{concentration in nM}$$

Reagent	Size	Resultant DNA Required
10fmol of P3e PolyA	2838bp	18.73ng
10fmol of PMe jRGECO1a	3965bp	26.17ng
10fmol of P5e Slc1a3b	12357bp	81.56ng
20fmol of pDestTol2_CryV	7426bp	98.03ng

P3e Poly A (18.73ng)	1μl
PMe jRGECO1a (26.17ng)	1μl
P5e Slc1a3b (81.56ng)	1μl
pDestTol2_CryV (98.03ng)	1μl
LR Clonase	2μl
TE Buffer	4μl

1μl of the LR reaction product was then added to 50μl of DH5 alpha cells and transformation was carried out in the same manner as for the BP reaction. Cells were incubated on a shaker at 37 degrees and then spread onto LB broth agar plates with Ampicillin and incubated overnight. The next day, 8 isolated colonies were selected from the agar plate and added to the PCR reagents listed below in table 5 to identify colonies which were positive for all 3 plasmids. Primers were designed and ordered which span across the vector and promoter, as well as slc1a3b and jRGECO1a and jRGECO1a to the vector.

Table 3.5: LR Reaction Colony PCR.

Reagents	Per Tube	Total Required
10x Taq Buffer	2μl	17μl
dNTPs	0.5μl	4.25μl
Forward Primer	1μl	8.5μl
Reverse Primer	1μl	8.5μl
MgCl ₂	2μl	17μl
DNA Pol	0.1μl	0.85μl
Template (colony)	1μl	8.5μl

MilliQ	12.4µl	105.4µl
--------	--------	---------

Gel electrophoresis was once again used to confirm the positive colonies from the PCR. The sample was run for 25 minutes at 150V in a 1% LMP agarose gel made with 100ml TAE Buffer, containing 2µl GelStar. The expected band sizes are listed on the gel image below which displays positive bands for samples 3,5,and 7 for two of the three sets of primers. As a result, these three colonies were mini-prepped (27106X4, QIAGEN) to increase the concentration of DNA to at least 1mg/ml.

Figure 3.3: LR Reaction Colony PCR Identified 2 positive colonies for *slc1a3b:jRGECO1a*.

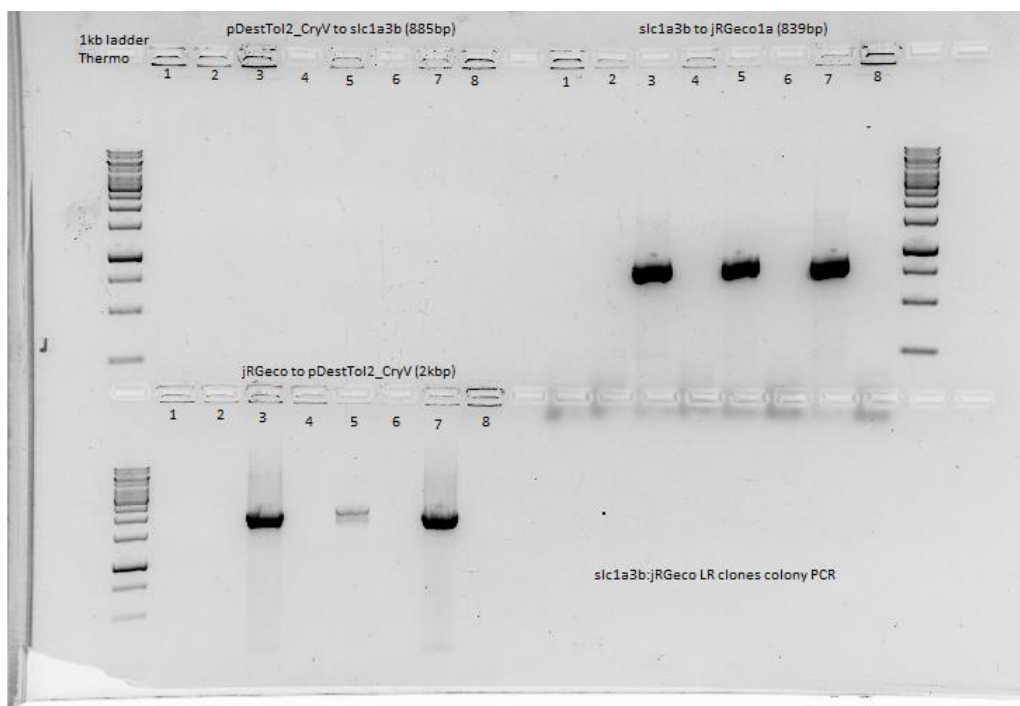
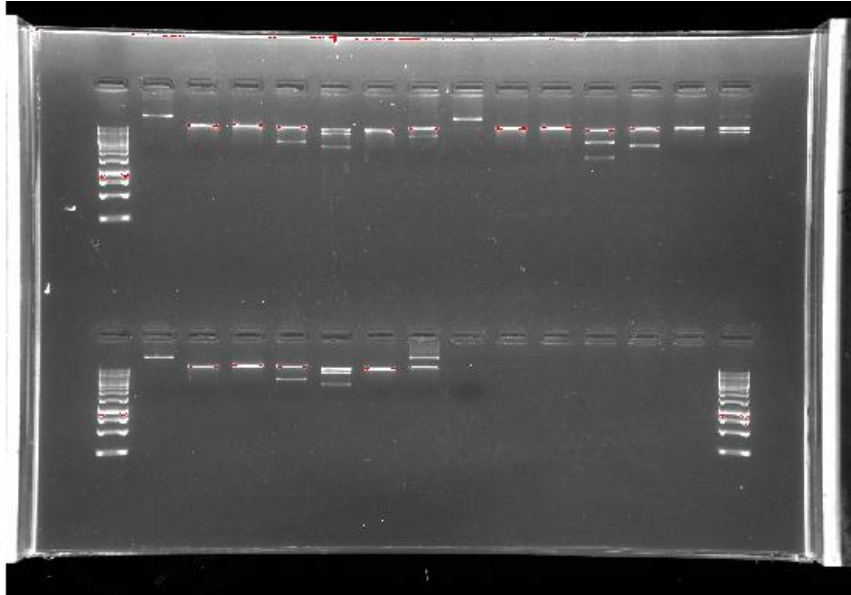


Figure 3.3: LR reaction colony PCR identified 3 positive colonies for *slc1a3b:jRGECO1a*. 8 bacterial colonies were selected from the agar plate and 3 separate PCR reactions ran on each colony. Reaction 1 tested for the presence of an 885bp region spanning across *pDestTol2* to the *slc1a3b* promoter. No colonies displayed a band for this region suggesting the primers were perhaps not functioning. The second PCR tested for presence of an 839bp region across the *slc1a3b* promoter onto *jRGECO1a* in which 3 lanes displayed a band of the correct size – lanes 3,5 and 7. The final reaction looked to identify a region between *jRGECO1a* to the *pDestTol2* which was approximately 2kbp in length. The same 3 wells identified a band of the correct size.

A restriction digest was then conducted on the miniprep DNA as a final confirmation that all constituents of the final plasmid were present. This data concludes that samples 3, 5 and

7 from the LR reaction colony PCR are all positive for our desired *slc1a3b:jRGECO1a* construct, the full map for which is displayed below.

Figure 3.4: Restriction Digest Gel Confirmation for *slc1a3b:jRGECO1a*.



*Figure 3.4: Restriction Digest Gel Confirmation for *slc1a3b:jRGECO1a*. Restriction digest of our complete plasmid confirmed correct sequencing. Each of the 3 samples were digested with a series of enzymes to test for correct sequencing. For each sample, the following was expected: Lane 1- ladder; Lane 2- Linearised (*EcoRI*); Lane 3- Linearised (*EcoRV*); Lane 4- 2 bands (*NdeI*), Lane 5- 2 bands (*SphI*), Lane 6- 1 band (*SalI*) and Lane 7- 2 bands (*NcoI*). Banding from the ladder was not optimal to calculate the size of each band but the comparison between expected values and the position along the gel compared to other bands present correlated as expected.*

Figure 3.5: Slc1a3b:jRGECO1a Plasmid Map

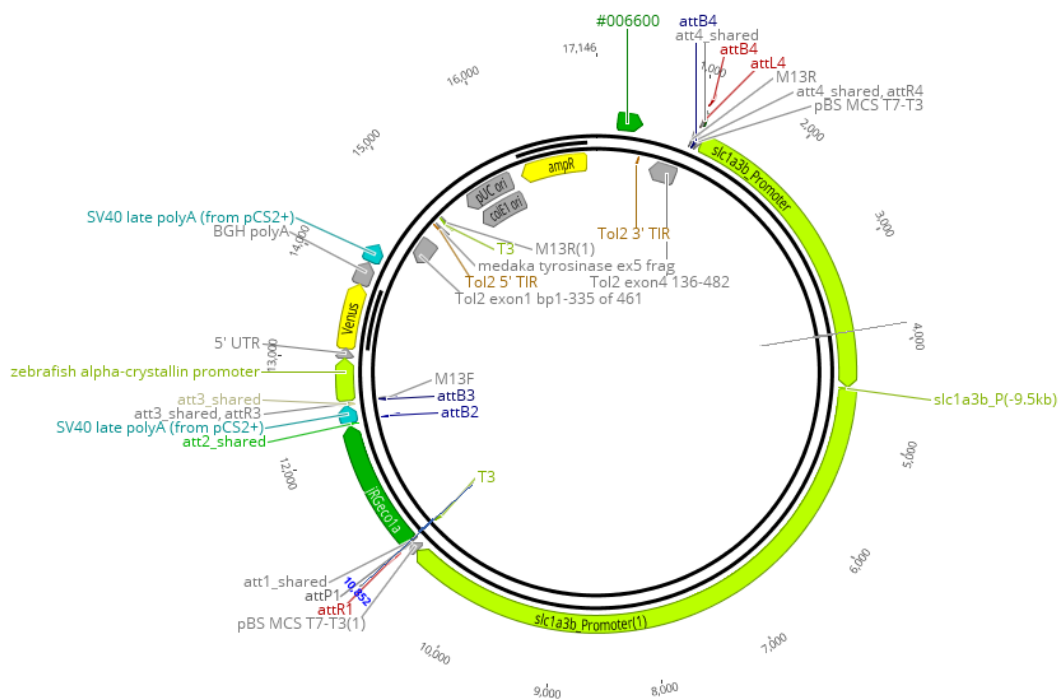


Figure 3.5: *Slc1a3b:jRGECO1a* Plasmid Map. The final *slc1a3b:jRGECO1a* construct had a total length of 17,146bp, comprising of *jRGECO1a* bound to the *slc1a3b* promoter, polyA tail and *tol2*.

Injection of *slc1a3b:jRGECO1a* into 1-cell stage embryos.

Fertilised nacre 1 cell stage embryos were injected with 75ng concentration of *slc1a3b:jRGECO* in accordance with protocols described in (Culp *et al.*, 1991). In addition to nacre embryos, the plasmid was also injected into 10days post-fertilisation *Tg(elavl3:H2B-GCaMP6s)* to create a double transgenic line in which neuronal calcium activity could be measured with GCaMP and astrocytic calcium activity measured with *jRGECO1a*.

2-Photon imaging of *slc1a3b:jRGECO1a* larvae.

Live imaging was performed using the NOBIC custom built 2-Photon microscope. *Tg(elavl3:H2B-GCaMP6s);Tg(slca3b:jRGECO)* 10 days post-fertilisation stage larvae were anaesthetised with mivacurium (1.25mg/ml in E3) Fish were mounted dorsal side up in 2% low melting point agarose prepared in standard E3 solution (5 mM NaCl, 0.17 mM KCl, 0.33 mM CaCl₂, 0.33 mM MgSO₄) into a series 20 chamber (Warner Instruments). The agarose surrounding the nose of the fish was carefully removed to allow the fish to detect olfactory stimuli. Food odour olfactory stimuli, obtained as described in Kermen *et al*, 2019 , was

applied using a perfusion system. Resultant calcium changes in astrocyte and neuronal activity in the optic tectum were then measured using our 2-photon microscope.

Data recordings were opened in ImageJ and the individual z-axis profile plotted for astrocytes across the optic tectum. Response traces for astrocytes which displayed activity a result of olfactory stimulation were transferred into IgorPro. Regions of neuronal activity were extracted based on estimates calculated from the direction of projections from that astrocyte. Regions of neuronal and astrocytic activity were then directly compared to look for similarities in their calcium activity during olfactory stimulation.

Results

4.1 Behaviour Assay

Work in the existing literature had shown that the input from the visual system was able to change olfactory perception (Morrot *et al.*, 2001). Additionally, evidence has shown that olfactory input can aid visual processing (Seigneuric *et al.*, 2010a, Zhou *et al.*, 2010, Kuang and Zhang, 2014) but whether it can completely change perception was not clear.

In our experiment, we wanted to utilise a dot that would be visually ambiguous, such that 50% of the time it would cause escape responses and 50% of the time trigger hunting behaviour. By then adding in an olfactory stimulus, we hoped to be able to alter the way this moving dot was perceived by the fish, such that if food odour was added the fish would demonstrate increased hunting behaviour towards the dot whereas in the presence of alarm substance, more avoidance behaviour would be seen (figure 4.1.1).

Figure 4.1.1: Experimental Design for Visual Perception Behaviour Test.

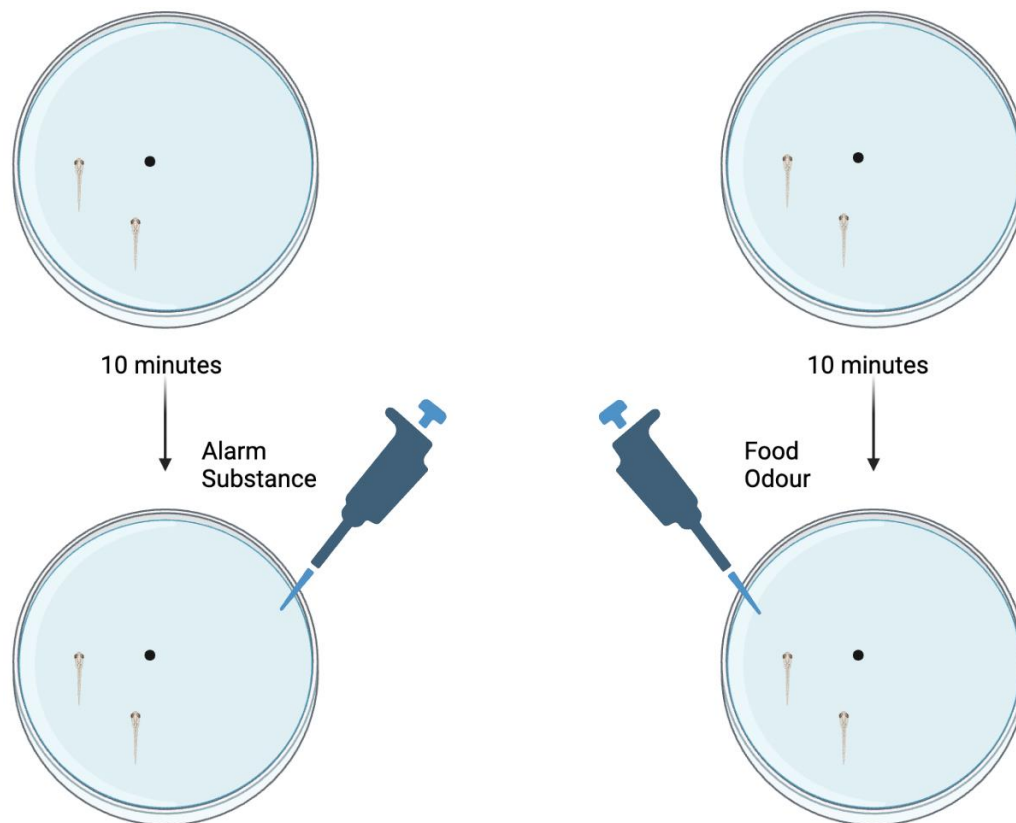


Figure 4.1.1: Experimental design for visual perception behaviour test. 2 fish were added into the imaging chamber and allowed time to acclimatise to their new environment. Visual stimulation then began with their behaviour tracked by a Basler USB3 acA1440-220um camera. After experimentation, olfactory stimuli were added in an attempt to alter the way the visual stimulus was perceived. A total of 40 fish were recorded and analysed for the alarm substance dataset and a total of 40 fish were also tested with food odorant. Figure made at Biorender.com.

After all data was collected, various parameters were then compared between the datasets. To quantify the amount of hunting or avoidance behaviour, we calculated: 1. Time spent in the centre of the dish (where the visual stimulus would present); 2. Distance (in pixels) to the moving visual stimulus; 3. Angle of the tail and 4. Angle of the eyes. The time spent in the centre of the dish and the distance to the visual stimulus provided an indicator for whether the fish was tracking the moving dot as a sign of hunting behaviour. In contrast to this, large angle tail movements were used as an indicator that fish was demonstrating avoidance behaviour whilst the angle of the eyes provided robust evidence of hunting behaviour. When zebrafish are hunting, it has been shown the eyes converge before striking for prey. In addition to this, we also monitored the number of frames where the fish were stationary or frozen. The alarm substance evokes freezing behaviour in larval zebrafish, so an additional minute was left after application to the dish to allow for freezing behaviour to subside. This

freezing data was compared between fish exposed to the alarm substance and food odour to ensure no statistically significant differences in other data could be due to increased freezing in fish exposed to the alarm substance (Figure 4.1.2). Repeated measures two-way ANOVA was conducted, and the results demonstrated addition of the odorants had no effect on freezing behaviour (interaction $p = 0.78$).

Figure 4.1.2: Fish Exposed to Alarm Substance and Food Odour Showed No Difference in Freezing Behaviour.

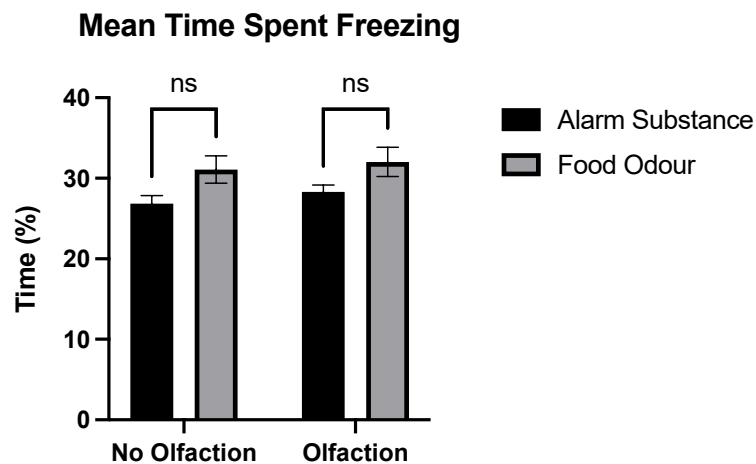


Figure 4.1.2: Fish Exposed to Alarm Substance and Food Odour Showed No Difference in Freezing Behaviour. 'Freezing' was classified as a fish moving not moving by any pixels in a single frame.). After the alarm substance was added, approximately a 2-minute period was allowed for freezing behaviour to subside before beginning the experiment. Repeated measures two-way ANOVA displayed no significant differences ($p=0.78$) in the amount of freezing displayed after addition of the olfactory stimuli (black = alarm substance, grey = food odour). Bars on graph represent mean \pm SEM. $N= 26$ fish.

We then progressed with analysing the percentage of time spent in the central portion of the imaging chamber and the mean distance to the moving visual stimulus ball. Here we hypothesised that the presence of food odour would have evoked more hunting behaviour towards the visual stimulus. This would present itself as increased tracking of the visual stimulus, thus more time spent in the centre of the chamber and a decreased distance to the ball in comparison to fish exposed to the alarm substance. The alarm substance exposed fish would perceive the ball as a potential threat and thus would have demonstrated a decreased amount of time in the centre of the chamber and a greater distance to the ball. Our repeated

measures two-way ANOVA identified a statistically significant difference for the interaction statistics between the two odourant groups when analysing the mean distance to the visual stimulus ($p = 0.0469$). The same statistical test also showed that fish exposed to the alarm substance spent a significantly reduced amount of time in the central part of the imaging chamber compared to the food odour exposed fish ($p=0.0165$). Fish treated with alarm substance spent 35.2% ($\pm 3.7\%$) of the time the stimulus was present in the centre of the imaging chamber, with a mean distance of 314 (± 6) pixels to the visual stimulus. Fish treated with the food odourant spent 51.5% ($\pm 4.7\%$) of the time when the stimulus was active in the centre of the chamber with an average distance of 272 (± 7) pixels to the stimulus.

Figure 4.1.3: Fish Exposed to Food Odorant Showed More Exploration Towards the Visual Stimulus.

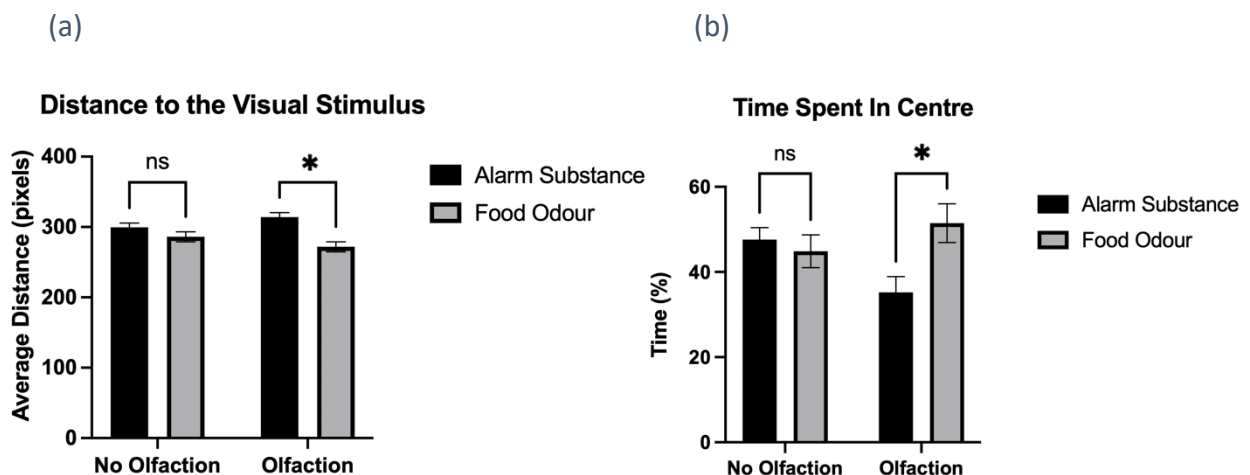


Figure 4.1.3: Fish Exposed to Food Odorant Showed More Exploration Towards the Visual Stimulus. (A) Fish exposed to the alarm substance (black bars) maintained a mean distance of 314 (± 6) pixels away from the visual stimulus. In comparison, the fish exposed to the food odorant (grey bars), swam closer to the visual stimulus – mean distance 272 (± 7) pixels (repeated measures two way ANOVA, interaction p value = 0.0469. Post-hoc test, $p=0.0001$ - Šidák's correction for multiple comparisons). Bars on graph represent mean \pm SEM. (B) Fish exposed to the food odorant (green trace) also showed an increased percentage of time spent in the central portion of the imaging chamber, where the visual stimulus would present (repeated measures two way ANOVA, interaction p value = 0.0165). Fish exposed to the food odour resided in this region for 51.5% ($\pm 4.7\%$) of the experiment, compared to just 35.2% (3.7%) in fish exposed to the alarm substance (post-hoc test, $p=0.0062$ - Šidák's correction for multiple comparisons). Bars on graph represent mean \pm SEM. $N=26$ fish for each condition.

In addition to positional information, using DeepLabCut we were also able to track the convergence of the eyes and angle of the tail during periods of the visual stimulation. If the moving dot was greater than 275 pixels away from the fish, the tracking information from the eyes and the tail was considered as not due to the visual stimulus and thus not analysed. For frames considered suitable to be analysed for responses to the visual stimulus, the amount of time spent with the eyes converged of convergences and J-bends was calculated for each fish. Our data showed that the average time spent with the eyes converged in response to the moving ball when treated with food odour was greater than when fish were exposed to the alarm substance (11.17 (+/- 0.94) seconds vs 8.19 (+/-0.81) seconds but this difference was not significant when compared on a repeated measures two-way ANOVA (interaction statistic - $p = 0.23$). In addition to the ANOVA, the baseline responses from the two control groups were subtracted from the number of events under the olfactory conditions to calculate the change in eye convergences and C-turns as a result of the olfactory stimulus. The resultant data was compared via unpaired t-test but again showed no significant change in vergence events. Food odour = +0.98 seconds +/- 1.08, Alarm substance = -0.91 seconds +/- 1.12. $p=0.11$).

Figure 4.1.4: Fish Exposed to Different Odourants Demonstrated No Significant Change in Eye Convergence.

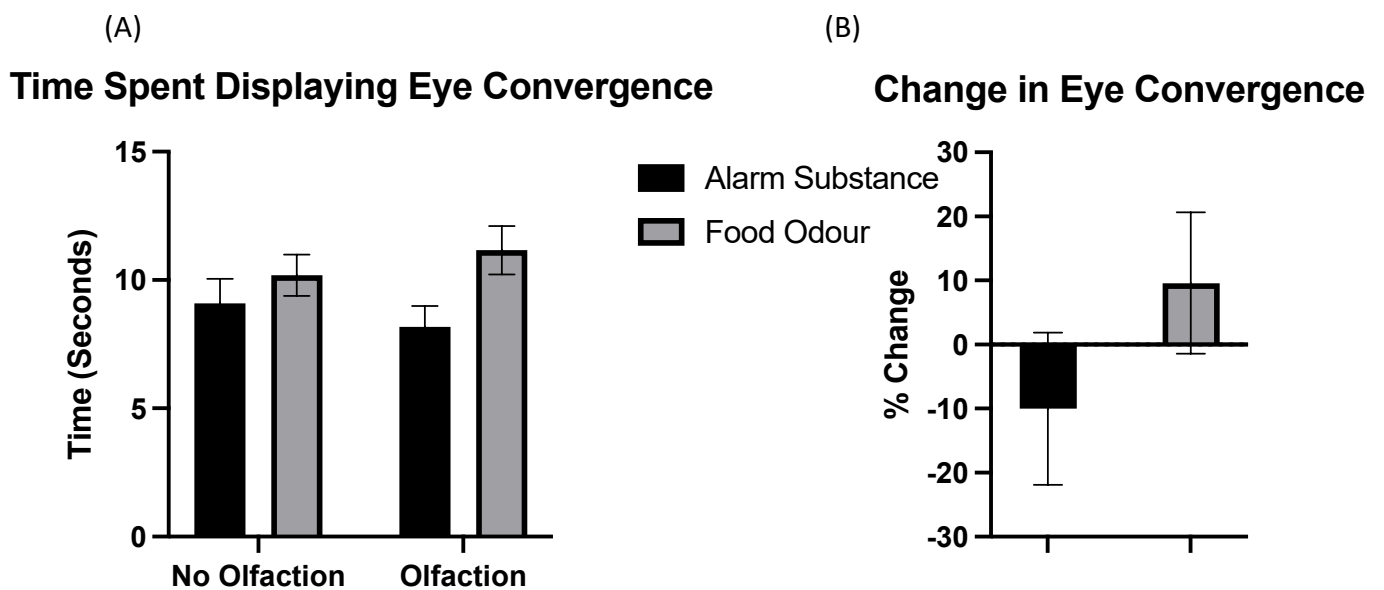


Figure 4.1.4: Fish Exposed to Different Odorants Demonstrated No Significant Change in Eye Convergence. Control groups for both alarm substance (black bars) and food odour (grey bars) treated fish displayed equal rates of eye convergence ($p=0.6188$). After addition of the odorants, fish exposed to the food odorant showed a slight increase in the average time spent with their eyes converged whilst the fish exposed to the alarm substance demonstrated a slight decrease. This difference was not significant for the interaction statistic in the RM-Two Way ANOVA ($p=0.23$). Bars on graph represent mean \pm SEM. ($N=26$ fish for each condition). (B) Data was also analysed by subtraction of the time spent displaying eye convergence in the controls from the olfactory conditions. The resultant data was tested for statistical significance via t-test (Food odour = $+0.98$ seconds \pm 1.08, Alarm substance = -0.91 seconds \pm 1.12. $p=0.11$). Bars on graph represent mean \pm SEM. $N=26$ fish for each condition.

Our final comparison allowed for quantification of high degree c-turns in response to the moving stimulus. These high angle turns would be seen as a redirection in response to the presence of the moving ball and could therefore be considered as an aversive response. Statistical analysis was conducted in the same way as for the eye convergence data. The repeated measures two-way ANOVA showed there was no significant changes in the number of aversive C-turns made under both conditions ($p=0.21$). Subtraction of the baseline turn events from the control conditions showed no change in the presence of food odour and a small decrease in the number of high angle turns in the presence of the alarm substance (-0.14 seconds \pm 0.06), but this was non-significant ($p=0.10$).

Figure 4.1.5: Treatment of Food Odour or Alarm Substance Had No Effect on the Number of High-Angle Turns Made.

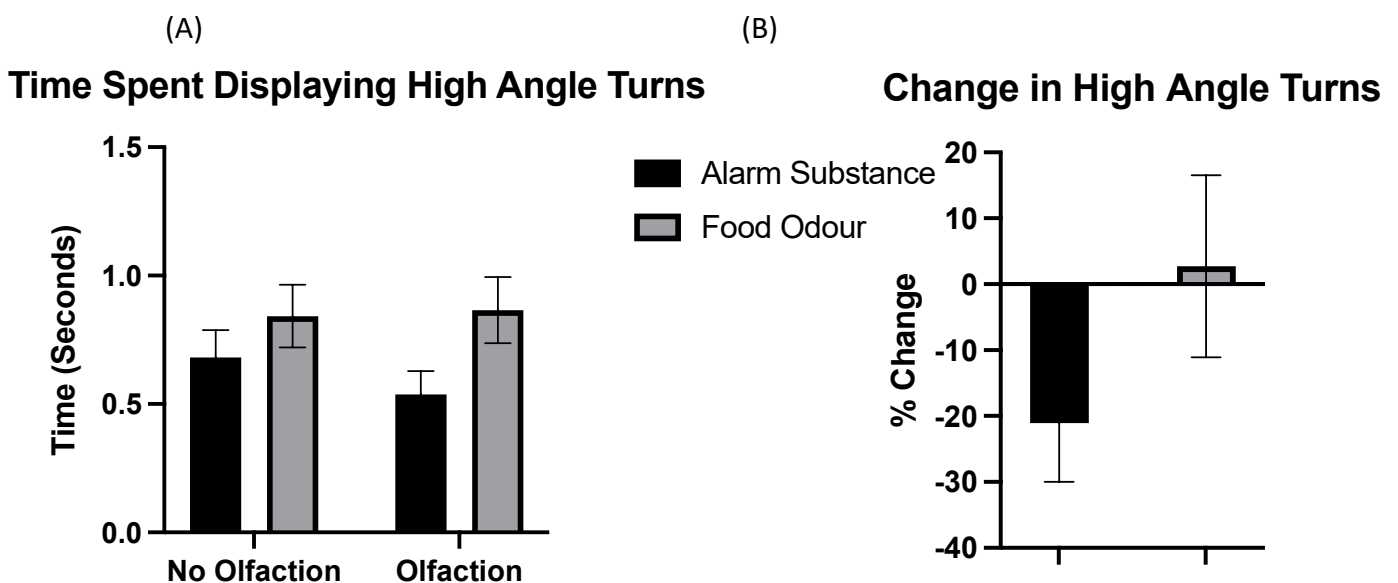


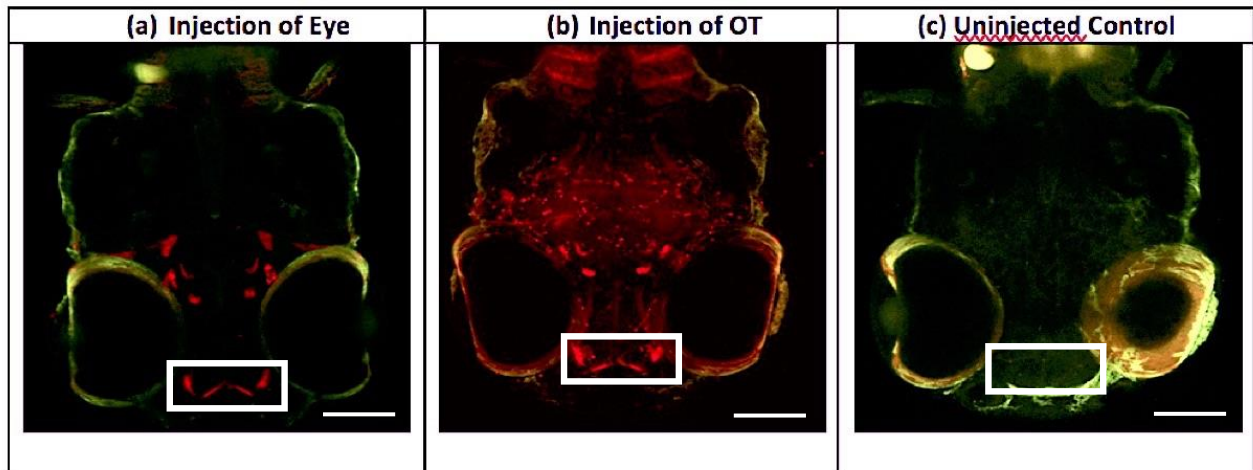
Figure 4.1.4: Treatment of Food Odour or Alarm Substance Had No Effect on the Number of High-Angle Turns Made. (a) Control groups for both alarm substance (black bars) and food odour (grey bars) treated fish showed no significant differences for the number of high angle turns during visual stimulation ($p=0.5328$). After addition of the odourants, fish exposed to the food odourant demonstrated very little change in the number of high degree bends whilst alarm substance treated fish demonstrated a slight decrease in the time spent displaying high degree turns which remained insignificant when compared to food odour treated fish (interaction statistic – $p=0.22$). Bars on graph represent mean \pm SEM. (b) Data was also analysed by subtraction of the time spent displaying high angle turns in the controls from the olfactory conditions. The resultant data was compared for statistical significance via t-test (Food odour = $+0.02$ seconds \pm 0.11, Alarm substance = -0.14 seconds \pm 0.06. $p=0.10$.) Bars on graph represent mean \pm SEM. $N=26$ fish.

4.2 Olfacto-Visual Neuronal Tracing.

It had previously been demonstrated that visual input had the capacity to alter olfactory perception. Our behaviour experiments were not able to conclusively demonstrate if olfaction was able to in turn also significantly change visually-evoked behaviours or perception. We decided to switch our attention to the neuronal circuitry of the brain and investigate where and how modulation as a result of visual/olfactory integration could occur. We therefore first wanted to visualise any neuronal projections from the olfactory bulbs to the retina and optic tectum, including the terminal nerve, and look for a presence of a neuronal feedback from the tectum back to the retina. To do this, 3days post-fertilisation PTU treated nacre zebrafish larvae were microinjected with 6% Tetramethylrhodamine dextran, 10,000 MW, Lysine fixable – Fluoro Ruby (Thermofisher) in both the eye and the optic tectum. The biotinylated dextran conjugate was used as a retrograde tracer, as this is endocytosed and actively transported along the axon towards the cell body. Labelling was seen in the olfactory bulbs as a result of injection to the tectum supporting the idea that the terminal nerve also projects to the optic tectum (figure 4.2.1(B)). As well as this, a large amount of labelling was seen elsewhere in the brain, including the pre-tectum, which was to be expected as the optic tectum has been proposed to function as an integratory hub. Injection in the eye also demonstrated labelling in the forebrain of the fish near to the olfactory bulbs which we again believe to be fibres of the terminal nerve, supporting work conducted by Koide et al. As well as this, fibres appeared to project from the retina, medially and posteriorly, into the midbrain

(figure 4.2.1(A)). Z-stacks were taken of the optic tectum and identified labelling of a small subset of periventricular cell bodies which may therefore act to provide centrifugal feedback from the optic tectum back to the retina (figure 4.2.1(d)).

Figure 4.2.1: The Terminal Nerve Projects from the Olfactory Bulbs to the Retina and Optic Tectum



(D) Retrograde labelling of tectal cells in samples injected in the eye of *Tg(NBT:GCaMP3) larvae*.

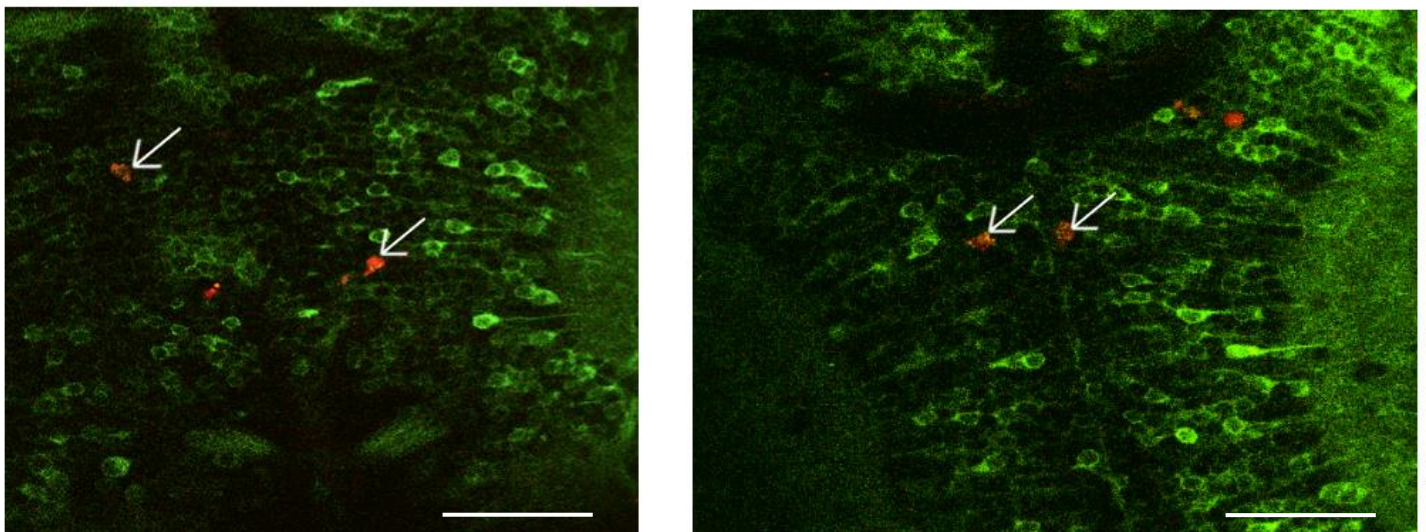


Figure 4.2.1: Max intensity projections acquired through 2-photon microscopy for the identification of neurons in the olfactory region of the zebrafish after injection of tetramethylrhodamine dextran, 10,000 MW, Lysine Fixable – Fluoro Ruby (ThermoFisher) into the Eye, Optic tectum and PBS injected controls. All fish were treated in PTU at 1days post-fertilisation . At 3days post-fertilisation fish were immobilised in low melting point agarose in order to be microinjected. After the procedure, the fish were released and returned to the incubator for 24 hours. The fish were then immobilised once more and imaged through 2-photon microscopy. Olfactory bulbs highlighted with white rectangles. (a) Injection in the eye labelled axons in the ventral forebrain around the region of the olfactory bulbs region which likely belong to the terminal nerve.

*Additionally, signal can be seen in neurons which appear to project from the midbrain back to the eye. N=4 (b) Tectal injection labelled the same subset of neurons in the olfactory region as seen from injection from the eye, confirming the terminal nerve likely projects to both the retina and the optic tectum. In addition to this, an abundance of other signal can be seen in the midbrain, consistent with the fact the tectum receives neuronal inputs from multiple brain areas and acts as an integratory hub. N=6 (c) Control fish injected with PBS showed no signal. N=2. Scale Bars for A-C Represent 100 μ m. (d) Identification of cell bodies in the optic tectum projecting to the retina through retrograde tracing. Larvae which were injected in the eye demonstrated a small number of cells within the optic tectum, which were labelled with rhodamine dextran (red), suggesting these could function to feedback information back to the retina. Green background represents neurons labelled in *tg(NBT:GCaMP3)* larvae. Scale Bars for D Represent 25 μ m.*

4.3 Predictive Coding and Sensory Integration.

Our initial hypothesis was that input from one sensory system can influence perception in another system by altering spontaneous activity in higher order centres.. To investigate this, we recorded the spontaneous activity in the optic tectum and habenula before, during and after olfactory stimulation. Anaesthetised 10days post-fertilisation *tg(elavl3:H2B-GCaMP6s)* larvae were immobilised in agarose, with the portion anterior to the nose of the fish carefully removed. E3 perfusion was provided for 10 minutes whilst spontaneous activity was recorded. The perfusion system then switched to either a food odorant, alarm substance or weak food odorant (control) for 5 minutes before reverting to E3 and a further 10 minutes of spontaneous activity was measured. Continuous perfusion allowed for minimising any mechanosensory effects when the odorants were applied. After experimentation, data files were registered for minor movement corrections and cellular responses were obtained by measuring relative changes in fluorescence intensity. K-means clustering grouped cells of interest which showed similar spiking patterns across the 3 test groups. Clustering created 4-8 clusters of responses per fish. Our focus on the clustering's results were to identify cells which demonstrate mechanosensory responses, which display consistent levels of spiking throughout the experiment, display increased spiking after stimulation and those which display decreased spiking after stimulation. Categories which did not display these profiles were not further analysed.

Control data showed responses were still seen when the perfusion system switched from E3 to an alternative E3 source suggesting mechanosensory responses were still present. The clustering results showed that out of a total of 8844 cells across 7 fish (mean = 1263 cells per fish), a total of 2024 (22.89%) were considered to be 'spiking'. Of these cells, 1205 (59.54%) demonstrated a consistent level of activity throughout the experiment, whilst 619 (30.58%)

showed a decrease in activity and 200 (9.88%) cells displayed an increase in the level of spiking activity (figure 4.3.1).

Figure 4.3.1: Spontaneous Activity Profiles for Cells Across the Optic Tectum and Habenula.

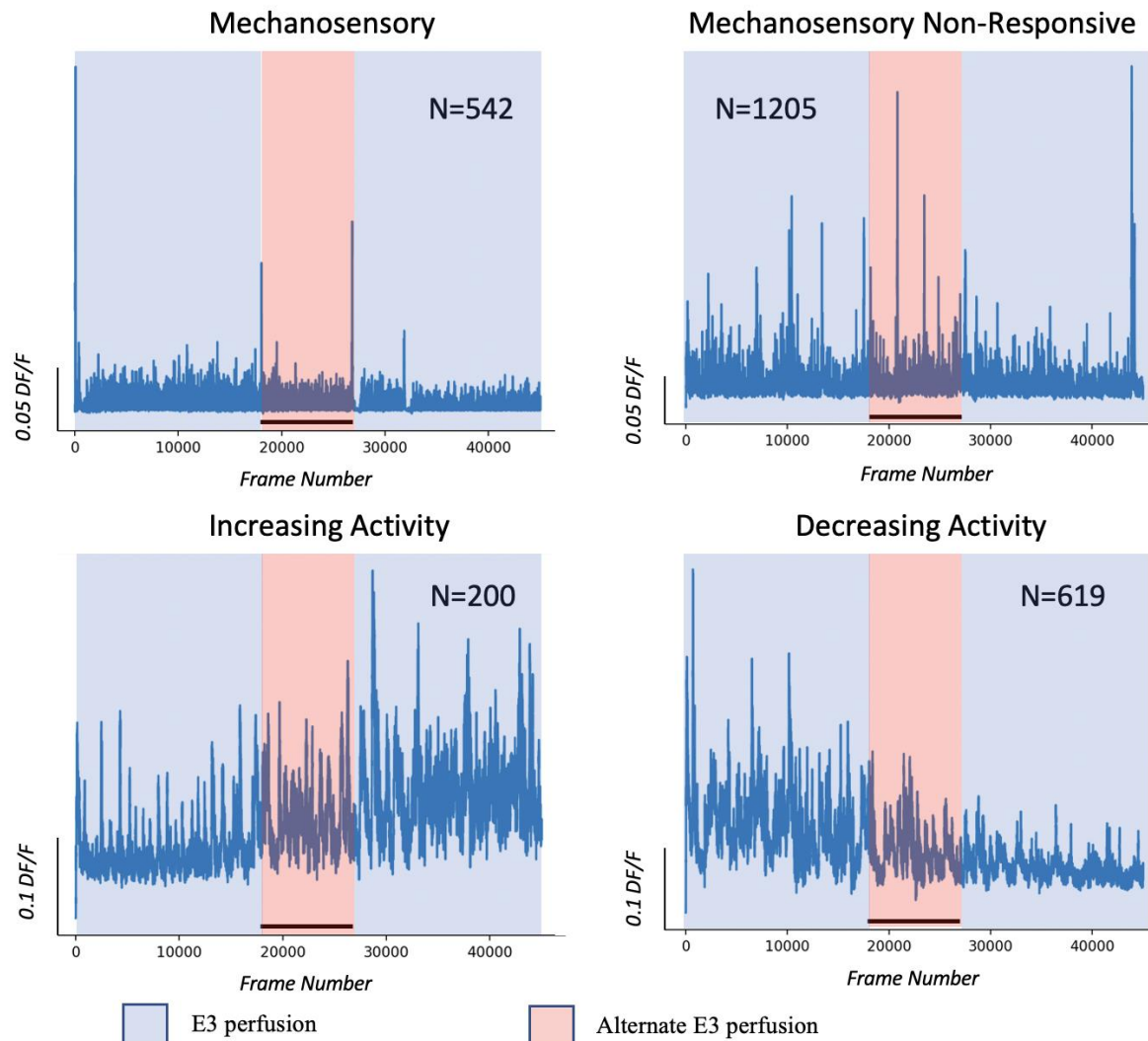
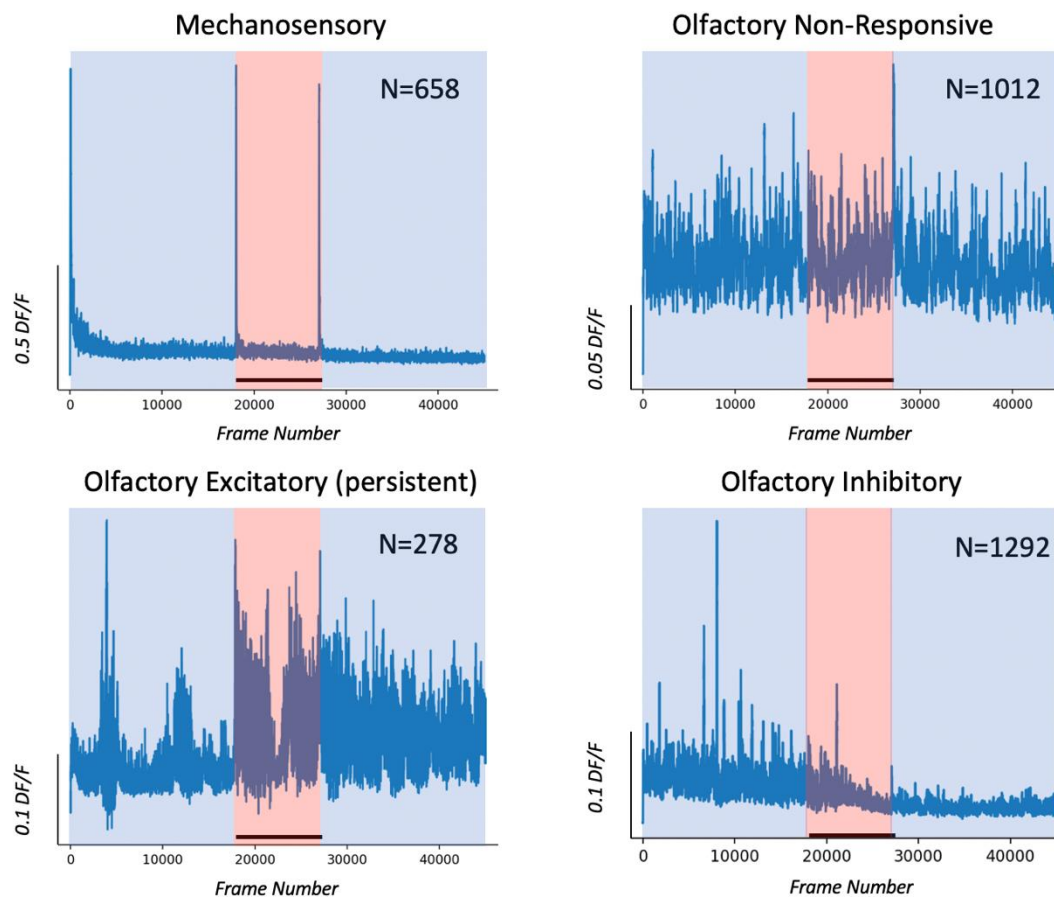


Figure 4.3.1: Spontaneous activity profiles for cells across the habenula and optic tectum. Fish were subject to 25 minutes of imaging during which spontaneous activity was recorded across the midbrain. In these control fish, perfusion of E3 was applied continuously throughout the experiment. After 10 minutes, perfusion switched from one tube of E3 to another to mimic changing from E3 to an olfactory stimulus in test fish (red background). Despite attempting to keep continuous perfusion throughout, K-means clustering identified 542 mechanosensory responses when the perfusion system switched from one tube of E3 to the other. Clustering also identified a total of 2024 cells (22.89% of all cells recorded) across 7 fish that displayed high levels of spontaneous spiking activity. Of these, 1205 displayed consistent levels of spiking throughout the recording. 200 cells showed a gradual increase in spiking activity throughout the experiment, whilst 619 cells displayed a gradual decrease in spiking activity.

In the fish presented with alarm substance, a total of 11,235 cells were identified across 10 fish in the analysis (mean = 1123 cells per fish). The k-means clustering identified that the of these, 2582 (23.0%) were considered spiking. Of these cells, the same four subgroups were concatenated and averaged. 1012 (39.19%) of the cells were spiked at a consistent frequency and amplitude throughout, 278 (10.77%) cells displayed an increase in spiking after the stimulus was applied whilst 1292 (50.04%) showed a decrease in activity. In addition to these, clustering identified an additional group of interest where neurons showed elevated activity in the period where the stimulus was applied (figure 4.3.2). This was not seen in control fish.

Figure 4.3.2: Alarm Substance Alters Spontaneous Activity in the Optic Tectum



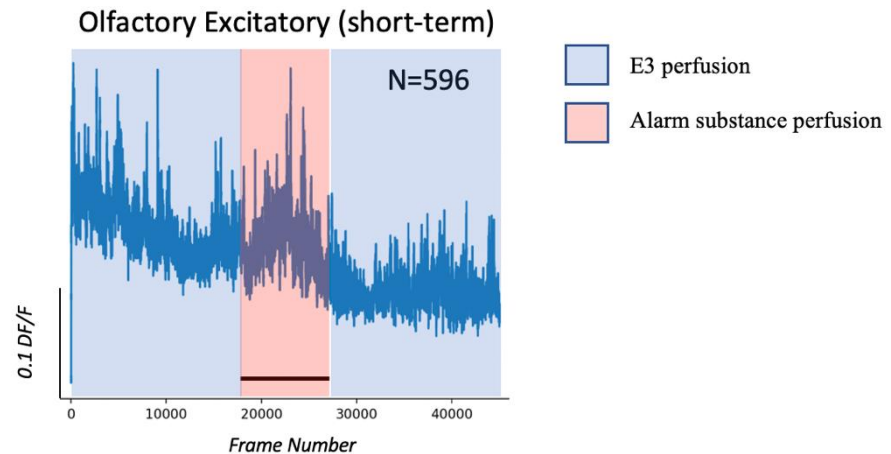


Figure 4.3.2: Application of the alarm substance alters spontaneous activity in the optic tectum. Average spontaneous activity profiles for clusters of cells across the habenula and optic tectum. Fish were subject to 25 minutes of imaging during which spontaneous activity was recorded across the midbrain. In these experiments, perfusion of E3 was applied for the first 10 minutes of the recording (blue background). After 10 minutes, perfusion switched from E3 solution to the alarm substance to provide an olfactory cue (red background) for 5 minutes. After this time, perfusion reverted to E3 for the final 10 minutes of the recording. Constant perfusion was maintained to attempt to minimise mechanosensory stimulation during odour application. K-means clustering identified 658 mechanosensory responses across 10 fish. A total of 11,235 cells were imaged across experiments with clustering identifying 2582 (23.0%) of those as highly spiking. 1012 demonstrated consistent levels of spiking throughout suggesting these were not responsive to olfactory stimulation. 278 cells displayed a sharp increase in activity at the onset of the stimulus which persisted for the remainder of the experiment. A further 596 cells displayed an increase in activity during stimulation before returning to the previous baseline level of activity. The final 1292 cells showed a steady level of activity prior to the stimulus onset but no spiking activity after the stimulus ended.

In the final test group, where fish were presented with food odour, a smaller number of cells were identified across all fish due to the level of fluorescence seen in this spawn being lower than others used in the experiments. In total, 6269 cells were identified (mean = 895 per fish), with 1336 (21.3%) spiking cells identified across all fish. Of these cells, 307 (22.98%) displayed consistent levels of activity throughout the recording, 355 (26.57%) showed an increase in spiking activity to our food odorant whilst 674 (50.45%) showed a decrease in spiking activity. In addition to these, we also identified a cluster of responding cells whose average trace displayed a decrease in activity during the period of stimulus presentation, opposite to that seen with the alarm substance previously (figure 4.3.3).

Figure 4.3.3: Application of Food Odour Alters Spontaneous Activity in the Optic Tectum

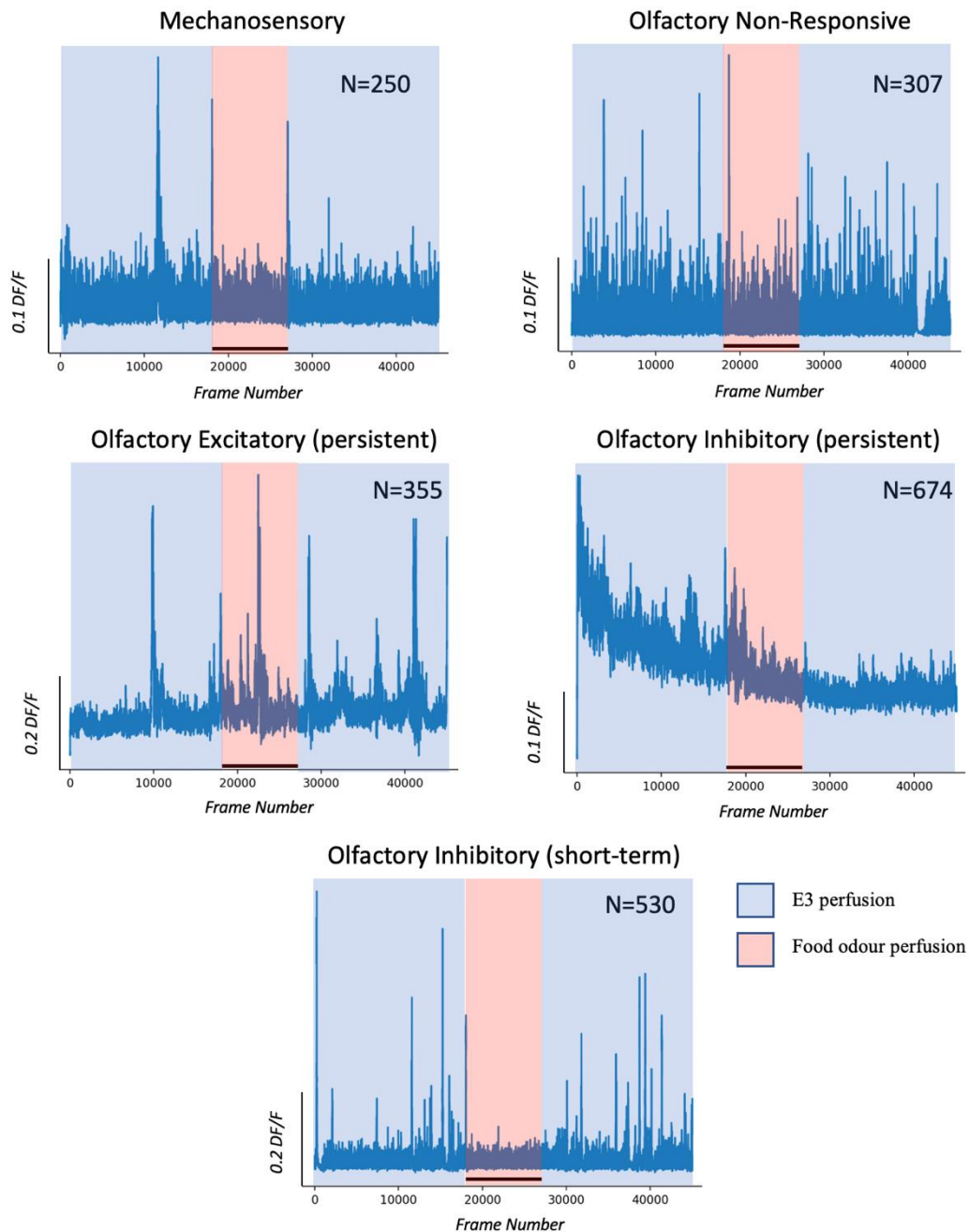


Figure 4.3.3: Application of food odorant alters spontaneous activity in the optic tectum. Average spontaneous activity profiles for clusters of cells across the habenula and optic tectum. Fish were subject to 25 minutes of imaging during which spontaneous activity was recorded across the midbrain. In these experiments, perfusion of E3 was applied for the first 10 minutes of the recording (blue background). After

10 minutes, perfusion switched from E3 solution to food odorant to provide an olfactory cue (red background) for 5 minutes. After this time, perfusion reverted to E3 for the final 10 minutes of the recording. Constant perfusion was maintained to attempt to minimise mechanosensory stimulation during odour application. K-means clustering identified 250 mechanosensory responses across 10 fish. A total of 6269 cells were imaged across experiments with clustering identifying 1336 (21.31%) of those as highly spiking. 307 demonstrated consistent levels of spiking throughout suggesting these were not responsive to olfactory stimulation. 278 cells displayed an increase in activity beginning the onset of the stimulus which persisted for the remainder of the experiment. 674 cells showed a steady level of activity prior to the stimulus onset but no spiking activity after the stimulus ended for the remainder of the experiment. The final cluster of 530 cells displayed spiking activity prior to and after the olfactory stimulus but spiking activity was inhibited during this period.

Table 4.3.1: Diversity of Changes in Spontaneous Activity Profiles in the Optic Tectum to Olfactory Stimuli

	<u>Control Fish</u>	<u>Alarm Substance</u>	<u>Food Odour</u>
<u>Total Cells</u>	8844	11,235	6269
<u>Spiking Cells</u>	22.89%	23.00%	21.31%
of which...			
<u>Consistent Spiking</u>	59.54%	39.19%	22.98%
<u>Increased Spiking</u>	9.88%	10.77%	26.57%
<u>Decreased Spiking</u>	30.58%	50.04%	50.45%

In order to confirm our responses were present in both the tectum and the habenula, individual response clusters were run through a custom python script allowing for visualisation of the cells within the cluster. Below are three examples taken from clusters in fish exposed to the alarm substance (figure 4.3.4(A-B)) and food odour (figure 4.3.4(C)). All three of these clusters demonstrate a change in spontaneous activity in response to application of the odorant and after visualisation of their constituent cells, we demonstrated that each cluster was formed from cells across the optic tectum and habenula.

Figure 4.3.4: Visualisation of Responding Clusters Demonstrated Cells Were Located in the Optic Tectum and Habenula.

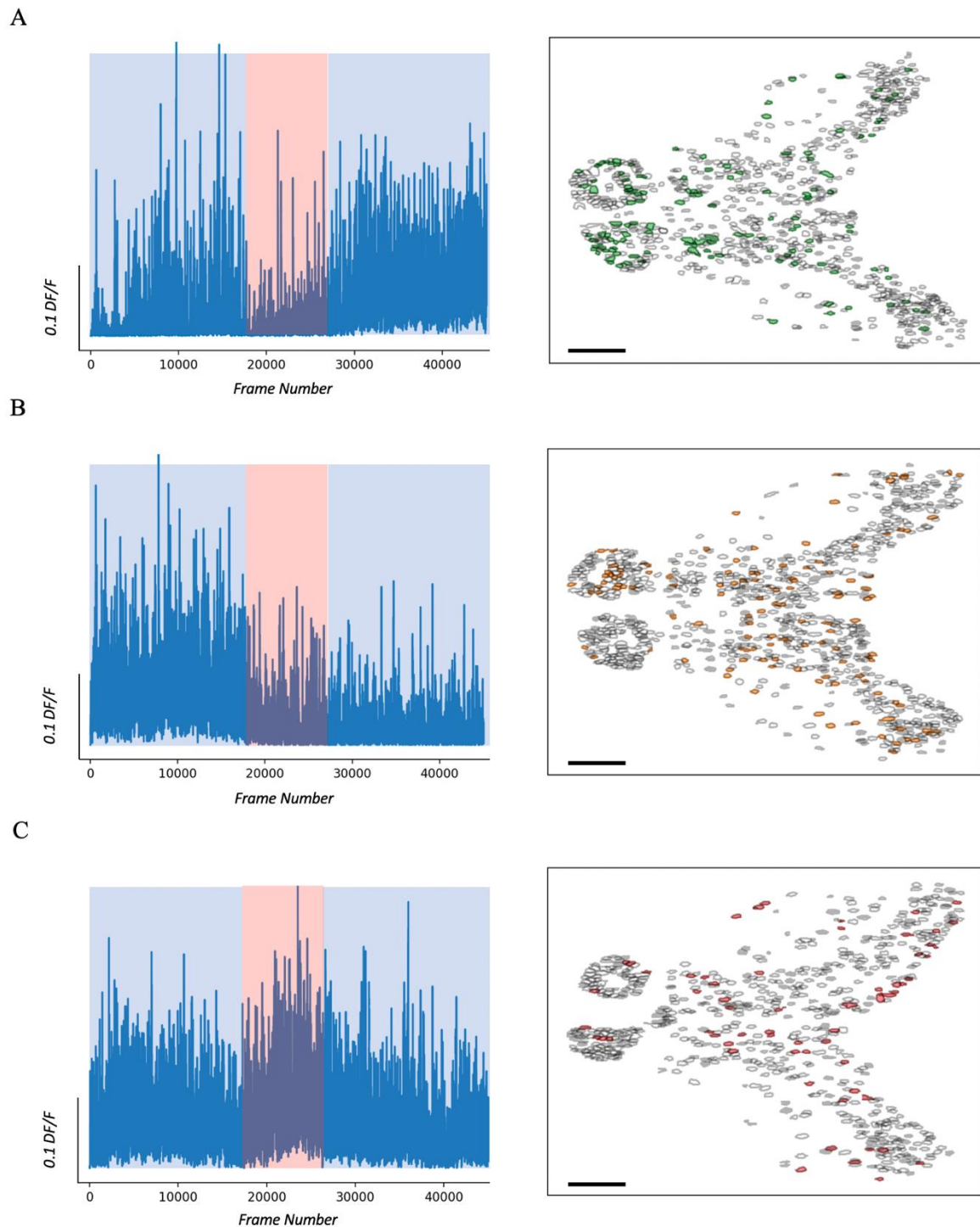


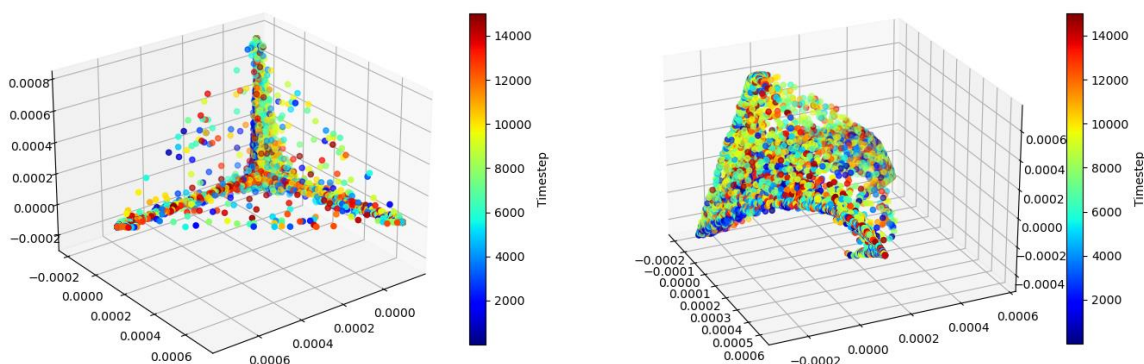
Figure 4.3.4: Visualisation of responding clusters demonstrated cells were located in the optic tectum and habenula. Individual clusters from the K-means clustering were cross checked to identify where the cells which formed the clusters were located within the brain. 3 responding clusters were selected from fish exposed to alarm substance (a, $n=125$ and b, $n=120$) and the food odorant (c, $n=76$). These demonstrated

that in all of the above cases, cells were present in both the left and right habenula as well as both tecti which formed the response cluster. Scale bars = 75 μ m.

In addition to the K-means clustering, we also conducted non-linear reduction analysis using Laplacian eigenmaps. The maps will preserve the local neuronal information only (responses between nearby neurons) and project data points into a low-dimensional space using the smallest eigenvectors from the Laplacian matrix. This allowed observation for how the collective activity, projected to a lower dimensional space, changed with time throughout our experiments.

The Laplacian eigenmaps were calculated initially for control experiments. Cellular responses were obtained by measuring relative changes in fluorescence intensity. To reduce the number of datapoints, the dataset was averaged by 3 so that memory capacity was not breached during the analysis. The eigenmaps from four of the seven control experiments can be found below in figure 4.3.5. The timesteps from before the stimulus (0-6000/blue) and after the stimulus (9000-15000/orange and red) shows during these periods the system resides in very similar states of activity as portrayed by the lack of correlation between similarly coloured dots.

Figure 4.3.5: Laplacian Eigenmaps for Control Fish Demonstrates the System Resided in a Similar State Before and After the Stimulus was Applied.



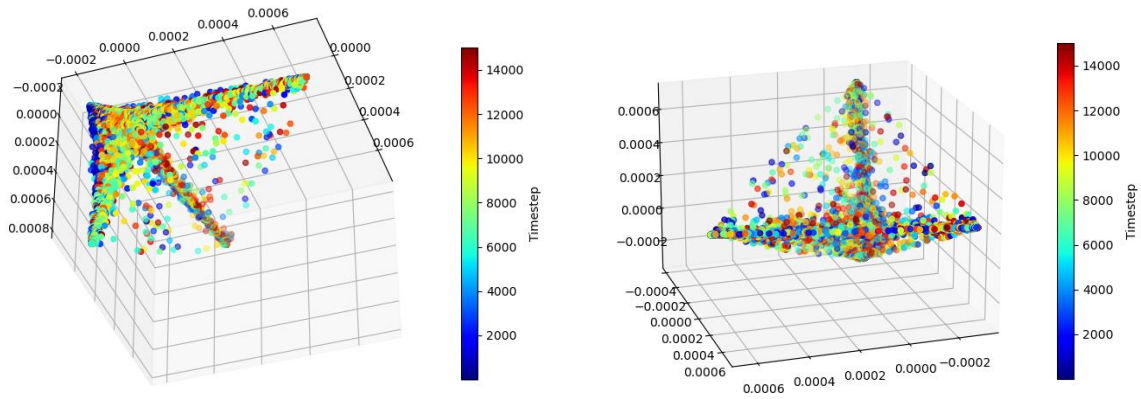
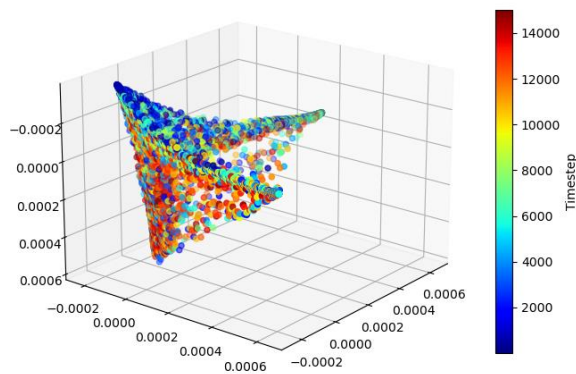


Figure 4.3.5: Laplacian Eigenmaps for Control fish Demonstrates the System Resides in a Similar State Before and After the Stimulus is Applied. The Laplacian eigenmaps from four out of 7 control fish which demonstrated that the system resided in similar states before ($t < 6000$) and after the stimulus ($t > 9000$).

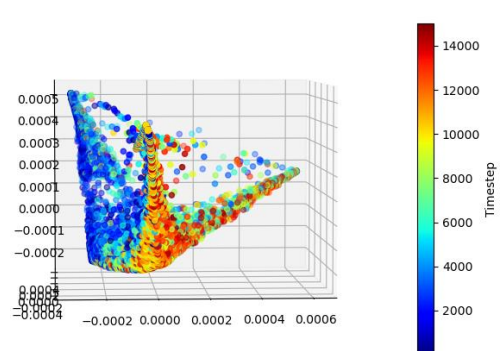
For fish treated with alarm substance, the Laplacian eigenmaps demonstrated different results. Figure 4.3.6 (A-C) below demonstrates that the system resided in a very different state in pre-stimulus period $t < 6000$ (blue dots) to the post stimulus period after the alarm substance was applied, $t > 9000$ (red dots). The same was also seen for when the food odorant was applied. Figure 4.3.6 (D-F) represent 3 of the Laplacian eigenmaps from fish which were presented with food odorant, and once more here, we can see a big shift in the state of activity pre and post stimulus.

Figure 4.3.6: Laplacian Eigenmaps for Fish Exposed to Olfactory Stimulus Demonstrates the System Resided in a Different State Before and After the Stimulus was Applied.

A



B



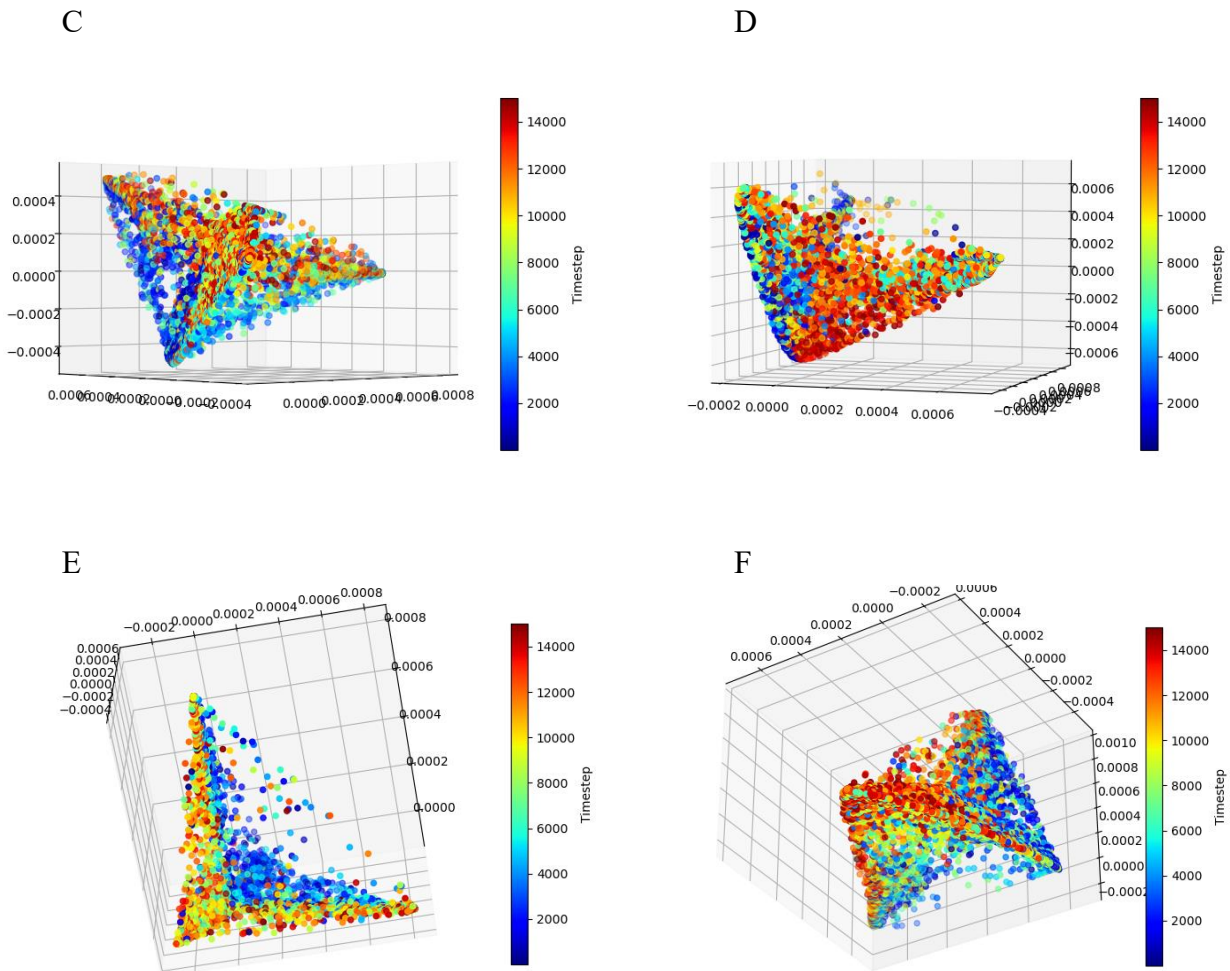


Figure 4.3.6: Laplacian Eigenmaps for Fish Exposed to Olfactory Stimulus Demonstrates the System Resided in a Different State Before and After the Stimulus was Applied. (A-C) Examples of some of the Laplacian eigenmaps from fish exposed to alarm substance demonstrated that the system resided in a very different state ($t < 6000$, blue dots) and after the alarm substance was applied ($t > 9000$, red dots). (D-F) Examples of some of the Laplacian eigenmaps from fish exposed to the food odorant demonstrated that the system resided in a very different state ($t < 6000$, blue dots) and after the odorant was applied ($t > 9000$, red dots).

4.4 Olfactory Adaptation

We saw in our previous work that olfactory stimuli were able to evoke changes in the spontaneous activity seen in the optic tectum. However, the use of different olfactory stimuli, in this case food and the alarm substance, evoked different levels of changes in the spontaneous activity. We decided to therefore to test whether different behaviourally relevant stimuli could evoke different forms of adaptations within the zebrafish olfactory system. For this we used the same two stimuli used previously, food and alarm substance in order to test two stimuli which evoke opposite behaviour reactions.

For these experiments, 5 days post-fertilisation *tg(Xla.Tubb:GCaMP3)* larvae were immobilised in 2% low-melting point agarose and imaged using 2-photon microscopy as described in section 3.4 of the methods. Larvae were exposed to 5 x 3-second presentations of either odour or an E3 media control via a glass pipette. In order to limit mechanosensory stimulation, the pipette was angled away from the nose of the fish to limit the amount of direct liquid flow (see figure 4.4.1 below). A separate set of experiments were initially conducted using luciferase yellow instead of our olfactory stimulus to ensure the odorant would still be detected by the fish as it diffused through the media.

Figure 4.4.1: Application of Olfactory Stimuli

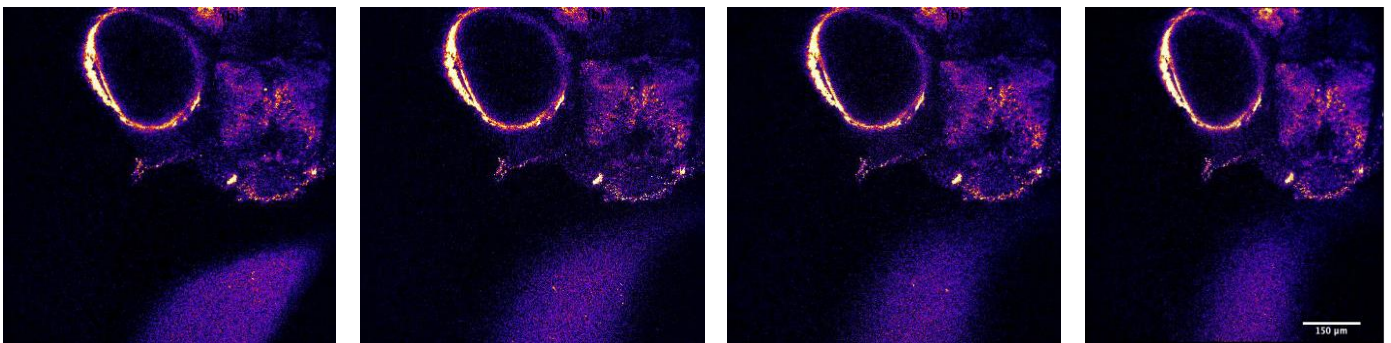


Figure 4.4.1: Application of Olfactory Stimuli. Application of olfactory stimuli was tested using lucifer yellow dye. Application was achieved using a glass pipette with tip diameter approximately $10\mu\text{m}$. The tip was angled away and anterior to the nose of the fish and dye allowed to diffuse back to the nose. This process limited mechanosensory stimulation but would still allow for olfactory detection to occur. Fish were mounted dorsal up with the anterior of the fish towards the bottom of the image. Scale bar = $150\mu\text{m}$.

The next stage of the experiment was to confirm once more that we were able to evoke olfactory responses in the olfactory bulbs. Fish were exposed to 5 presentation of the olfactory odorant and the resultant calcium responses recorded from the olfactory bulbs. Due to using a cytoplasmic GCaMP reporter (figure 4.4.2(A)), it was difficult to separate the cell bodies from dendrites and axons therefore we decided to use a voxel-wide analysis approach. Analysis of 5 fish identified 1755 responding voxels to the food odorant. The average response trace (figure 4.4.2 (B)) showed that repetitive presentation of the stimulus caused a significant depression – a decrease of the response amplitude. The amplitude of the first response was about 1.7x higher than that of the fifth response (0.96 ± 0.016 vs 0.55 ± 0.017) ($p < 0.0001$, $n = 1755$ voxels, 5 fish) giving an adaptation index of 0.267. Adaptation dynamics can be fitted

with a single exponent, with the adaptation time constant (τ) being 44.45 ± 9.46 seconds, which is much slower than in the visual system (2-10 seconds, (Nikolaev *et al.*, 2013)).

Figure 4.4.2: Application of Food Odorant Evoked Olfactory Responses.

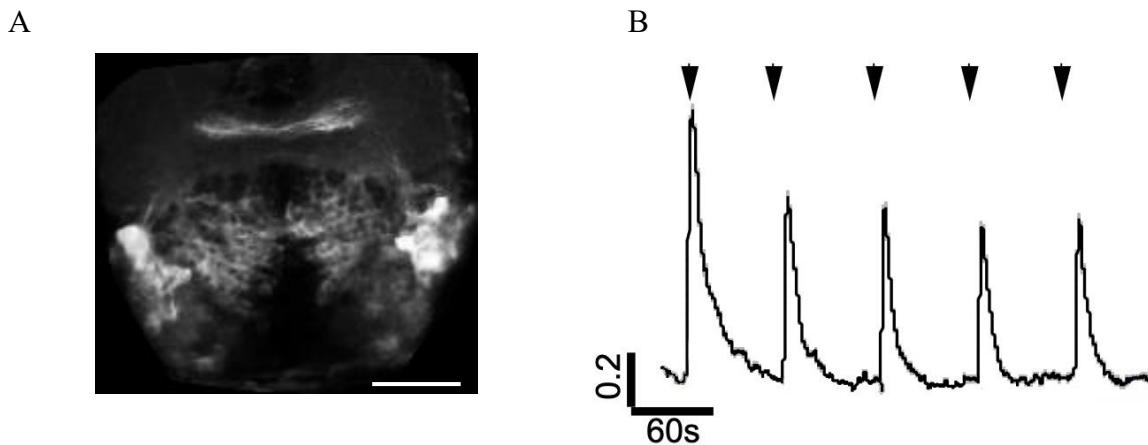


Figure 4.4.2: Application of Food Odorant Evoked Olfactory Responses. Application of food stimulus to *tg(Xla.Tubb:GCaMP3)* zebrafish evoked olfactory responses. (A) Calcium responses were recorded from the olfactory bulbs and ventral telencephalon using 2-photon microscopy. Scale bar represents $25\mu\text{m}$. (B) The average response trace was plotted from voxel wise analysis, with smoothing fits, of neurons in telencephalon in response to 5 repeats of a food based olfactory stimulus. Shadows represent SEM. Black arrows indicate olfactory stimulus presentation. $N=5$ Fish

Diversity of Olfactory Adaptations.

Visual systems of mammals and other vertebrates exhibit different forms of adaptation (depressing vs facilitating) and also different speeds of adaptation. We, therefore, aimed to define whether olfactory neurons also exhibit such diversity of adaptations. To test this, we performed analysis of the adaptation dynamics of fluorescence in individual voxels. We performed both a manual and an automated analysis to categorize individual traces based on their adaptation characteristics across 10 fish. From the responded voxels, five main subgroups were identified and the voxels within each group were averaged together to create an average trace (figure 4.4.3). The 5 subgroups were: adapting (34.7%, adaptation index = 0.65 ± 0.01), strongly adapting (17.3%, adaptation index = 0.99 ± 0.01), non-adapting (18.9%, adaptation index = -0.04 ± 0.001), sensitising (15.9%, adaptation index = -0.24 ± 0.01) and hyperpolarising responses (13.2%).

Figure 4.4.3: The Zebrafish Olfactory System Displays a Diversity of Adaptations.

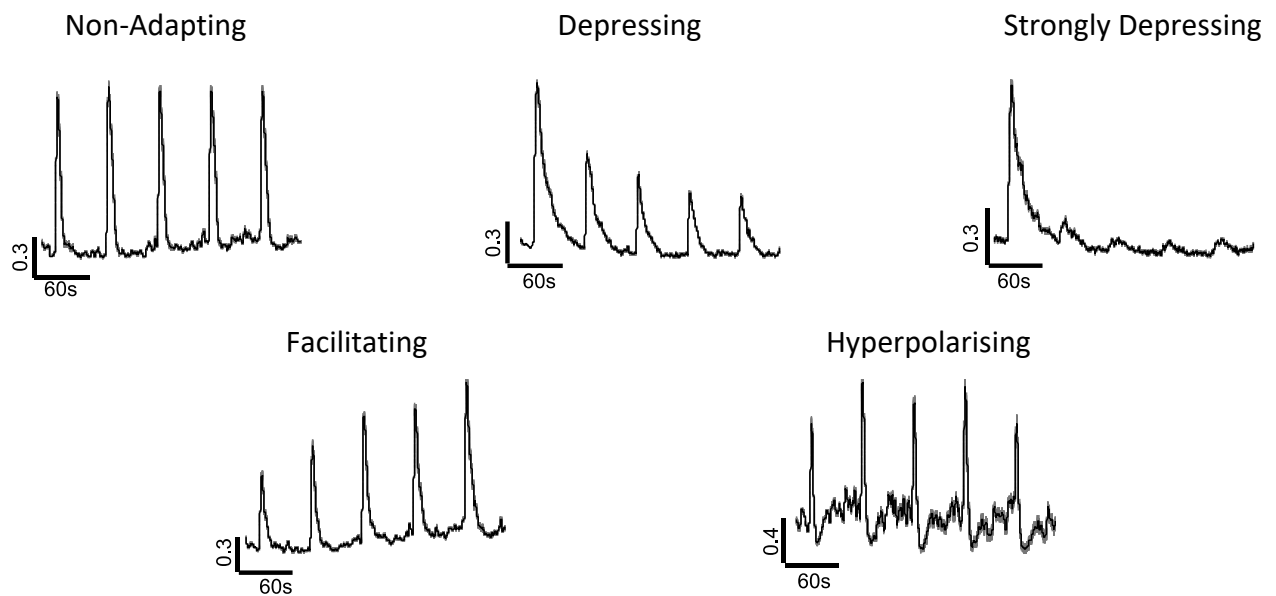


Figure 4.4.3: The zebrafish olfactory system displays a diversity of adaptations. Voxel wise analysis identified a total of 1755 responding voxels. Manual analysis of these voxels displayed 5 main response profiles: 1. Non-adapting ($n=183$), 2. Depressing ($n=846$), 3. Strongly Depressing ($n=311$), 4. Facilitating ($n=269$) and 5. Hyperpolarising ($n=89$). Traces for each group were extracted and averaged to calculate the average response trace for each profile. Average traces were plotted, with smoothing fits. Shadows represent SEM.

As mentioned, the same analysis was also conducted using an automated system to select the soma of individual neurons. The results from this analysis identified the same 5 main subgroups of adapting cells, as shown below in figure 4.4.4. In both cases, most of the voxels exhibited increase in fluorescence upon application of food odour. However, the final subgroup behaved similarly to OFF cells, i.e., decreased fluorescence upon food odour application and/or subsequently depolarized at the stimulus offset. These cells were much better identified by the automated analysis likely due to difficulties in identifying negativity in the skewness of data during the voxel wise analysis.

Figure 4.4.4: Manual and Automated Analysis Display the Same Diversity of Adaptations.

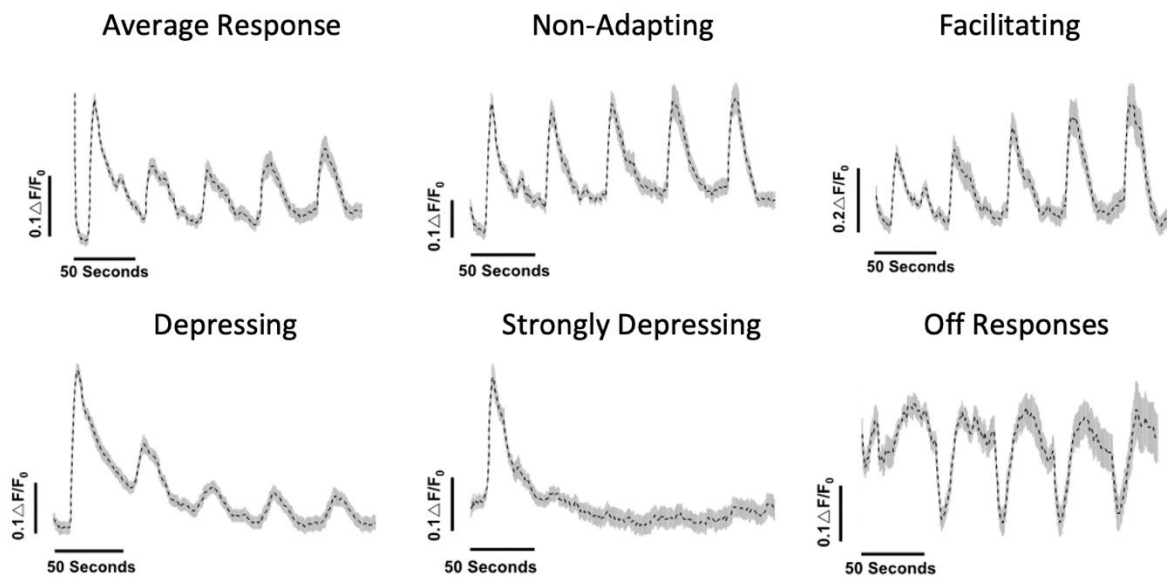


Figure 4.4.4: Manual and automated analysis display the same diversity of adaptation. Advanced ROI analysis was used to detect different response profiles across 10 responding 5days post-fertilisation larvae. 5 main response profiles were identified and plotted alongside the average response of all ROIs. Analysis identified a total of 2412 ROIs across the olfactory bulbs and ventral telencephalon of 10 fish, of which 190 demonstrated olfactory responses. 66 of those showed adaptation, a further 33 only responded to the first presentation of odorant, 36 ROIs were identified that demonstrated no adaptation, 30 ROIs displayed sensitisation and 25 ROIs showed hyperpolarising responses. Due to the difficulty of segmentation of cytoplasmic GCaMP, some ROIs were larger than a single cell. Shadows represent standard error of the mean.

For each individual voxel we also calculated its adaptation index defined as the ratio of the differences between the first and fifth response amplitude to the sum of the first and fifth response amplitude (see Methods). The distribution of the adaptation indices (Figure 4.4.5) is broad with some voxels exhibiting positive adaptation index (meaning depression) and others exhibiting negative adaptation index (meaning facilitation). This data demonstrates that, like in the visual system (Nikolaev *et al.*, 2013, Kastner and Baccus, 2011), the olfactory system exhibits opposing forms of plasticity in response to food odour presentation.

Figure 4.4.5: Distribution of Adaptation Indices in the Zebrafish Olfactory System.

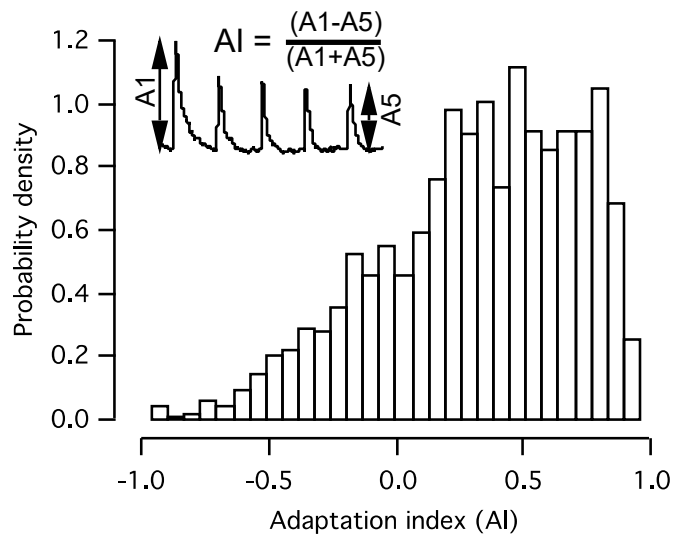


Figure 4.4.5: Distribution of adaptation indices in the zebrafish olfactory system. The adaptation index, defined as (amplitude of 1st response – amplitude 5th response) / (amplitude 1st response + amplitude of the 5th response), was calculated for all responding voxels in the previous experiment. All resultant values for the adaptation index would lay between -1 and 1, with -1 representing maximal facilitation, and 1 represent maximal depression. The distribution of adaptation indices above display that the majority of responding voxels had an adaptation index greater than 0, and thus were displayed depression. It is also clear however that the olfactory system, like the visual system, is also home to several voxels which display facilitation, as seen by the distribution of voxels with an adaptation index of less than 0.

To investigate whether the diversity of adaptation responses is preserved during development, we repeated the experimental process once more, this time using zebrafish at later larvae stages (10-17days post-fertilisation) with volumetric imaging. This allowed us to continuously record the changes in levels of calcium in cells simultaneously at different depths in the telencephalon and olfactory bulbs in a single experiment. As well as this, we could also conduct a comparison of the responses to our odorant in fish for which the stimulus would be novel (5days post-fertilisation) and those which would recognise the odorant as meaning the smell of food.

Upon analysis of the volumetric imaging data, all individual voxel response traces were compiled together for each recording depth from every experiment and averaged to give an overall average response trace. The average once again showed most cells were adapting to

the stimulus (50.8%), with the same main classes of response types seen as in the younger fish (Figure 4.4.6(A)). Overall, in older zebrafish, we found a similar representation for each subtype as described for the 5days post-fertilisation zebrafish (Figure 4.4.6(B)), suggesting that opposing forms of plasticity are not a temporary characteristic of the undeveloped olfactory system and are not limited to stimuli that were not experienced by the animal before.

Figure 4.4.6: Diversity of Olfactory Adaptations Persists in Older Larval Zebrafish.

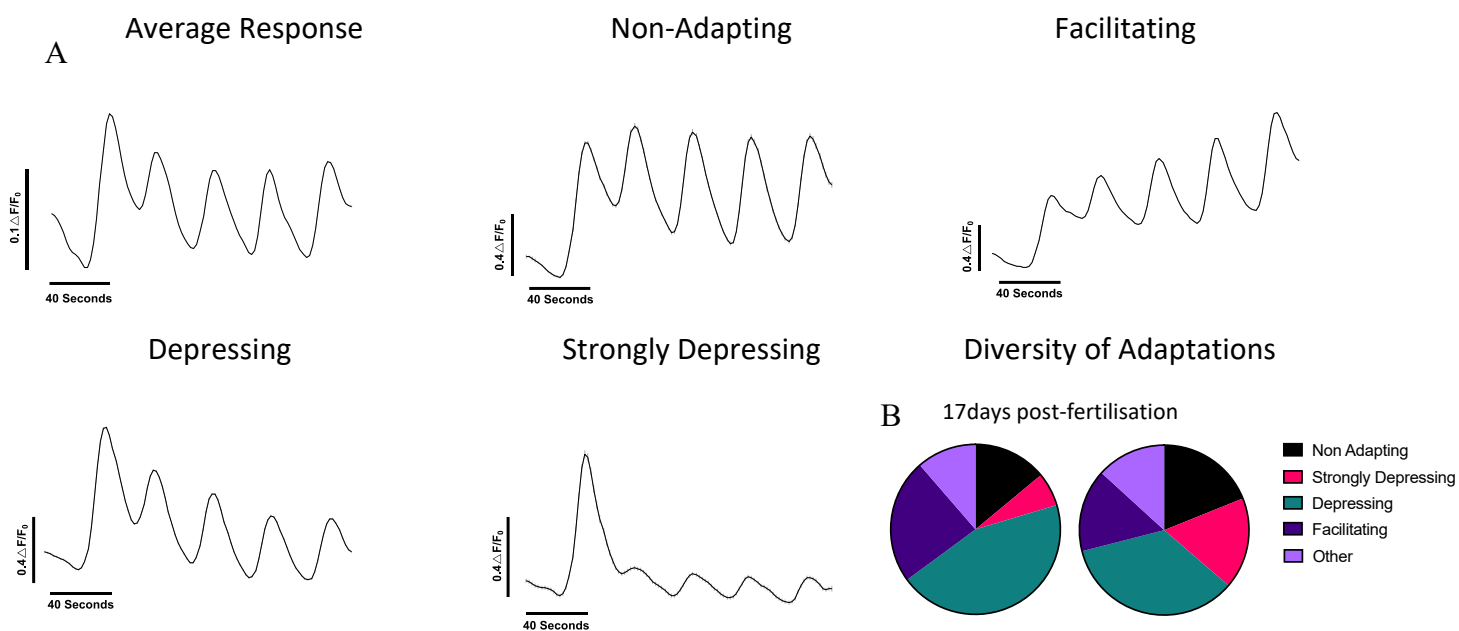


Figure 4.4.6: Diversity of olfactory adaptations persists in older larval zebrafish. (A) Volumetric imaging and 2-photon microscopy identified the same 4 main response profiles in 10-17days post-fertilisation *Tg(NBT:GCaMP3)* larvae in response to 5 presentations of the same food odorant. Voxel wise analysis followed by manual sorting of responding traces was conducted for 6 different planes of depth for each of 6 fish. A total of 16,547 responding traces were obtained from cells in the olfactory bulbs and telencephalon. Out of the responding traces, 7368 (44.5%) were adapting, 2315 (13.9%) showed no adaptation, 3926 (23.7%) sensitised to the stimulus, and 1058 (6.3%) strongly adapted. Shadows represent SEM. (B) Comparison and quantification of the number of ROIs in each subgroup for both 5days post-fertilisation larvae and older larvae and the adaptation they portrayed. Pizza plots demonstrate that similar percentages of cells could be found for each subgroup in both 5days post-fertilisation and older larvae, with the only noticeable difference between the quantity of depressing and strongly depressing cells.

Diversity of Adaptations is not Reflected in the Brain Structure.

Spatial distribution of glomeruli is invariant both between the left and right olfactory bulbs of the same animal and across different animals (Lodovichi, 2021). This topography and the combinatorial pattern of activation are both essential to confer odour identity. We investigated if similar topography existed regarding the short-term plasticity displayed in different areas of the olfactory system. To test this, we mapped the position of all sorted traces voxels with different dynamics (Figure 4.4.7(A)). The adaptation index was calculated for all responding voxels to provide visual representations of the brain areas displaying depression and facilitation (Figure 4.4.7(b-C)). The distribution of depressing, non-adapting and facilitating voxels along anterior-posterior and left-right axes demonstrates a very high degree of correlation. This suggests that several depressing, non-adapting and facilitating voxels can be found across the olfactory bulbs and telencephalon, meaning the diversity of adaptations is not reflected in the brain structure.

Figure 4.4.7: Diversity of Adaptations is not Reflected in the Brain Structure.

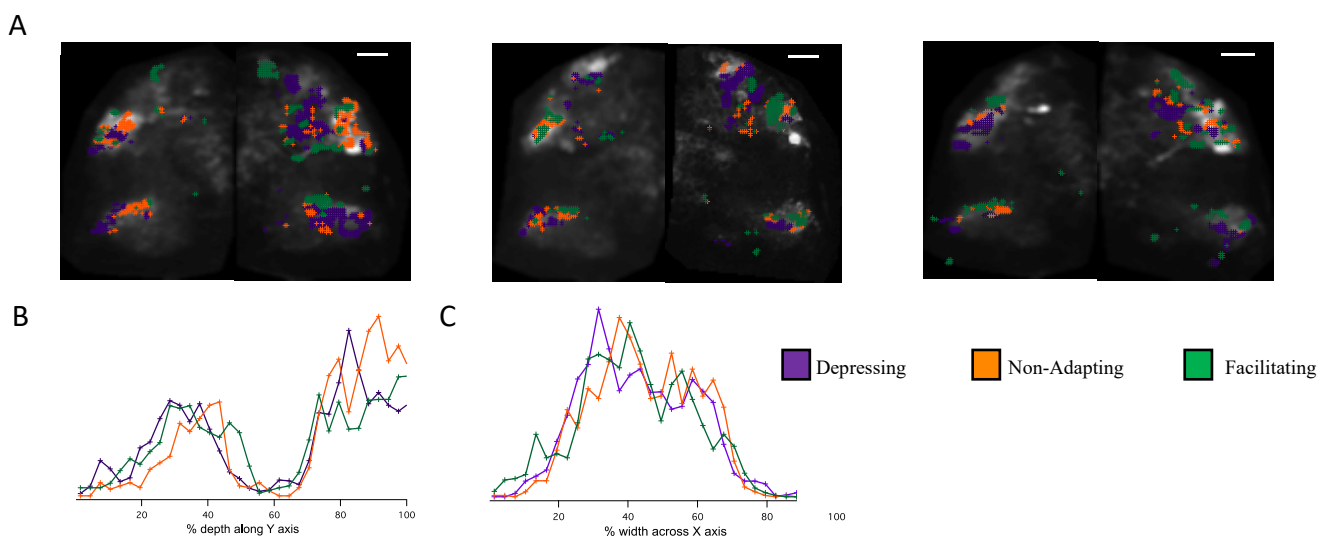


Figure 4.4.7: Diversity of adaptations is not reflected in the brain structure. (A) Responding voxels mapped as a function of X and Y onto the average image for different planes of recording from the volumetric imaging in a 14days post-fertilisation *nbt:GCaMP3* larva. Adapting, non-adapting and sensitising traces can be seen in medial and lateral regions of both the olfactory bulbs and telencephalon. After calculation of adaptation index, voxels with an AI of less than -0.2 were classed as sensitising (green), between -0.2 and 0.2 as non-adapting (orange) and greater than 0.2 were adapting (purple). The positions of adapting, non-adapting and sensitising voxels were mapped as a function of X and Y. No statistically significant differences were present for positions of adapting, non-adapting and sensitising traces along either the depth (B) of the fore brain or the width (C). This suggests the diversity of adaptations are not reflected in the brain

structure. Legend: *Depressing traces (purple), non-adapting traces (orange) and sensitising traces (green).* Scale bars represent 15 μ m.

The Alarm Substance Evokes Different Olfactory Adaptations Compared to Food Odour.

The experiments discussed previously evidence that a food odour evokes a range of adaptations across the zebrafish olfactory system. Regarding behaviour, a food odour would be classed as an attractive stimulus which triggers a set of behaviour programmes including hunting. The question we now wanted to answer was if odours which evoke different behaviours, such as aversive odours e.g., the alarm substance, will display different adaptations in the olfactory system.

To investigate this, we tested the plasticity of neurons which responded to the alarm substance, schreckstoff, in the olfactory system. The alarm substance is released when the skin of a fish becomes damaged, for example by a predator, and alerts other nearby fish to a potential danger through activation of the olfactory system. Danger signals such as this elicit immediate behaviour effects. Given the differences in behaviour evoked by our two stimuli as well as the vastly different relevance of each stimulus, we hypothesised that the adaptation in the olfactory system would also differ.

For these experiments, the application of the odorant and analysis was conducted as described previously for our food odorant. Responding voxels were separated based on skewness and the resultant dataset reduced to a total of 5000 responding voxels to aid with data handling and prevent memory capacity errors. These were then further sorted manually to categorise the adaptations shown and remove any non-responding traces. The average response trace to schreckstoff was calculated from the sorted voxels within the olfactory bulbs and telencephalon. The average response trace demonstrates facilitation (Figure 4.4.8, $AI = -0.15 \pm 0.0128$, $p < 0.05$, $n = 1245$ voxels, 5 fish) which is significantly greater than the AI seen for responses to the food odourant where the average trace displayed depression.

Figure 4.4.8: Olfactory Neurons Display Facilitation to Repeated Presentations of Alarm Substance.

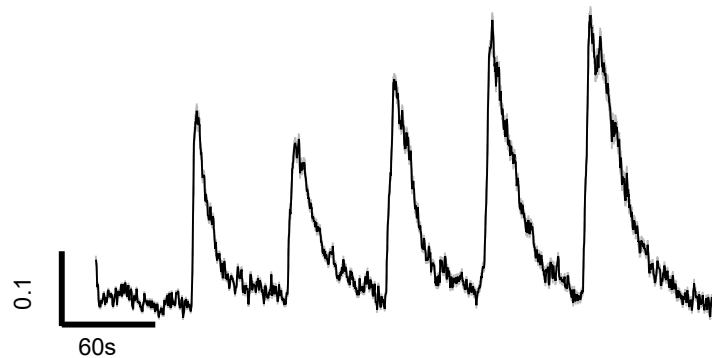


Figure 4.4.8: Olfactory Neurons Display Facilitation to Repeated Presentations of Alarm Substance. The average response trace, with smoothing fits, to 5 presentations of alarm substance Responses to the alarm substance display a much greater level of facilitation on average, with an average adaptation index of -0.15 ± 0.0128 . $N= 5$ fish, 1245 voxels.

We once more investigated the diversity of responses to the alarm substance. From looking at the average trace, it was evident that the average amplitude of the second response was lower than the average amplitude of the first response, suggesting the presence of depressing cells also. Manual sorting of the responding voxels identified the presence of depressing, non-adapting and facilitating voxels to repeated presentations of the alarm substance (Figure 4.4.9 (a)). Of the 1245 responding voxels, 465 (37.35%) displayed depression, 612 (49.15%) showed facilitation and for the remaining 168 (13.50%) no adaptation was seen. This distribution differs to that seen to the food odorant where most voxels display depression (Figure 4.4.9(b)).

Figure 4.4.9: Diversity of Adaptations to the Alarm Substance in Olfactory Bulbs.

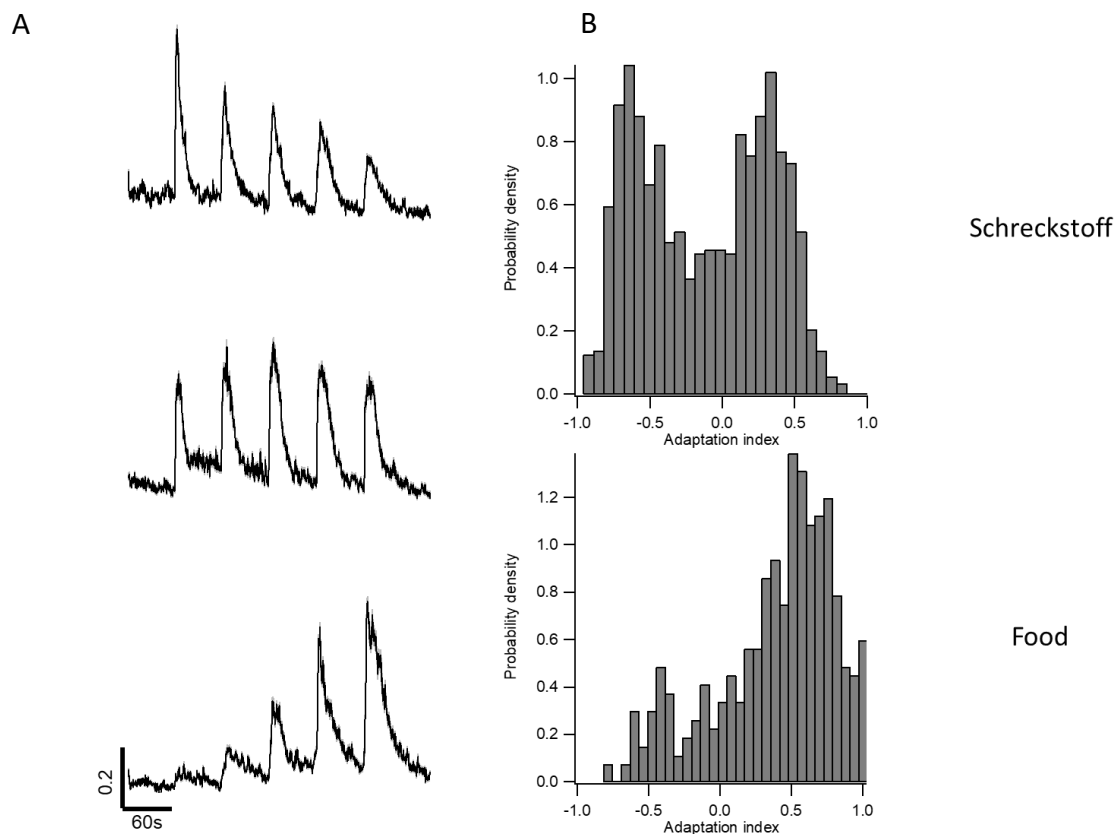


Figure 4.4.9: Diversity of adaptations to the alarm substance in the olfactory bulbs.(A) . Manual sorting of the responding voxels identified the presence of depressing, non-adapting and facilitating voxels to repeated presentations of the alarm substance (Figure 4.4.9 (a)). Of the 1245 responding voxels, 465 (37.35%) displayed depression, 612 (49.15%) showed facilitation and for the remaining 168 (13.50%) no adaptation was seen. (B) Distribution of adaptation indices between food odour and alarm substance displayed a great increase in the presence of facilitating voxels to alarm substance in comparison to food odour. Approximately 20% of responding traces in the food data displayed facilitation. In comparison, almost 50% of traces in the alarm substance displayed this phenomenon.

Interestingly, we also noticed the presence of facilitating voxels within the olfactory epithelium in response to the alarm substance. The level of GCaMP6 expression in the olfactory epithelium under both the NBT and HuC promoters were unfortunately extremely low, reducing our signal to noise ratio but we were able to identify the presence of depressing, non-adapting and facilitating voxels (n=4 fish, 826 voxels). Of the 826 total responses identified, 77 (9.3%) displayed depression, 171 (20.7%) showed no adaptation and 373 (45.2%) were classified as facilitating.

Figure 4.4.10: Diversity of Adaptations to the Alarm Substance in Olfactory Epithelium.

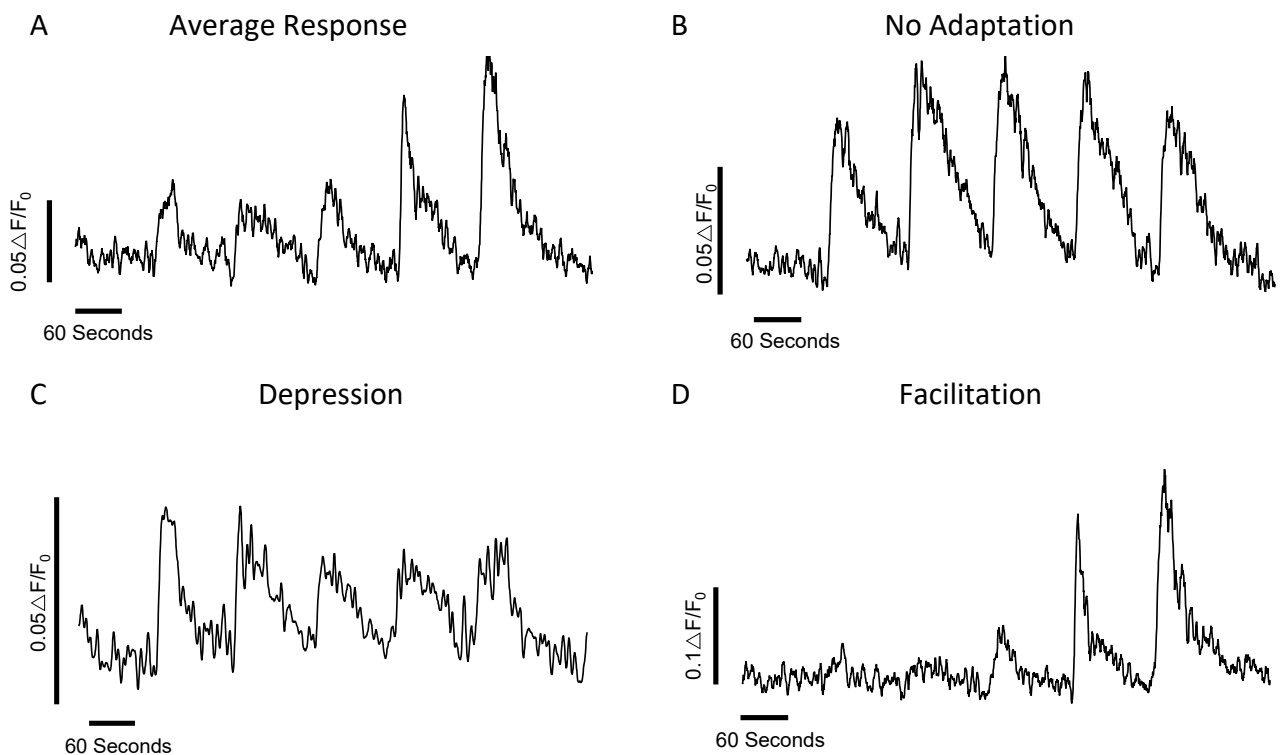


Figure 4.4.10: Diversity of adaptations to the alarm substance in the olfactory epithelium. (A) . The average response trace, with smoothing fits, to 5 presentations of alarm substance from neurons in the olfactory epithelium. Responses to the alarm substance display on average facilitation to subsequent presentations with an average adaptation index of -0.35. $N=4$ fish, 826 voxels. Manual sorting of the responding voxels identified the presence of, non-adapting (B), depressing (C) and facilitating (D) voxels to repeated presentations of the alarm substance. Of the 826 total responses identified, 77 (9.3%) displayed depression, 171 (20.7%) showed no adaptation and 373 (45.2%) were classified as facilitating.

The effects of the alarm substance across the many neural circuits it can modulate is not fully understood. We therefore wanted to investigate if any changes in the way the olfactory system is able to function can be detected before and after exposure to the alarm substance. To investigate this, I amended the experimental design such that five applications of food were applied anterior to the nose of the fish, followed by a single application of the alarm substance and then a further five applications of the food stimulus. On average, responses were seen to all 10 presentations of food odorant, suggesting the olfactory system is still sensitive to other stimuli after exposure to the alarm substance (figure 4.4.11).

Figure 4.4.11: The Olfactory System Remains Sensitive After Alarm Substance Exposure.

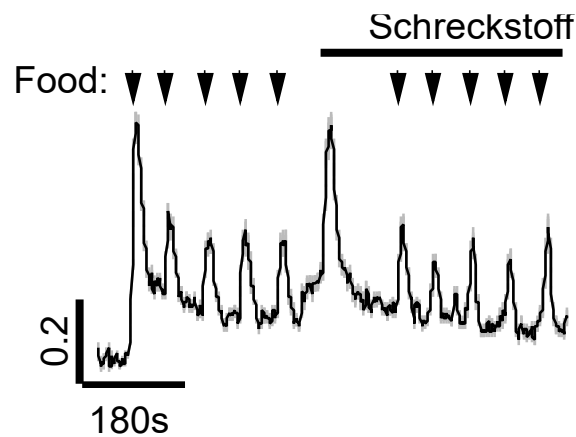


Figure 4.4.11: The olfactory system remains sensitive after alarm substance exposure. The average response trace, with smoothing fits, to 5 presentations of food odorant followed by a single larger exposure to the alarm substance. A final 5 presentations of food odour were then applied to the fish. The average response clearly demonstrates that the olfactory system is still sensitive to food odour after exposure to schreckstoff. Shadows represent SEM. N=6 fish.

The average response amplitude to the food odorant was reduced after schreckstoff exposure and the amount of adaptation seen decreased from an AI of 0.53 before exposure to AS to an AI of 0.11 after ($p < 0.05$, $n = 6$ fish). Because the whole population of neurons depresses on average, the above result can be explained by continued depression of responses to food odour rather than inhibition of response to food by Schreckstoff application. To rule this out, we have analysed the effect of Schreckstoff in each adapting class. We demonstrated that the inhibitory effect of the alarm substance was observed in facilitating and non-adapting terminals and therefore cannot be explained by depression of food responses which may have been present without the addition of alarm substance (figure 4.4.12). These results demonstrate that alarm substance strongly inhibits the responses of the olfactory neurons to other odours.

Figure 4.4.12: The Effect of Alarm Substance on Food Odour Responses

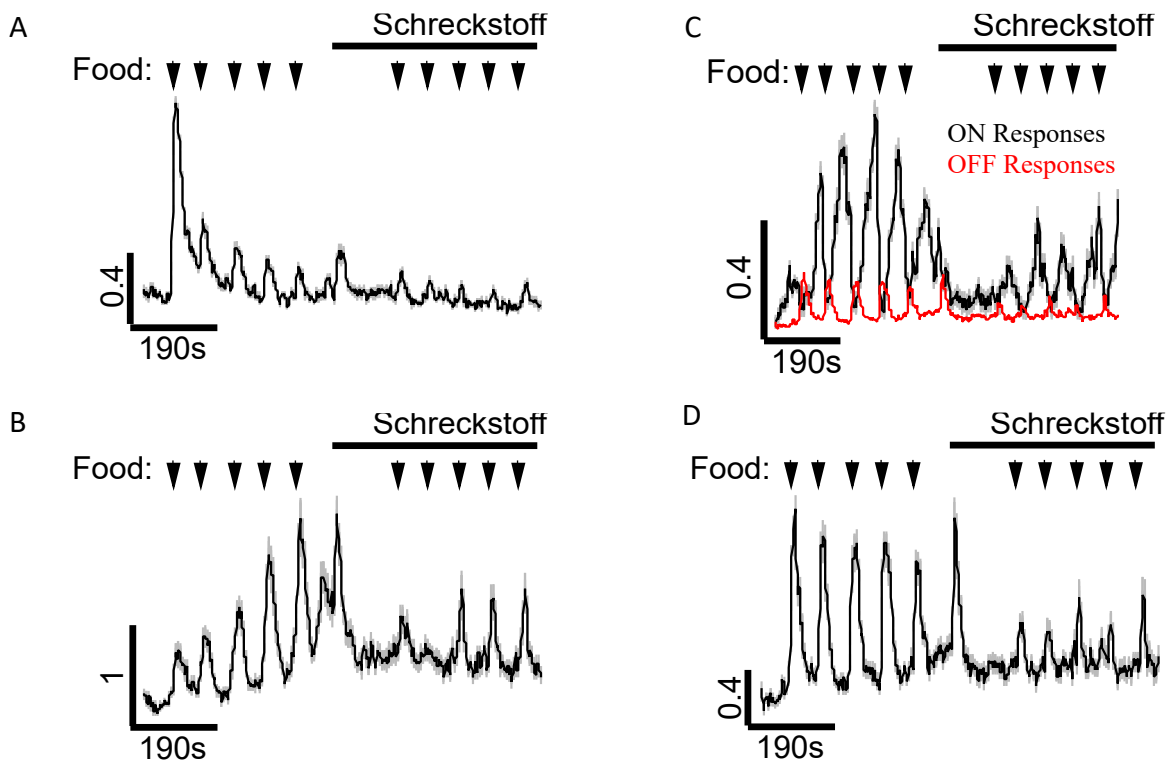


Figure 4.4.12: The effect of alarm substance on food odour responses. The average traces, with smoothing fits, to neurons in the olfactory bulbs responding to 5 presentations of food odorant followed by a single larger exposure to the alarm substance. A final 5 presentations of food odour were then applied to the fish. All responding voxels were concatenated and manually sorted to select for depressing (A), facilitating (B), 'OFF' responding cells (C) and non-adapting cells (D) to the first 5 presentations of food. The full-length traces were then averaged to identify the effects of alarm substance on each of these sub-groups. N=6 fish. Shadows represent SEM.

Mechanisms of Olfactory Sensitisation.

Sensitisation is a phenomenon which had not yet been described in the olfactory bulbs. In the retina, sensitisation is regulated by adaptation of GABAergic interneurons onto the sensory neurons. To dissect the mechanism behind sensitisation in the olfactory bulbs, we applied the GABA_A receptor inhibitor, PTZ, to 5 days post-fertilisation fish to block centrifugal inhibition from the granule cells onto the mitral cells. Five applications of food odorant were first applied before exposing the fish to PTZ. After application and a 10-minute incubation period,

a further five food applications were presented to the fish in a second recording. Both datasets were reduced by selecting every n^{th} trace to give a dataset of 5000 traces in order to aid with data handling and prevent memory capacity errors. The traces were manually sorted to select for traces displaying facilitation and all other responding traces. 610 responding voxels were identified to the food stimulus before PTZ exposure compared to 1511 responding voxels after PTZ exposure. The average trace after PTZ displayed a larger adaptation index than before PTZ was applied (figure 4.4.13).

Figure 4.4.13: The Effect of PTZ on Responses to Food Odour Application

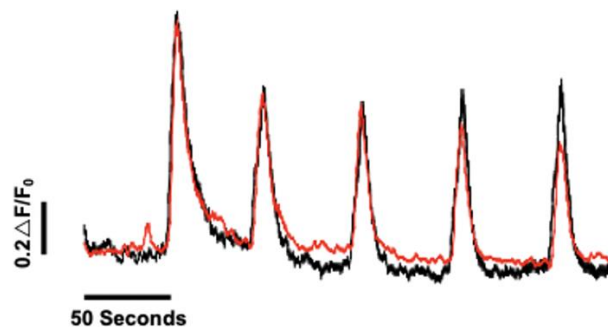
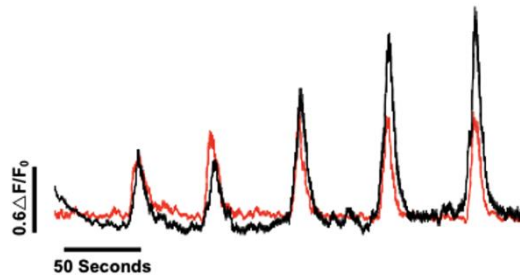


Figure 4.4.13: The effect of PTZ on responses to food odour application. The average response trace, with smoothing fits, from the responding traces manually sorted from the refined 5000 voxel dataset from neurons in the olfactory bulbs to 5 presentations of food odour delivered before (black trace) or after (red trace) PTZ exposure. The average response after PTZ exposure demonstrates a slightly larger adaptation index. $N=10$ fish.

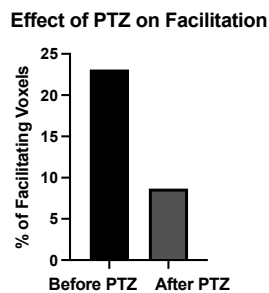
The facilitating traces were identified and separated out from the analysis. The average response trace demonstrated that facilitating traces before PTZ exposure showed a higher degree of sensitisation (figure 4.4.14(A)). In addition, before PTZ exposure, 23.11% of responding voxels demonstrated a facilitation, whereas after PTZ exposure, just 8.67% of voxels demonstrated a facilitation (figure 4.4.14(B)). The adaptation index of these voxels also increased from -0.45 before PTZ to -0.29 afterwards (figure 4.4.14(C)).

Figure 4.4.14: PTZ exposure decreased the number and increased the adaptation index of facilitating voxels.

A



B



C

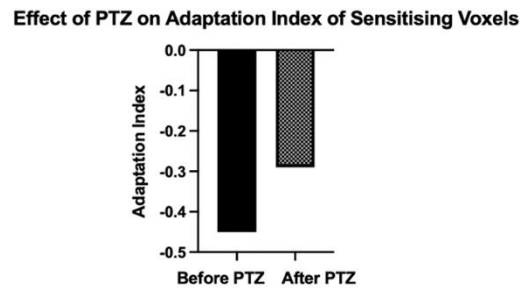


Figure 4.4.14: PTZ exposure decreased the number and increased the adaptation index of facilitating voxels. (A) The average response trace, with smoothing fits, from facilitating neurons in the olfactory bulbs to 5 presentations of food odour, before (black) and after (red) exposure to PTZ. Facilitating voxels were manually selected and plotted to create the average trace. $N=10$ fish. (B) The % of facilitating voxels decreased from 23.11% of responding traces before PTZ exposure to just 8.67% of voxels after PTZ exposure. (C) In addition to this, the adaptation index of these facilitating voxels increased from -0.45 before PTZ exposure to -0.29 after PTZ exposure.

Despite this, I was hesitant to accept these results as they were taken from 2 separate recordings which may have had mild planar differences and it wasn't possible to track changes within the same cell between the two recordings. As a result, I repeated the experiment once more as a single continuous recording, with 5 applications of food, a single prolonged application of PTZ into the imaging chamber followed by a 10-minute incubation period, and a final 5 applications of food odour. The 10-minute incubation period was excluded from the

analysis. This method allowed us to identify facilitating voxels to the first 5 applications of food odour and track changes to their adaptation to the second set of odour applications after PTZ exposure. Analysis identified that cells displaying facilitation prior to PTZ application displayed an average AI of -0.37, however after application this increased to a depressing AI of 0.29 (figure 4.4.13).

Figure 4.4.15: The Effect of PTZ on Olfactory Sensitisation.

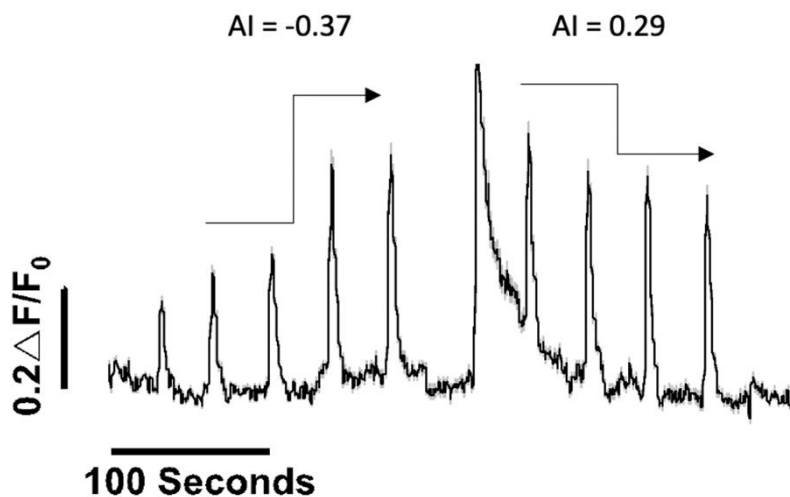


Figure 4.4.15: The effect of PTZ on olfactory sensitisation. The average response trace, with smoothing fits, for neurons which exhibited facilitation to the initial 5 presentations of food odour. After the first 5 presentations of food odour, PTZ was added to the imaging chamber and a further 5 presentations of food odour applied after a 10-minute incubation period. PTZ application and the incubation period was removed from the analysis. The average response trace demonstrates facilitating voxels show an adaptation index of -0.37 to the food odorant before PTZ exposure. After exposure, these voxels stop facilitating and begin to depress, with an AI = 0.29. N=2 fish. Shadows represent SEM.

4.5 Effect of Olfactory Input on Tectal Processing

It was now evident from experiments I had already completed that different olfactory stimuli both evoke different levels of adaptation in the olfactory bulbs and alter the spontaneous activity in the optic tectum to differing levels. The next logical question to then ask was what effect does this change in spontaneous activity due to olfactory input have on the way in which visual information is being processed?

To investigate this, 10-17days post-fertilisation *tg(Xla.Tubb:GCaMP3)* larvae were immobilised in 3.5% agarose and mounted into our custom-built chamber. A small moving spot visual stimulus similar to that used in the behaviour experimentation which would visually mimic prey was projected onto the side of the chamber along the visual field of the left eye (figure 4.5.1). The moving dot passed along the chamber wall 4 times before a 30-second pause. The stimulus would then repeat for a total of 10 repeats.

Figure 4.5.1: Imaging Chamber for Application of Olfactory and Visual Stimuli

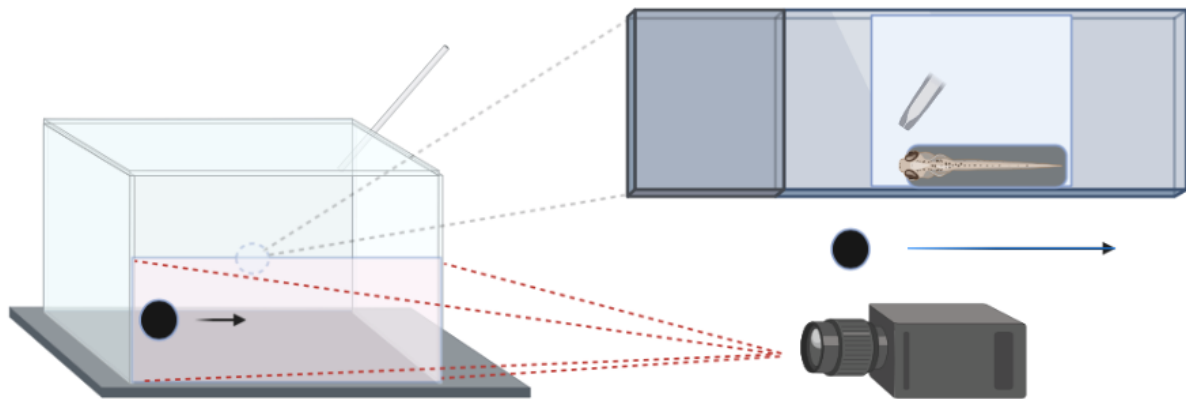


Figure 4.5.1: Imaging chamber for application of olfactory and visual stimuli. An Optoma PK320 projector connected to a Linux laptop was used to apply moving spot visual stimuli onto the wall of the imaging chamber across the visual field of the left eye. Fish were mounted onto a coverslip in 3.5% agarose with the agarose removed from the nose to allow for olfactory stimuli to be applied via glass pipette. The coverslip was placed onto a glass slide with 2 magnets attached on the posterior to attach onto magnets mounted on the base of the imaging chamber. This allowed for fish to be raised from the base of the imaging chamber to improve visual stimulation.

We first wanted to conduct this experiment without any olfactory stimulation thus to gauge the basal levels of processing across the different layers of the tectum. After conducting experiments, we once more conducted voxel wise analysis, with the focus being on the neuropil of the optic tectum as this is the region containing most synapses and input from other brain areas. The data demonstrated an adaptation across the neuropil of the optic tectum as a whole. This is demonstrated in figure 4.5.2 below. Here we can see that after the

first 3 repeats of the moving ball have concluded, the responses present for repeats 4 through 10 remain approximately equal. The responses to repeats 4 and 5 were combined to give an average response over this epoch and the same was conducted for repeats 6 and 7. These responses display no significant difference in the amplitude of response or adaptation in this period.

Figure 4.5.2: Tectal Responses to a Moving Ball Visual Stimulus Adapt Over Time.

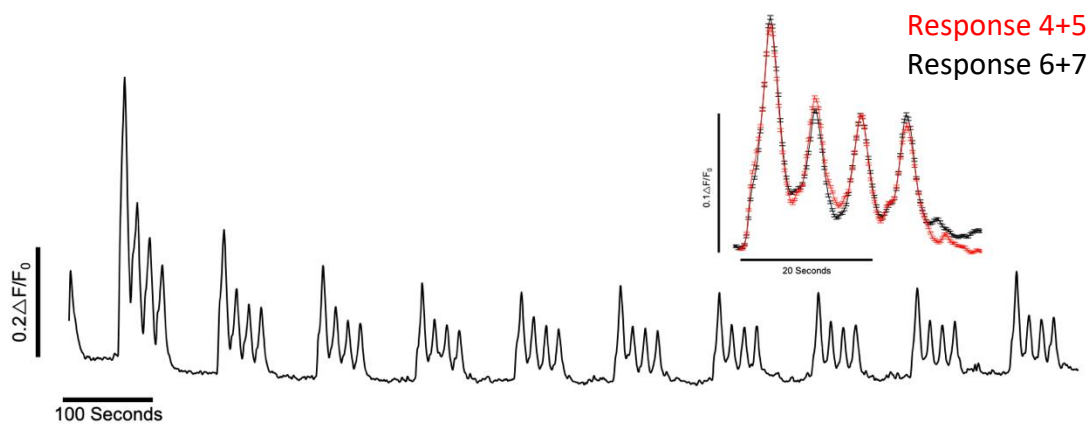


Figure 4.5.2: Tectal responses to a moving ball visual stimulus adapt over time. Average response trace, with smoothing fits, obtained from the right neuropil of the optic tectum in response to 10 repeats of 4 presentations of a moving dot stimulus. The tectal response across the neuropil adapts over time showing on average a depression. Responses to our repetitive stimulus showed adaptation both between repeats of the stimulus within each set and between sets. The adaptation plateaued after the first 3 sets of responses with the amplitude of response and level of adaptation becoming consistent between repeats 4 through 10. Responses to repeats 4+5 (red trace) and responses 6+7 (black trace) were combined to give an average response in this period to the stimulus. No differences in the response amplitude or adaptation could be seen in this period.

Further dissection of the data demonstrated that in the retinal ganglion cell input receiving layers of the stratum opticum and stratum fibrosum et griseum, we see a lesser adaptation than in the output layer of the stratum periventriculare. This would suggest that the tectum can function to filter incoming visual information (Figure 4.5.3). Once again, no significant difference was seen between responses for repeats 4 and 5 of the stimulus and responses to repeats 6 and 7.

Figure 4.5.3: Different Layers of the Optic Tectum Display Differing Levels of Adaptation.

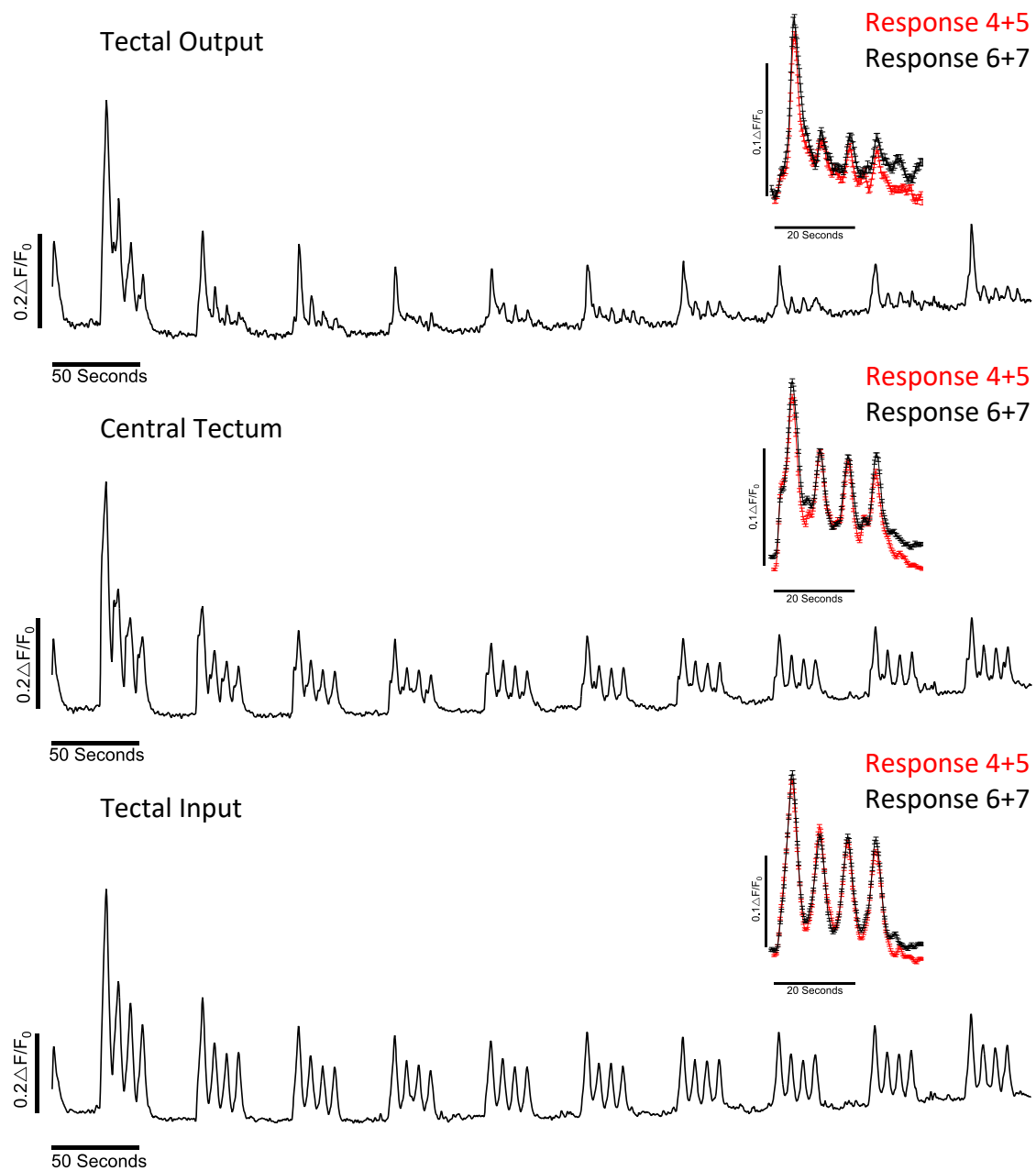


Figure 4.5.3: Different layers of the optic tectum display differing levels of adaptation. Average response trace, with smoothing fits, from the right neuropil of the optic tectum in response 10 repeats of 4 presentations of a moving dot stimulus. The tectal response across the neuropil adapt over time. The neuropil was separated into three equal-sized portions across the lateral-medial axis to compare the level of adaptation in the different layers of the neuropil. Responses to our repetitive stimulus showed adaptation across all three analyses both within each set and between sets of repeats. The greatest level of adaptation occurred in the most medial section of the neuropil, containing the stratum periventriculare, responsible for output from the tectum, suggesting the tectum acts to filter visual information. Once more, responses to

repeats 4+5 (red trace) and responses 6+7 (black trace) were combined to give an average response in this period to the stimulus. No differences in the response amplitude or adaptation could be seen in this period in any of the 3 layers.

How does olfaction effect processing of visual information in the optic tectum?

We hypothesised that during bimodal stimulation, the amount of adaptation, in particular in the SPV would decrease as the stimulus may now be considered more important to the fish. To investigate this hypothesis, a second set of experiments were conducted where the same stimulus would pass across the visual field of the fish, but this time repeats 1 through 5 would not contain any olfactory stimulation whilst repeats 6 through 10 would align with a puff of food odour anterior to the nose of the fish as the ball begins to pass across the visual field. I then repeated the same analysis as conducted previously for data without the olfactory stimulus. The average response trace for the neuropil of the optic tectum again showed a similar level of adaptation between each set of repeats of the moving ball stimulus compared to the previous control experiment (figure 4.5.4). After application of the food odour, the first two sets of visual stimuli saw a slight reduction in the level of adaptation to the visual stimulus within each repeat however this was not as large as hypothesised and there was no change in the overall amplitude of the responses.

Figure 4.5.4: Effect of Olfaction on Visual Processing in the Optic Tectum

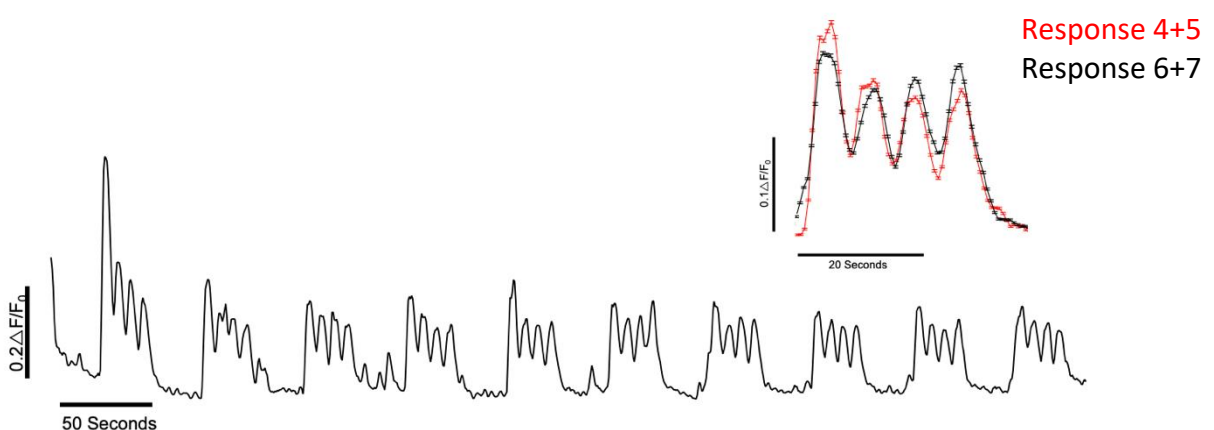


Figure 4.5.4: Effect of olfaction on visual processing in the optic tectum. Average response trace, with smoothing fits, obtained from the right neuropil of the optic tectum in response 10 repeats of 4 presentations of a moving dot stimulus. The tectal response across the neuropil adapt over time, showing on average a depression. Olfactory stimulation was applied as visual stimulus repeats 6 through 10 began.

Responses to repeats 4+5 (red trace) and responses 6+7 (black trace) were combined to give an average response in this period before and after olfactory stimulation was applied. The average response trace showed there was a slight reduction in adaptation, with less depression being seen between across presentations of the ball in repeats 6 and 7.

To investigate this further, once more we looked at the separate layers of the optic tectum to identify if certain layers exhibited a stronger change in adaptation than others. Our data showed that similar differences in adaptation were present across the medial, lateral and mid layers of the neuropil and displayed no major differences before or after olfactory stimulation (Figure 4.5.5).

Figure 4.5.5: Effect of Olfaction on Adaptation to Visual Stimulation Across Different Layers of the Optic Tectum

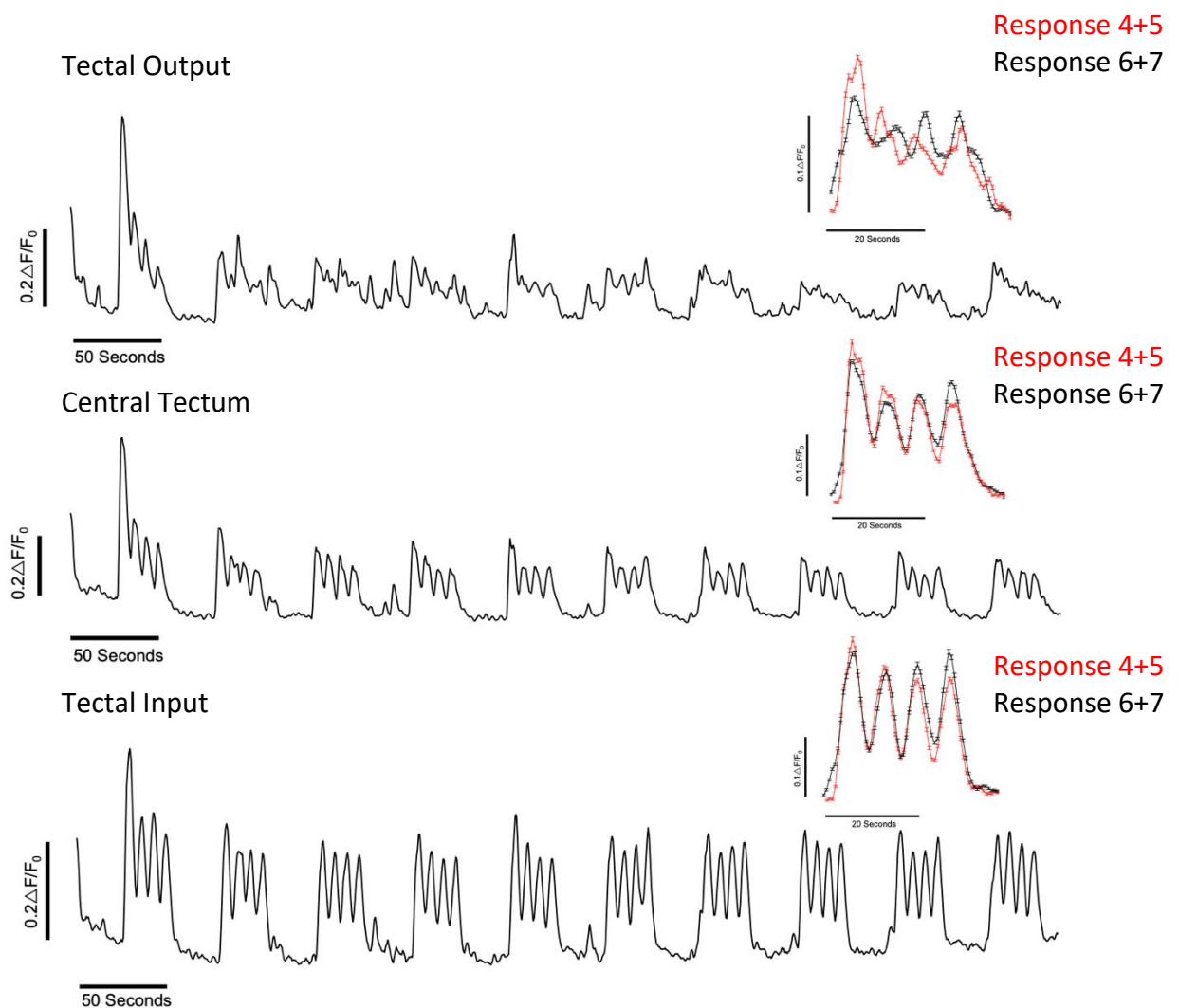


Figure 4.5.5: Effect of olfaction on adaptation to visual stimulation across different layers of the optic tectum. Average response trace, with smoothing fits, from the right neuropil of the optic tectum in response 10 repeats of 4 presentations of a moving dot stimulus. The tectal response across the neuropil adapt over time. The neuropil was separated into 3 equal sized portions across the lateral-medial axis to compare the level of adaptation in the different layers of the neuropil. Responses to our repetitive stimulus showed adaptation across all 3 analyses both within each set and between sets of repeats. Responses to repeats 4+5 (red trace) and responses 6+7 (black trace) were combined to give an average response in this period to the stimulus to identify any differences between responses before and after olfactory stimulation. Small differences in the level of adaptation were observed across each layer of the tectum, with a reduction in depression being seen. No change in the amplitude of the responses was observed.

4.6 Visual Responses in the Olfactory Bulbs

We have now investigated in depth how olfaction can affect visual processing in the optic tectum. What I was yet to consider is how visual input may or may not alter olfactory processing. My first investigation was to provide a visual stimulus and observe if we could see any responses in the olfactory bulbs or olfactory epithelium. We hypothesised that this would not be the case and once again the two systems would interact at the level of influencing predictions.

In these experiments, *tg(elavl3:GCaMP6s)* 5days post-fertilisation larvae were immobilised in 2% agarose and mounted in our custom-built visual stimulation chamber described previously in figure 4.5.1. The same small moving dot visual stimulus was applied to fish as 10 single pass repeats. 2-Photon calcium imaging of the olfactory bulbs (figure 4.6.1(A)) was conducted to record intracellular calcium level olfactory bulb neurons during the experiment. After experimentation, the responses within the olfactory bulbs were extracted in IgorPro using an automated analysis system which extracted the calcium data for individual soma (4.6.1(B)). All traces were compiled into a single dataset and manually sorted to select out visually responsive cells. This analysis demonstrated that visual stimulation was able to evoke responses in neurons of the olfactory bulbs (figure 4.6.1(C)).

Figure 4.6.1: Visually Responsive Cells Are Present in the Olfactory Bulbs.

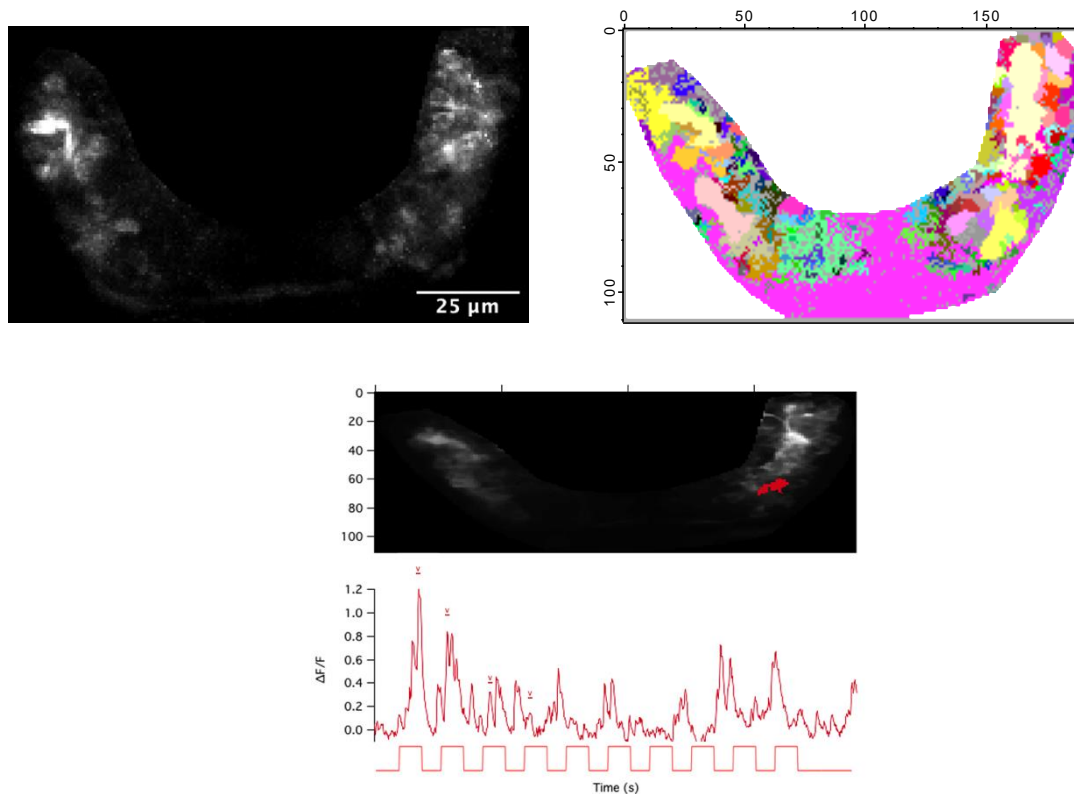


Figure 4.6.1: Visually responsive cells are present in the olfactory bulbs. 7days post-fertilisation *tg(Xla.Tubb:GCaMP3)* larvae were immobilised in 2% agarose and mounted in our visual stimulation imaging chamber. (A) Averaged Image of the field of view recorded for experimentation. The ventral telencephalon was removed from the analyses as this was known to contain visually responsive cells, leaving behind just the olfactory bulbs. (B) Automated analysis was used to identify individual soma and extract their calcium responses. Soma identification was not perfect, with sometimes multiple cell bodies being combined into a single ROI. (C) Individual soma were identified which displayed response to our moving ball visual stimulus. The stimulus consisted of 10 repeats of 4 presentations of the same moving dot stimulus used on visual experimentation in the optic tectum. In this example, responses can be seen to the first four presentations of the stimulus (marked by 'v') which then completely depress and become non-responsive by the fifth presentation.

In total, across 5 fish, 20 ROIs were identified, giving a mean of 4 visually responsive 'cells' per fish in a single plane of the olfactory bulbs. The average traces displayed a high level of adaptation, with responses seen clearly to the first 3 presentations of the visual stimulus but becoming less clear for the remainder of the experiment (figure 4.6.2).

Figure 4.6.2: Visual Responses to a Moving Ball Visual Stimulus Within the Olfactory Bulbs.

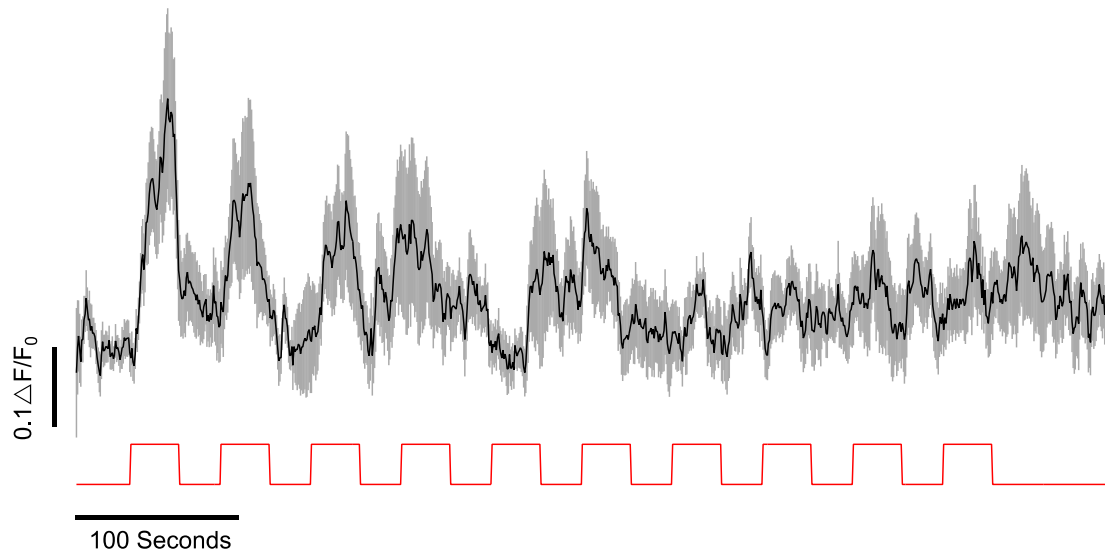


Figure 4.6.2: Visual Responses to a Moving Ball Visual Stimulus Within the Olfactory Bulbs. Average response trace of 20 ROI's identified across the olfactory bulbs of 4 *tg(Xla.Tubb:GCaMP3)* zebrafish larvae. The stimulus on/off trace was plotted below the average calcium response in red as an identifier for when responses should be seen. Shadows represent SEM.

As this experiment was conducted in a cytoplasmic GCaMP, even with the automated analysis, identifying individual cells within the olfactory bulbs was difficult. We therefore later repeated an experiment in the *tg(elavl3:H2B-GCaMP6s)* which demonstrates better definition of the olfactory bulb border as well as better expression in the olfactory epithelium. In this data, we once again saw cells within the olfactory bulbs responding to a visual stimulus and even small responses within the olfactory epithelium (figure 4.6.3).

Figure 4.6.3: Visual Responses Can Also Be Seen in the Olfactory Epithelium

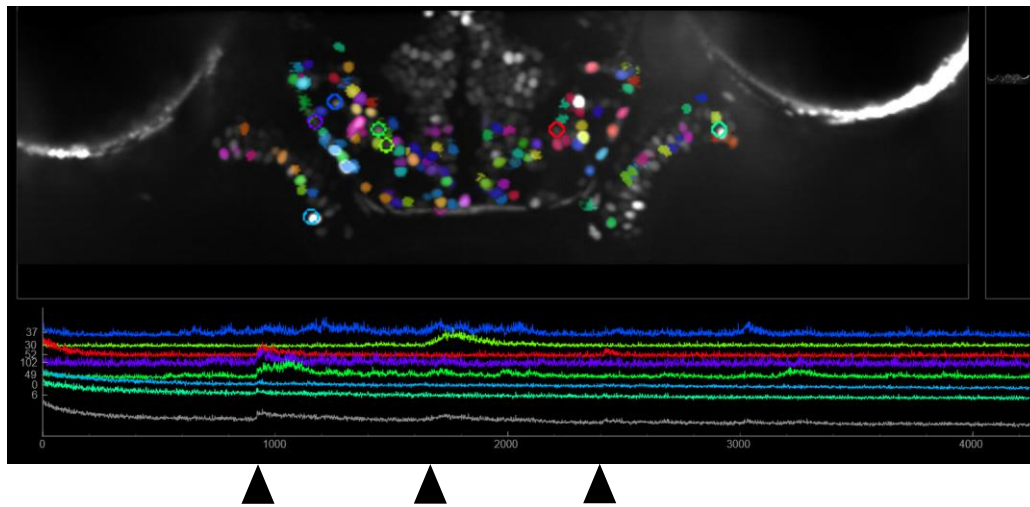


Figure 4.6.3: Visual responses can also be seen in the olfactory epithelium. Suite2p cell identification across the olfactory bulbs and epithelium. Fish were immobilised in agarose and mounted in our custom-built imaging chamber. The moving ball visual stimulus was passed across the visual field of the fish 3 times, as indicated by the black arrowheads. Responses were identified in 5 cells across the olfactory bulbs and 2 cells in the olfactory epithelium also displayed small responses to the first presentation. These cells are indicated on the average image plot by coloured circles. These experiments confirmed cells in the olfactory bulbs respond to visual stimulation.

As well as this, we also wanted to see if the visually responsive cells also had the capability to respond to olfactory stimuli. In addition, it would demonstrate if olfactory input had any effect on the visual responses. For this experiment, the moving ball was once again passed across the visual field of the fish, for the first half of the experiment no olfactory stimulus was present, but after the first 5 visual stimuli, a prolonged puff of food odorant was added to the chamber. These experiments demonstrated that in addition to the visually responsive cells previously discussed, some cells in the olfactory bulbs had the capacity to respond to the moving ball stimulus only after application of the olfactory stimulus (figure 4.6.4).

Figure 4.6.4: Olfaction Enhances Olfactory Bulbs Visual Responses.

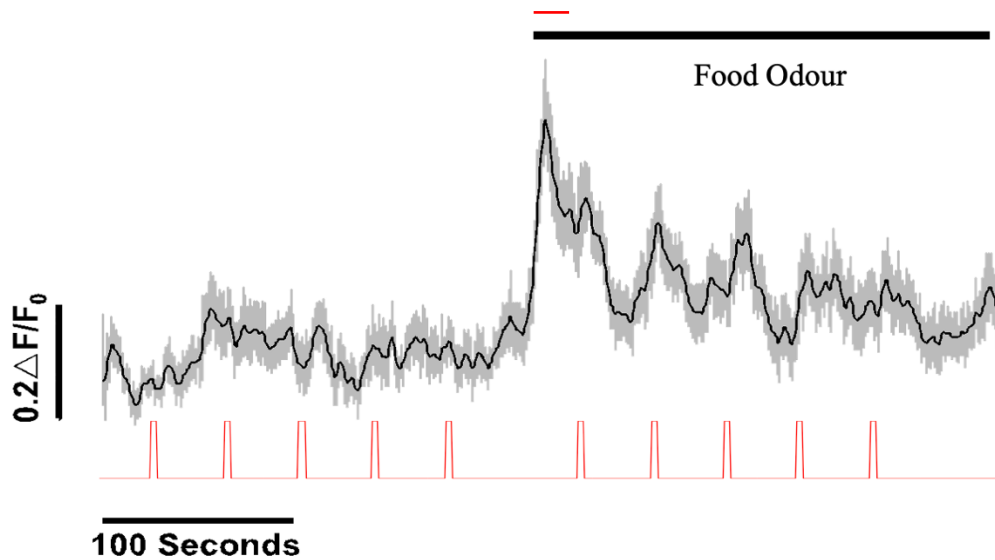


Figure 4.6.4: Olfaction enhances olfactory bulb visual responses. Average response trace, with smoothing fits, to cells identified across the olfactory bulbs which identified visual responses only after application of food odour was applied. Across 3 fish, a total of 7 ROIs were identified and averaged together to give the above response trace. These cells display no response to the first 5 presentations of the moving ball when no olfactory stimulus is present but do respond after food odour is applied halfway through the experiment. Shadows represent SEM. $N=3$ fish.

In addition to this, cells were noted that showed an increase in response amplitude to the visual stimulus after application of food odour (figure 4.6.5(A)). A further cell was identified which displayed possible OFF responses and sensitisation to the visual stimulus again after application of odour (figure 4.6.5 (B)). This diversity of responses requires further experimentation to explore in full.

Figure 4.6.5: Individual Cell Responses to a Moving Ball Visual Stimulus Within the Olfactory Bulbs Display Diversity.

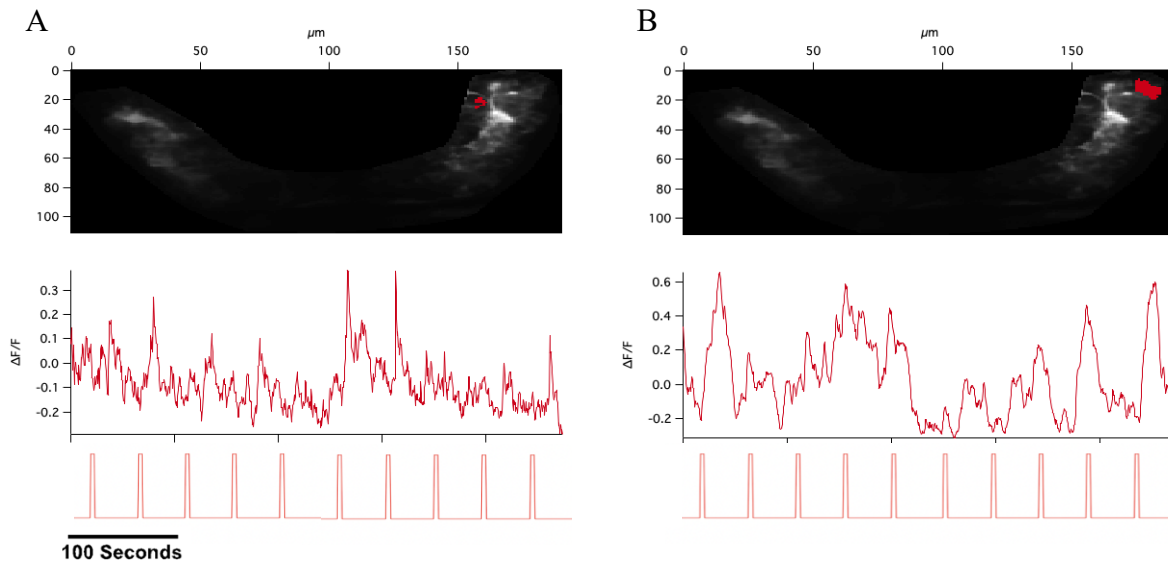


Figure 4.6.5: Individual cell responses to a moving ball visual stimulus within the olfactory bulbs display diversity. Analysis of individual cell responses in fish responding to visual stimuli after olfactory activation identified a diversity in the response profile. The cell responding in figure (A) displayed responses to the moving ball stimulus prior to olfaction but these responses then showed a possible initial increase in the amplitude of response after the food odour was delivered. The cell in response (B) may have been displaying facilitation to the stimulus, with the response amplitude increasing with each pass of the moving ball and appeared to also be responding to the end of the stimulus, much like an OFF response in the retina.

Further experimentation is required here to investigate this phenomenon further, across a larger population of fish to ensure responses are stimulus specific and not spontaneous events after undergoing olfaction.

4.7 Regulation of Changes in Spontaneous Activity

It became evident that olfactory input was altering the level of spontaneous activity in the optic tectum and thus likely changing the way in which visual information was being processed. In order to understand how this was occurring, I created a transgenic line of zebrafish expressing the jRGECO1a under the promoter for the astrocytic GLAST protein, a membrane glutamate transporter, *slc1a3b*.

I made the plasmid using the established gateway cloning protocol. The protocol involved the creation and ultimately fusion of P3E PolyA tail, PME jRGECO1a and P5E *slc1a3b*. Our lab already had a stock of P3E PolyA-tail and we received P5E *slc1a3b* as a gift from the Monk

Lab. I therefore had to first create PME jRGECO1a before the LR reaction to combine the constituent parts in a donor vector could take place. The 75ng/ μ l of plasmid was initially injected into 1 cell stage naere embryos alongside 50ng Tol2 and Phenol Red to visualise the injection material. Positively expressing embryos were selected at 2days post-fertilisation . At 10days post-fertilisation , larvae were imaged using 2-photon microscopy. Expression of our plasmid displayed a high degree of variety between embryos, but in the best cases, jRGECO1a expression could be seen in radial glia and astrocytes across the brain as demonstrated in figure 4.7.1 below.

Figure 4.7.1: Expression of *slc1a3b*:jRGECO1a Across the Zebrafish Brain.

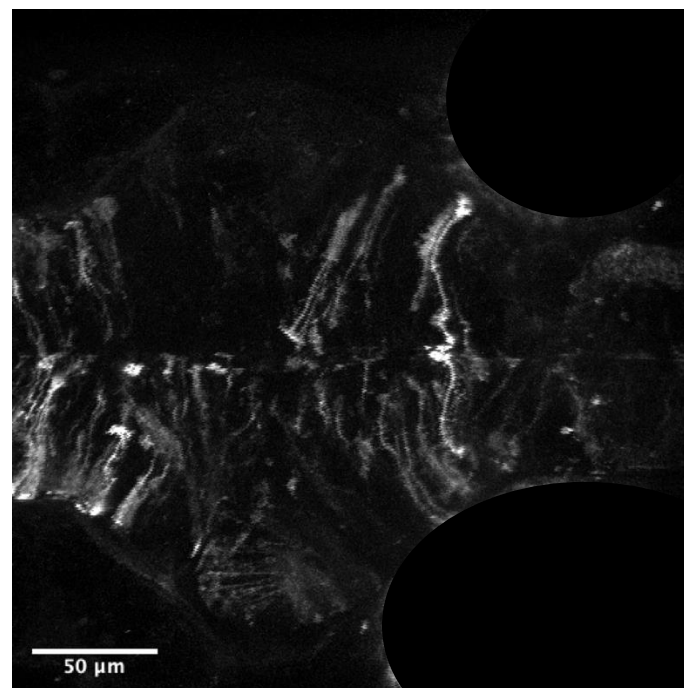


*Figure 4.7.1: Expression of *slc1a3b*:jRGECO1a across a section of the zebrafish brain after injection of *slc1a3b*:jRGECO1a into 1 cell stage fertilised embryo. Fish is orientated such that the head/anterior is on the right side of the field of view and posterior to the left. They eyes have been blacked out from the average image. The injection of *slc1a3b*:jRGECO1a led to excellent visualisation of radial glia and astrocytes across the zebrafish brain, including the optic tectum. Expression levels were diverse between fish, with the numbers of glia labelled ranging from 5-50 per fish. Scale bar = 50 μ m.*

Fish which displayed high levels of expression were then imaged further to record the intracellular levels of calcium. Following a similar experimental design to experiments in section 4.3, a period of spontaneous activity was recorded in astrocytes and radial glia in the optic tectum before providing olfactory stimulation with food odour. After stimulation, a further period of spontaneous activity was recorded to analyse the effects of olfaction on tectal astrocytes and glia. The results demonstrated the astrocytes and glia in the tectum displayed an increased level of activity when food odour was applied (figure 4.7.2).

Figure 4.7.2: Tectal Astrocytes Display Responses to Food Odour Delivery.

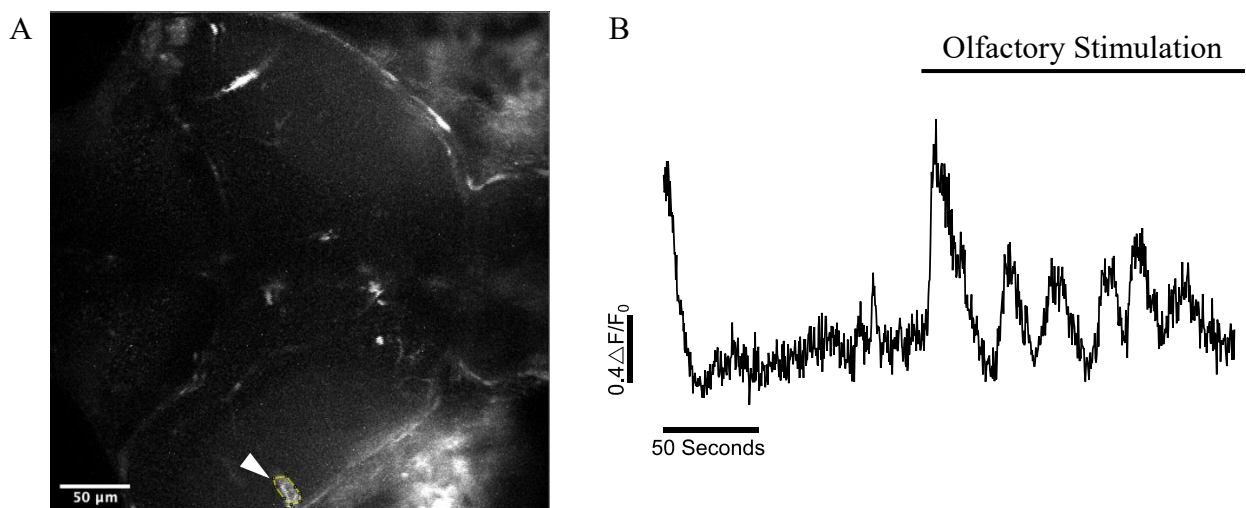


Figure 4.7.2: Tectal astrocytes display responses to food odour delivery. *Tg(slc1a3b:jRGECO1a)* fish were anaesthetised in mivacurium and mounted in 2% agarose. Agarose was removed from the nose of the fish. Fish were imaged using 2-photon microscopy to image calcium activity in astrocytes and glia for 5 minutes at 30Hz. Odorants were perfused into the chamber between 4000 and 5000 frames. There was no washout of odorant thus it remained in the chamber until the end of experimentation. Astrocytes were selected in imageJ, and calcium responses were exported into IgorPro for each cell. White arrow/yellow circle on figure A identifies the glial cell used in figure B.

To confirm that a correlation existed between neuronal and astrocytic activity within the optic tectum when olfactory stimuli were applied, the experiment had to be repeated in double transgenic *Tg(slc1a3b:jRGECO1a)(Elavl3:H2B-GCaMP6s)* larvae. 1 cell-stage injections were repeated on *tg(Elavl3:H2B-GCaMP6s)* fish and double transgenics were selected and imaged at 10days post-fertilisation using 2-photon microscopy. The same experimental protocol was

repeated whereby food odour was applied after a period of spontaneous activity was recorded. Our results showed that once again, food odour had the capacity to cause spiking activity in astrocytes. Direct comparison of neurons in the region where the cell appeared to project showed that increases in calcium after odour delivery between the neurons and astrocyte directly correlated (figure 4.7.3).

Figure 4.7.3: Spiking Between Tectal Neurons and Astrocytes Are in Anti-Phase After Olfaction.

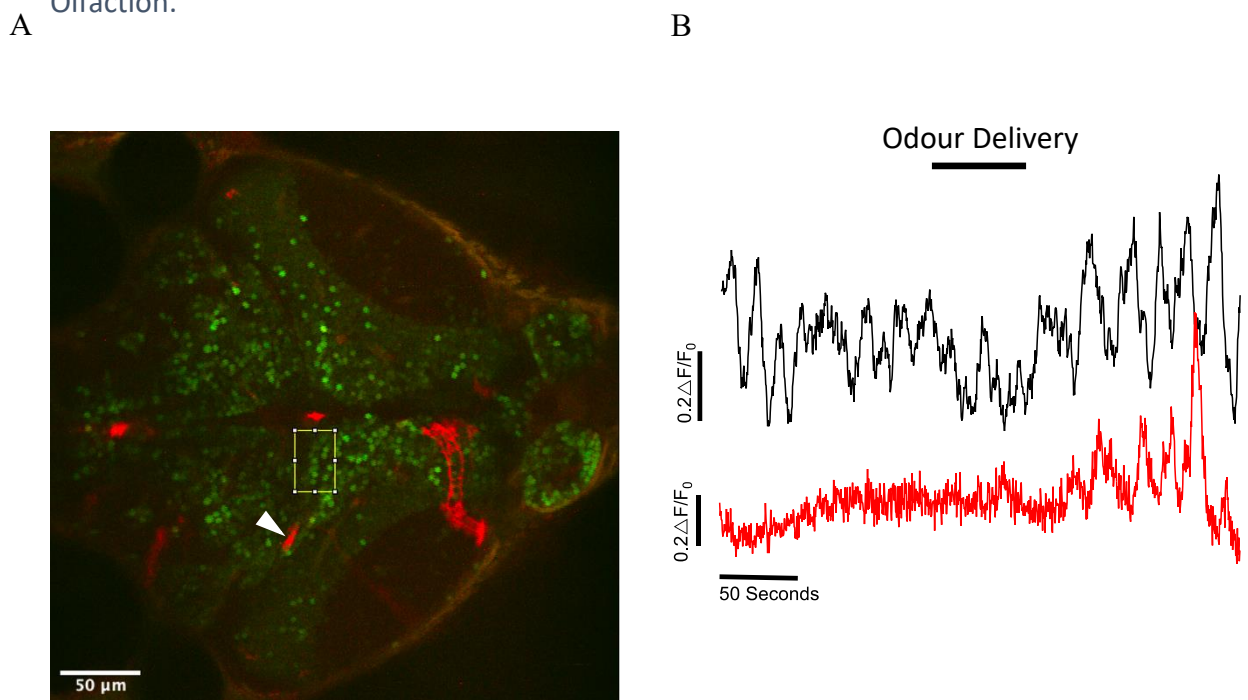


Figure 4.7.3: Spiking between tectal neurons and astrocytes show correlation after olfaction. *Tg(slc1a3b:jRGECO1a)(Elavl3:H2B-GCaMP6s)* fish were anaesthetised in mivacurium and mounted in 2% agarose. Agarose was removed from the nose of the fish. Fish were imaged using 2-photon microscopy to image calcium activity in astrocytes and glia for 5 minutes at 30Hz. Odorants were perfused into the chamber between 4000 and 5000 frames. There was no washout of odorant thus it remained in the chamber until the end of experimentation. Astrocytes were selected in imageJ, and calcium responses exported into IgorPro for each cell. Neuronal regions of interest were also identified based on the region of the brain the astrocytes appeared to project, and once again exported into IgorPro for further analysis. The white arrow in the figure indicates the astrocyte whose calcium responses are displayed in figure B (red trace). The yellow box displays the neuronal ROI analysed for figure B based the astrocytes expected trajectory (black trace). The two responses can be seen to be in anti-phase, whereby the peaks of the astrocyte's response correlate with the troughs in the neuronal trace.

Discussion

Neuronal Tracing Studies.

Our neuronal tracing studies aimed to demonstrate that neurons project from the olfactory bulbs to both the retina and the optic tectum. We were indeed able to achieve this and in addition, we identified a subset of tectal cells which project back to the retina. From what is now known from other studies in the field, we now have a system whereby the tectum acts to filter and process multi-modal information from the retina, lateral line, auditory system and terminal nerve. This information is then relayed onto pre-motor regions and areas of the brain which regulate behaviour. We now also hypothesise that this information is sent back to the retina whereby we expect some further modulation or error correction could occur on the local circuitry. This modulation may work alongside input from the olfactory system as demonstrated by previous work (Esposti *et al.*, 2013).

Further work will be needed to identify these cells and their axonal projections to trace where in the retina these may synapse, and what is the function of the synaptic interactions they form.

Can Olfaction Influence Visual Perception?

Our behavioural studies on visual and olfactory integration offered evidence that olfaction was able to alter behaviour to an ambiguous visual stimulus. In our experiment, by simply adding a food stimulus to the chamber, our visually ambiguous moving dot triggered an increase in hunting behaviour by the larvae. This was depicted by a greater amount of time spent in the central portion of the chamber where the stimulus was present and a decreased average distance to the visual stimulus. In contrast to this, when the alarm substance was added to the chamber, a different set of behaviours could be seen. After the initial freezing response was finished, fish preferred to stay around the borders of the chamber and there was an increased distance between the fish and the visual stimulus. When fish are hunting, the eyes converge to focus on prey to an angle greater than 65 degrees. As a result, we also used DeepLabCut to track the amount of hunting events each fish makes in the presence of alarm substance and food odour when the visual stimulus is within the chamber. We saw that in the presence of food odour, the trend of the data showed a slight increase in the number

of vergence events after addition of food odour and a decrease in the number of vergence events after addition of the alarm substance, however this was not statistically significant.

Our DeepLabCut data for tracking the tail angle of the fish did not provide any significant differences. We had initially hypothesised that we would be able to use this as a marker to display increased aversion in the alarm substance exposed fish. This is most likely not suitable however due to the fact that after exposure to the alarm substance, fish have been shown to swim in a more rigid manner, with fewer swim bouts and smaller angular tail movements (Jesuthasan *et al.*, 2020). As the fish also spent more time around the border, they were less likely to see the visual stimulus. Further experiments using closed-loop imaging on BonZeb (Guilbeault *et al.*, 2021) where the visual stimulus presents and moves along with the position of the fish may be able to provide more counts of visually driven behaviour in both conditions. The number of c-turns could then once more be calculated to test for escapes to the stimulus and perhaps also compared to the latency of swim bouts under each condition as a second marker for aversion. Zebrafish have also been shown to orient their tail in different ways to different behaviours. As mentioned, c-turns have been characterised as an aversive tail movement (approximately 60°) to quickly swim away in a different direction, but j-bends are used by the zebrafish as a re-orientating mechanism (approximately 20°) before striking for prey (Semmelhack *et al.*, 2014). At present, all of our tail analysis looks at the cumulative angle of the whole tail, but the j-bend only uses the most distal portion of the tail (Patterson *et al.*, 2013). Repeating the analysis but just look at the distal tip of the tail vs the whole tail may allow us to better separate the tail kinematics and characterise both hunting and aversive tail behaviours to the visual stimulus. We may also have been able to improve the amount of hunting we saw by changing the visual stimulus from a black dot on a white background projected onto the bottom of the chamber to a small ultraviolet dot projected from above. When fish are hunting, it has been shown that they use specialised ultraviolet cones in the retina for detection of prey. These have a specific spatial organisation within the retina which aids the fish in hunting in such a way that they attack prey from underneath (Yoshimatsu *et al.*, 2019). As a result, our stimulus may be better suited to project above the imaging chamber in order to better replicate how a zebrafish would hunt. Increasing the size of our population for the experiments and the resolution we recorded our behaviour at to improve the stability of tracking on DeepLabCut may both be sufficient to provide some statistical significance in

our results. I believe repeating our experiments with these ideas in mind would give us a clearer and more definitive view as to whether olfaction can modulate visual behaviours and/or perception.

At present, although some of our data points towards this being the case, we cannot conclude with certainty that this is the case. Work conducted previously demonstrated that the food based olfactory odourant methionine has the capacity to alter dopaminergic signalling in the retina (Esposti *et al.*, 2013, Maaswinkel and Li, 2003a). However, alongside research done by Koide *et al.*, it was shown that methionine does not activate the *gnrh3* pathway so the mechanism for this interaction is currently unknown (Koide *et al.*, 2018). If future experimentation can confirm that olfactory stimuli are able to evoke changes in visually driven behaviour, further work will also have to be carried out to investigate where along the visually circuitry this olfactory modulation takes place.

Vision and Olfaction May Integrate at the Level of Influencing Predictions.

As it is unclear how modulation of vision through olfaction could occur, we decided to investigate this at the level of changing predictions. The predictive coding framework explains that each sensory system creates estimates or priors of the environment (Friston, 2010). We hypothesised that the visual and olfactory systems may interlay some of their sensory information upon each other in order to provide a more accurate representation of the environment and thus alter these priors or predictions to better react to upcoming environmental changes. Spontaneous bursts of activity are commonly seen across the brain and appear to oscillate with up and down states of brain activity (Koren and Denève, 2017). This activity is therefore not completely random and instead exhibits unique spatiotemporal patterning meaning it can be used as a signature of predictive coding. We demonstrated that application of two behaviourally distinct olfactory stimuli were both able to change the level of spontaneous activity of numerous cells across the optic tectum, with some cells showing an increase in their neuronal activity and other cells showing decreases in their neuronal activity in response to application of olfactory stimuli.

In addition to this, through conducting non-linear reduction analysis using Laplacian eigenmaps, we also observed how the collective activity, projected to a lower dimensional space, changed with time throughout our experiments. Mapping of our calcium response traces from the optic tectum and habenula demonstrated that in the controls, the majority of our fish remained in a similar state of brain activity throughout the experiment, with the system not being affected by perfusion of E3. In contrast to this, most of the food and alarm substance experiments demonstrated very different results. A distinct shift could be seen amongst the location of the system before and after the olfactory stimulus was applied. This data provides evidence to support that we also saw a spatiotemporal shift in spontaneous activity, which agrees with the predictive coding framework. This data suggests that olfaction may be able to influence predictions in the visual system through changes in spontaneous activity. It was worth noting however that a couple of exceptions were present for each test group, e.g., a shift in activity could be seen in the control or not seen after olfaction. As a result of this, to confirm the result, I will aim to conduct some further experimentation to increase our sample size.

What remains unclear is what effect this altering of spontaneous activity has on visual processing and perception. We analysed the responses to a repetitive moving ball stimulus before and after application of an olfactory stimulus, and although perhaps a minor change in the adaptation could be seen, this was not substantial enough to be statistically significant and may have just been a result of a smaller population size when olfaction was added. My analysis done in this section only looked at the average of the tectum (or layers of) and little consideration was made to individual responding voxels. Our spontaneous activity experiments showed that some cells decreased their activity whilst other cells increased their levels activity. It may be that some individual voxels across the neuropil demonstrated reduced responses after olfaction whilst others displayed increased response amplitudes after olfaction. By averaging these together in our analysis, the result would be seeing little to no change as the effects may cancel each other out. I intend on further dissecting this analysis over the coming weeks to identify if this is the case or not.

Future work could also seek to identify if different stimuli, either visual or olfactory, could evoke a greater effect than what we saw in our experiments. It may also be that olfactory

stimulation can tighten receptive fields. Animals rely on olfaction to navigate through complex olfactory landscapes; therefore, it may be possible that this information is also used to alter visual receptive fields to aid with navigation.

Effects of Visual Stimulation of Olfactory Processing.

We had previously seen that vision and olfaction interact at the level of influencing spontaneous activity in the optic tectum, we therefore wanted to investigate if the same phenomenon was present in the olfactory bulbs. Upon investigating of this, we encountered surprising results. It became clear that visual stimuli evoke robust responses in cells across the olfactory bulbs and even some small responses could be seen in the olfactory epithelium. The presence of small responses in the olfactory epithelium was particularly surprising as we did not expect much integration or processing to occur here. We hypothesise that these responses are due to centrifugal input from other brain areas. The olfactory bulbs receive centrifugal input from the raphe, a set of serotonergic nuclei as well as the terminal nerve (Brunert *et al.*, 2016, Maaswinkel and Li, 2003a). As the terminal nerve originates in the olfactory bulbs however, it is unlikely to carry any visual information at this point. We therefore hypothesise that these responses are a form of regulatory input from the raphe. This could be tested by using a serotonin inhibitor and repeating the same experiments to investigate if responses are still present.

Further investigation will also be required to understand if visual stimuli have long-lasting effects on the level of spontaneous activity seen across olfactory cells as we saw in the optic tectum. It is also unclear how visual input may alter olfactory processing, and in turn, how this integration affects behaviour. Due to the time limitations of my project these are all questions I wanted to investigate during my PhD however unfortunately I was not able to do so.

Astrocytes May Regulate Changes in Spontaneous Activity in the Optic Tectum.

Our data showed that the integration of olfactory and visual was present across the brain. What we had yet to do was display any evidence of how this integration occurred. Work conducted by the Ahrens lab had already demonstrated a role for astrocytes in regulating neuronal activity in response to swim failures (Mu *et al.*, 2019) and given the extensive

network of connections astrocytes form across the brain, they would be functionally primed to be able to coordinate the activity of neurons across the sensory modalities. We therefore hypothesised that astrocytes and radial glia may be able to regulate neuronal changes across the brain to different sensory stimuli.

Early experimentation using our *slc1a3b:jRGECO1a* zebrafish line has identified that the application of olfactory stimuli also alters the level of calcium activity seen in radial glia and astrocytes across the zebrafish optic tectum. This may highlight an additional role for astrocytes in modulating neuronal activity. When both the astrocytes and neurons calcium activity were imaged simultaneously in our experiment, it was noted that calcium transients in both the astrocytes and neurons were locked in antiphase, suggesting an interaction may indeed be occurring between the two cell types.

Further experimentation is required to continue to investigate this correlation between astrocytic and neuronal activity to understand how the two are interacting and what effect this interaction has on sensory processing. Our analysis method involved estimation of the region of the tectum that we believed the astrocyte may be interacting with neurons in. I would like to in future analyse the synaptic activity of neurons in the optic tectum using the iGluSnFR synaptic glutamate reporter alongside an astrocytic marker. This would allow us to analyse more accurately if synaptic glutamate can be regulated by astrocytes during both visual and olfactory stimulation (Dürst *et al.*, 2019). At present, a pan-neuronal synaptic glutamate reporter has yet to be made but this would be something that could be very beneficial to the wider neuroscience community. Laser ablation of astrocytes or pharmacological inhibition of these across the brain may also be able to provide more definitive answers as to whether astrocytes are able to integrate information between sensory modalities and result in the changes in spontaneous activity observed in the optic tectum.

These early observations provide further support for the need to investigate the function of astrocytes in modulating neural circuits. Work from the Monk lab to identify a potential *bona fide* astrocyte in the zebrafish was used as a platform for this work and appear to be concurrent with that of the Ahrens lab demonstrating that astrocytes have the capacity to

modulate neuronal activity in the brain (Chen *et al.*, 2020, Mu *et al.*, 2019). We aim to hopefully now build on this further to investigate how and where this modulation may occur.

Different Behaviourally Relevant Olfactory Stimuli Evoke Different Adaptations.

Our results demonstrate that like in the retina, some olfactory stimuli evoke different forms of adaptation ranging from very strong depression to facilitation. In addition, attractive and aversive olfactory stimuli demonstrated differing numbers of depressing and facilitating cells.

Danger signals, like the alarm substance, elicit very fast behavioural effects alongside changes in neuronal computations to increase the organisms' sensitivity to threats in both adult zebrafish and younger larvae (Jesuthasan *et al.*, 2020). Larval zebrafish exhibit prolonged periods of immobility in response to schreckstoff exposure alongside widespread and prolonged activation of multiple brain regions. This includes but is not limited to the OBs, posterior tuberculum, lateral habenula, and superior raphe, even after stimulus removal (Jesuthasan *et al.*, 2020). As a result of this phenotype, we had expected that persistent exposure to the alarm substance would evoke stronger responses with each presentation (i.e., we should observe facilitation. Our data showed application of strongly aversive alarm substance led to a much greater number of facilitating cells than application of food odour. The alarm substance functions to act as a warning to nearby fish that a predator is nearby. Upon administering repeated presentations of alarm substance, this would likely be portrayed by this fish as increasing severity of the warning signal. As a result, facilitation to the stimulus would be expected as more information should be transferred regarding the importance of the sensory detection.

Food odour on the other hand displayed much fewer facilitating voxels than alarm substance and a greater diversity of depressing and non-adapting voxels. This caused us to question why different behaviourally relevant stimuli cause different levels of adaptation in sensory neurons. Food is an important stimulus that requires complex processing (Tabor *et al.*, 2004). The animal must be able to recognise the stimulus, localise where it is in the environment, before finally executing complex hunting behaviours. Therefore, a diversity of adaptations with their ability to optimise the neuronal response to future changes in the intensity of olfactory stimulation may be necessary. Conversely, the alarm substance does not require

such complex processing and the behavioural response is arguably much simpler compared to hunting (Kermen *et al.*, 2020). As a result of this, a simple single presentation may be sufficient for fast execution of the appropriate behavioural program (freeze response). It is plausible that this quick behavioural phenotype could be initiated by depressing cells across the olfactory bulbs. Those which display facilitation may then provide information on the severity of the danger at hand. This idea requires further investigation but nevertheless our data demonstrate that different behaviourally relevant stimuli display different forms of adaptation and therefore opposing forms of adaptations across different sensory modalities may play an important role in the processing of sensory information. In addition to this, it has also been shown that neuronal information for food and fear odours are sent to different brain regions. Food odours activate hypothalamic regions in the zebrafish brain to trigger these complex foraging behaviours whereas alarm substance has been shown to activate nuclei in the dorso-medial and ventral ventral telencephalon and the preoptic area (Kermen *et al.*, 2020, Faustino *et al.*, 2017). It is therefore not surprising that differences in the early processing and short-term plasticity to these stimuli can also be seen.

The synaptic plasticity and memory hypothesis asserts that activity dependent plasticity is able to encode memories and facilitate storage within the brain (Takeuchi *et al.*, 2014, Ryan *et al.*, 2015). The fact that two behaviourally different stimuli in our experiments assert very different short term plasticity patterns in the olfactory system is concurrent with the information that may be carried in these differences in short term plasticity within these early synaptic responses that in turn may aid olfactory or neural processing as a whole as well as memory formation in higher centres (Zhou *et al.*, 2020).

Both adaptation and facilitation have been researched in the retina and cortex in both zebrafish and mice (Nikolaev *et al.*, 2013, Kastner and Baccus, 2011, Heintz *et al.*, 2022). In the retina, pharmacological block of GABAergic feedback using PTZ converted facilitating bipolar cell terminals into depressing ones (Nikolaev *et al.*, 2013). This led to the conclusion that facilitation in sensory cells arises as a result of depression of the inhibitory interneurons. Application of PTZ in our own experiments conducted for figure 4.4.14 showed that PTZ was able to conduct a partial inhibition of facilitation in the olfactory system but by no means complete. The data displayed in the subsequent figure was more convincing and concurrent

with mechanisms displayed for facilitation in the retina. However, additional experimentation will be required to increase our n number and be sure of the results. Furthermore, identifying facilitating synapses in the olfactory epithelium suggests a different mechanism of facilitation may be present in the olfactory system as there is no GABAergic feedback from granule cells or periglomerular cells to the olfactory epithelium. More direct methods such as expression of halorhodopsin in the inhibitory granule cells and silencing by light may give more conclusive results as to whether other mechanisms contribute to facilitation within the olfactory bulb but closer analysis at the synaptic level may be required to investigate facilitation in the olfactory epithelium.

Challenges Faced

As with any PhD project, I encountered problems throughout the duration of my candidature. Firstly, regarding zebrafish, almost all experimentation was conducted on *tg(Xla.Tubb:GCaMP3)* or *tg(elavl3:H2B-GCaMP6s)* lines. Although brighter at younger ages, the *elavl3/HuC* promoter expresses a much dimmer level of fluorescence beyond 10days post-fertilisation. As a result, there was some inconsistency in the brightness of fish we imaged around this age resulting in variation in cell counts in our spontaneous activity experiments. In general, we tried to use the *tg(elavl3:H2B-GCaMP6s)* in experiments on fish under 10days post-fertilisation and the *tg(Xla.Tubb:GCaMP3)* line for experiments over 10days post-fertilisation but this was not always possible.

Aside from zebrafish lines, my project was severely impacted by COVID-19. Being a collaboration project, I was due to spend the first 2 years of my project working at the University of Sheffield (September 2018-September 2020) and the final 2 years in Singapore. Unfortunately, due to the pandemic, the Singapore borders were shut and access to the country was not possible in September 2020. At this point, I was not able to obtain a definitive date for when I would be able to move to Singapore and my rental property in Sheffield reached the end of its tenancy. Given the uncertainty about when I would be able to go to Singapore, I had no choice but to move back in with my parents in South Derbyshire and commute to the lab which was both logistically difficult and expensive, impacting how often I would be able to attend the lab. Furthermore, due to being a part of a large laboratory in

Sheffield, access hours were restricted, and an attendance rotor was put in place for days when we could come access the lab for experimentation, once again restricting the frequency at which I could conduct experiments.

Finally in July 2021 I was able to move to Singapore and begin work in the Jesuthasan lab at A*STAR. Sadly, on my first day in the lab, upon turning on the 2-Photon system we discovered the laser was no longer operational and required replacing. Due to both impacts from COVID-19 and the Suez Canal blockage, a replacement laser took until March 2022 to arrive – severely impacting my experimentation timeline. A second 2-photon system was being built which we could access at Nanyang Technological University however the laser purchased for this system was faulty and imaging was sub-optimal. I was able to gain valuable experience however by assisting in the development of this system and troubleshooting various engineering problems throughout the process.

Conclusions

Despite the challenges faced, we have been able to demonstrate multiple findings across this thesis. Firstly, I have demonstrated that olfactory stimulation is able to alter how visual stimuli are perceived by fish, with the same stimulus being perceived as aversive or a potential source of food with just a change of olfactory cue. Mechanistically, we have then shown that olfactory stimuli can influence predictions in the main visual processing centre, the optic tectum. Additionally, visual stimulation can be seen to evoke responses in olfactory cells in the olfactory bulbs and olfactory epithelium. Further experimentation will be required to understand what effect this sensory integration has on perception.

Finally, we have demonstrated that olfactory adaptations are both present and diverse to repetitive stimulation. Levels of depression and facilitation vary between different behaviourally relevant olfactory cues suggesting that opposing forms of adaptations across different sensory modalities may play an important role in the processing of sensory information.

Visual-olfactory integration is both present and diverse across the zebrafish brain and is likely essential in the optimisation of processing in both sensory systems.

References

- Ahuja, G., Sb, N., V, Z., V, S., Kowatschew D, Y, O. & Si, K. 2015. Kappe neurons, a novel population of olfactory sensory neurons. *Scientific Reports*, 4.
- Akerboom, J., Chen, T.-W., Wardill, T. J., Tian, L., Marvin, J. S., Mutlu, S., Calderón, N. C., Esposti, F., Borghuis, B. G., Sun, X. R., Andrew Gordus, Orger, M. B., Portugues, R., Engert, F., Macklin, J. J., Alessandro Filosa, Aggarwal, A., Kerr, R. A., Ryousuke Takagi, Kracun, S., Shigetomi, E., Khakh, B. S., Baier, H., Leon Lagnado, Wang, S. S.-H., Bargmann, C. I., Kimmel, B. E., Vivek Jayaraman, Svoboda, K., Kim, D. S., Schreiter, E. R. & Looger, L. L. 2012. Optimization of a GCaMP Calcium Indicator for Neural Activity Imaging. *Journal of Neuroscience*, 32.
- Akerboom, J., Calderón, N. C., Tian, L., Wabnig, S., Prigge, M., Tolö, J., Gordus, A., Orger, M. B., Severi, K. E., Macklin, J. J., Patel, R., Pulver, S. R., Wardill, T. J., Fischer, E., Schüler, C., Chen, T.-W., Sarkisyan, K. S., Marvin, J. S., Bargmann, C. I., Kim, D. S., Kügler, S., Lagnado, L., Hegemann, P., Gottschalk, A., Schreiter, E. R. & Looger, L. L. 2013. Genetically encoded calcium indicators for multi-color neural activity imaging and combination with optogenetics. *Frontiers in Molecular Neuroscience*, 4.
- Aleström, P., D'angelo, L., Midtlyng, P. J., Schorderet, D. F., Schulte-Merker, S., Sohm, F. & Warner, S. 2020. Zebrafish: Housing and husbandry recommendations. *Lab Anim*.
- Altieri, N. 2014. Multisensory integration, learning, and the predictive coding hypothesis. *Frontiers in Psychology*, 4.
- Amsellem, S., Höchenberger, R. & Ohla, K. 2018. Visual-Olfactory Interactions: Bimodal Facilitation and Impact on the Subjective Experience. *Chemical Senses*, 43, 329-339.
- Angelaki, D., Gu, Y. & Deanegelis., G. C. 2009. Multisensory integration: psychophysics, neurophysiology, and computation. *Current Opinion in Neurobiology*, 19, 452-458.
- Antinucci, P. & Hindges, R. 2018. Orientation-selective retinal circuits in vertebrates. *Frontiers Neural Circuits*.
- Avanesov, A. & Malicki, A. J. 2010. Analysis of the retina in the zebrafish model. *Methods in Cell Biology*, 153-204.
- Axel, R. 1995. The molecular logic of smell. *Scientific American*, 273, 154-159.
- Baden, T., Euler, T. & Berens, P. 2020. Understanding the retinal basis of vision across species. *Nature Reviews Neuroscience*, 21, 5-20.
- Bannister, L. 1965. The fine structure of the olfactory surface of teleostean fishes. *The Quarterly Journal of Microscopical Science*, 106, 333-342.
- Behrens, U. & Wagner, H. 2004. Terminal nerve and vision. *Microscopy research technique*, 65, 25-32.
- Bergmann, K., Santoscoy, P. M., Lygdas, K., Nikolaeva, Y., Macdonald, R. B., Cunliffe, V. T. & Nikolaev, A. 2018. Imaging Neuronal Activity in the Optic Tectum of Late Stage Larval Zebrafish. *Journal of Developmental Biology*, 6.
- Biechl, D., Tietje, K., Ryu, S., Grothe, B., Gerlach, G. & Wullimann, M. F. 2017. Identification of accessory olfactory system and medial amygdala in the zebrafish. *Sci Rep*, 7, 44295.
- Bilotta, J. & Saszik, S. 2001. The zebrafish as a model visual system. *International Journal of Developmental Neuroscience*, 19, 621-629.
- Bodick, N. & Levinthal, C. 1980. Growing optic nerve fibers follow neighbors during embryogenesis. *PNAS*, 77, 4374-4378.

- Bollmann, J. 2019. The Zebrafish Visual System: From Circuits to Behavior. *Annual Reviews Visual Science*, 5, 269-293.
- Brunert, D., Tsuno, Y., Rothermel, M., Shipley, M. T. & Wachowiak, M. 2016. Cell-Type-Specific Modulation of Sensory Responses in Olfactory Bulb Circuits by Serotonergic Projections from the Raphe Nuclei. *Journal of Neuroscience*.
- Buchanan, T., Tranel, D. & Adolphs, R. 2003. A specific role for the human amygdala in olfactory memory. *Learning and Memory*, 10, 319-325.
- Burg, E. V. D., Olivers, C. N. L., Hickey, C. & Theeuwes, A. J. 2008. Pip and pop: nonspatial auditory signals improve spatial visual search. *Journal of Experimental Psychology: Human Perception Performance*, 34, 1053-1065.
- Burg, E. V. D., Talsma, D., Olivers, C. N., Hickey, C. & Theeuwes, A. J. 2011. Early multisensory interactions affect the competition among multiple visual objects. *Neuroimage*, 55, 1208-1218.
- Burgoyne, R. 2007. Neuronal calcium sensor proteins: generating diversity in neuronal Ca²⁺ signalling. *Nature Reviews Neuroscience*, 8, 182-193.
- Butler, A. B. & Hodos, W. 2005. *Comparative Vertebrate Neuroanatomy: Evolution and Adaptation.*, Hoboken, New Jersey, John Wiley and Sons Inc.
- Byrd, C. A. & Brunjes, P. C. 1995. Organization of the olfactory system in the adult zebrafish: histological, immunohistochemical, and quantitative analysis. *J Comp Neurol*, 358, 247-59.
- Cajal 1889. Nota preventiva sobre la estructura de la médula embrionaria. *Gac. Méd. Cat.*, 12, 132-174.
- Calvo-Ochoa, E. & Byrd-Jacobs, C. A. 2019. The olfactory system of zebrafish as a model for the study of neurotoxicity and injury: implications for neuroplasticity and disease. *International Journal of Molecular Sciences*, 20, 1639.
- Chen, J., Poskanzer, K. E., Freeman, M. R. & Monk, K. R. 2020. Live-imaging of astrocyte morphogenesis and function in zebrafish neural circuits. *Nature Neuroscience*, 1297-1306.
- Chen, T.-W., Wardill, T. J., Sun, Y., Pulver, S. R., Renninger, S. L., Baohan, A., Schreiter, E. R., Kerr, R. A., Orger, M. B., Jayaraman, V., Looger, L. L., Svoboda, K. & Kim, D. S. 2013. Ultra-sensitive fluorescent proteins for imaging neuronal activity. *Nature*, 499, 295-300.
- Cheng, R.-K., Jeusthasan, S. J. & Penney, T. B. 2014. Zebrafish Forebrain and Temporal Conditioning. *Philosophical Transactions of The Royal Society B*, 369.
- Cheung, K. Y., Jesuthasan, S. J., Baxendale, S., Hateren, N. J. V., Marzo, M., Hill, C. J. & Whitfield, T. T. 2021. Olfactory Rod Cells: A Rare Cell Type in the Larval Zebrafish Olfactory Epithelium With a Large Actin-Rich Apical Projection. *Frontiers In Physiology*, 12.
- Chhetri, J., Güven, N. & Jacobson, G. 2014. Zebrafish – on the move towards ophthalmological research. *Eye*, 28.
- Chia, J. S. M., Wall, E. S., Wee, C. L., Rowland, T. a. J., Cheng, R.-K., Cheow, K., Guillemin, K. & Jesuthasan, S. 2019. Bacteria evoke alarm behaviour in zebrafish. *Nature Communications*.
- Choi, J.-H., Duboue, E. R., Macurak, M., Chanchu, J.-M. & Halpern, M. E. 2021. Specialized neurons in the right habenula mediate response to aversive olfactory cues. *eLife*.
- Connaughton, R. N. a. V. 1995. *Bipolar Cell Pathways in the Vertebrate Retina*.

- Corbetta, M. & Shulman, G. L. 2002. Control of goal-directed and stimulus-driven attention in the brain. *Nature Reviews Neuroscience*, 3, 201-215.
- Culp, Nüsslein-Volhard & Hopkins 1991. High-frequency germ-line transmission of plasmid DNA sequences injected into fertilized zebrafish eggs. *PNAS*, 88, 7953-7957.
- Dana, H., Sun, Y., Mohar, B., Hulse, B. K., Kerlin, A. M., Hasseman, J. P., Tsegaye, G., Tsang, A., Wong, A., Patel, R., Macklin, J. J., Chen, Y., Konnerth, A., Jayaraman, V., Looger, L. L., Schreiter, E. R., Svoboda, K. & Kim, D. S. 2019. High-performance calcium sensors for imaging activity in neuronal populations and microcompartments. *Nature Methods*, 16, 649-657.
- Decarvalho, T. N., Akitake, C. M., Thisse, C., Thisse, B. & Halpern, M. E. 2013. Aversive cues fail to activate fos expression in the asymmetric olfactory-habenula pathway of zebrafish. *Frontiers in Neural Circuits*.
- Deitmer, J., Verkhratsky, A. & Lohr, C. 1998. Calcium Signalling in Glial Cells. *Cell Calcium*, 24, 405-416.
- Demattè, M. L., Sanabria, D. & Spence, C. 2009. Olfactory Discrimination: When Vision Matters? *Chem Senses*, 34.
- Denk, W., Yuste, R., Svoboda, K. & Tank, D. 1996. Imaging calcium dynamics in dendritic spines. *Current Opinion in Neurobiology*, 6, 372-378.
- Denuex, T., Kaszas, A., Szalay, G., Katona, G., Lakner, T., Grinvald, A., Rózsa, B. & Vanzetta, I. 2016. Accurate spike estimation from noisy calcium signals for ultrafast three-dimensional imaging of large neuronal populations in vivo. *Nature Communications*, 7.
- Dom Miceli, J. R., Jean-Paul Rio and Monique Medina 1995. GABA immunoreactivity in the nucleus isthmo-opticus of the centrifugal visual system in the pigeon: A light and electron microscopic study. *Visual Neuroscience*, 12, 425-441.
- Doron, N. N. & Ledoux, J. E. 2000. Organisation of projections to the lateral amygdala from auditory and visual areas of the thalamus in the rat. *J Comp Neurol*, 417, 385-386.
- Dorostkar, M. M., Dreosti, E., Odermatt, B. & Lagnado, L. 2010. Computational processing of optical measurements of neuronal and synaptic activity in networks. *Journal of Neuroscience Methods*, 141-150.
- Dowling, J. E. 2013. Olfaction and Vision Meet in the Retina. *Neuron*, 06.
- Dreosti, E., Llopis, N. V., Carl, M., Yaksi, E. & Wilson, A. S. W. 2014. Left-Right asymmetry is required for the habenulae to respond to both visual and olfactory stimuli. *Current Biology*, 24, 440-445.
- Dunn, T. W., Mu, Y., Narayan, S., Randlett, O., Naumann, E. A., Yang, C.-T., Schier, A. F., Freeman, J., Engert, F. & Ahrens, M. B. 2016. Brain-wide mapping of neural activity controlling zebrafish exploratory locomotion. *eLife*.
- Dürst, C. D., Wiegert, J. S., Helassa, N., Kerruth, S., Coates, C., Schulze, C., Geeves, M., Török, K. & Oertner, T. G. 2019. High-speed imaging of glutamate release with genetically encoded sensors. *Nature Protocols*.
- Easter, S. & Nicola, G. 1996. The Development of Vision in the Zebrafish. *Developmental Biology*, 180, 646-663.
- Echeverry, F. A., Ijaz, S. & Pereda, A. E. 2022. Recording Synaptic Transmission from Auditory Mixed Synapses on the Mauthner Cells of Developing Zebrafish. *eNeuro*, 9.
- Elsaesser, R. & Paysan, J. 2007. The sense of smell, its signaling pathways, and the dichotomy of cilia and microvillus in olfactory sensory cells. *BMC Neuroscience*.

- Esposti, F., Johnston, J., Rosa, J. M., Leung, K.-M. & Lagnado, L. 2013. Olfactory Stimulation Selectively Modulates the OFF Pathway in the Retina of Zebrafish. *Neuron*, 79, 97-110.
- Fadool, J. M. 2003. Development of a rod photoreceptor mosaic revealed in transgenic zebrafish. *Developmental Biology*, 258, 277-290.
- Faustino, A., Monteiro, A. T. & Oliveira, R. 2017. Mechanisms of social buffering of fear in zebrafish. *SCIENTIFIC REPORTS*.
- Faveri, F. D., Marcotti, W. & Ceriani, F. 2021. Sensory adaptation at ribbon synapses in the zebrafish lateral line. *Journal of Physiology*, 599, 3677-3696.
- Filippo Del Bene, Claire Wyart, Estuardo Robles, Amanda Tran, Loren Looger, Ethan K Scott, Ehud Y Isacoff & Baier, H. 2010. Filtering of visual information in the tectum by an identified neural circuit. *Science*, 330, 669-673.
- Fore, S., Palumbo, F., Pelgrims, R. & Yaksi, E. 2017. Information processing in the vertebrate habenula. *Seminars in Cell and Developmental Biology*.
- Friedrich, R., Jacobson, G. & Zhu, A. P. 2010. Circuit Neuroscience in Zebrafish. *Current Biology*, 20.
- Friedrich, R. W., Habermann, C. J. & Laurent, G. 2004. Multiplexing using synchrony is the zebrafish olfactory bulb. *Nature Neuroscience*, 7.
- Friedrich, R. W. & Korsching, S. I. 1998. Chemotopic, Combinatorial and Non-Combinatorial odorant representations in the olfactory bulb revealed using a voltage-sensitive axon tracer. *Journal of Neuroscience*, 18, 9977-9988.
- Friston, K. 2010. The free-energy principle: a unified brain theory? *Nature Reviews Neuroscience*, 11, 127-138.
- Gottfried, J. A. & Dolan, R. J. 2003. The Nose Smells What the Eye Sees: Crossmodal Visual Facilitation of Human Olfactory Perception. *Neuron*, 39, 375-386.
- Guilbeault, N. C., Guerguiev, J., Martin, M., Tate, I. & Thiele, T. R. 2021. BonZeb: open-source, modular software tools for high-resolution zebrafish tracking and analysis. *Nature Scientific Reports*.
- Hartmann, S., Vogt, R., Kunze, J., Rauschert, A., Kuhnert, K.-D., Wanzenböck, J., Lamatsch, D. & Witte, K. 2018. Zebrafish larvae show negative phototaxis to near-infrared light. *PLoS One*.
- Heintz, T., Hinojosa, A., Dominiak, S. & Lagnado, L. 2022. Opposite forms of adaptation in mouse visual cortex are controlled by distinct inhibitory microcircuits. *Nature Communications*.
- Helmbrecht, T. O., Maschio, M. D., Donovan, J. C., Koutsouli, S. & Baier, H. 2018. Topography of a Visuomotor Transformation. *Neuron*, 100, 1429-1445.
- Hikosaka, O. 2010. The habenula: from stress evasion to value-based decision-making. *Nature Reviews Neuroscience*, 11, 503-513.
- Howe, K., Clark, M. D., Torroja, C. F., Torrance, J., Camille Berthelot & Matthieu Muffato, J. E. C., Sean Humphray, Karen McLaren, Lucy Matthews, Stuart McLaren, Ian Sealy, Mario Caccamo, Carol Churcher, Carol Scott, Jeffrey C. Barrett, Romke Koch, Gerd-Jorg Rauch, Simon White, William Chow¹, Britt Kilian, Leonor T. Quintais, José A. Guerra-Assunção, Yi Zhou, Yong Gu, Jennifer Yen¹, Jan-Hinnerk Vogel, Tina Eyre, Seth Redmond, Ruby Banerjee, Jianxiang Chi, Beiyuan Fu, Elizabeth Langley, Sean F. Maguire, Gavin K. Laird, David Lloyd, Emma Kenyon, Sarah Donaldson, Harminder Sehra, Jeff Almeida-King, Jane Loveland, Stephen Trevanion, Matt Jones, Mike Quail, Dave Willey, Adrienne Hunt, John Burton, Sarah Sims, Kirsten

- Mclay, Bob Plumb, Joy Davis, Chris Clee, Karen Oliver, Richard Clark, Clare Riddle, David Elliot, Glen Threadgold, Glenn Harden, Darren Ware, Sharmin Begum, Beverley Mortimore, Giselle Kerry, Paul Heath, Benjamin Phillimore, Alan Tracey, Nicole Corby, Matthew Dunn, Christopher Johnson, Jonathan Wood, Susan Clark, Sarah Pelan, Guy Griffiths, Michelle Smith, Rebecca Glithero, Philip Howden, Nicholas Barker, Christine Lloyd, Christopher Stevens, Joanna Harley, Karen Holt, Georgios Panagiotidis, Jamieson Lovell, Helen Beasley, Carl Henderson, Daria Gordon, Katherine Auger, Deborah Wright, Joanna Collins, Claire Raisen, Lauren Dyer, Kenric Leung, Lauren Robertson, Kirsty Ambridge, Daniel Leongamornlert, Sarah McGuire, Ruth Gilderthorp, Coline Griffiths, Deepa Manthravadi, Sarah Nichol, Gary Barker, Siobhan Whitehead, Michael Kay, Jacqueline Brown, Clare Murnane, Emma Gray, Matthew Humphries, Neil Sycamore, Darren Barker, David Saunders, Justene Wallis, Anne Babbage, Sian Hammond, Maryam Mashreghi-Mohammadi, Lucy Barr, Sancha Martin, Paul Wray, Andrew Ellington, Nicholas Matthews, Matthew Ellwood, Rebecca Woodmansey, Graham Clark, James D. Cooper, Anthony Tromans, Darren Grafham, Carl Skuce, Richard Pandian, Robert Andrews, Elliot Harrison, Andrew Kimberley, Jane Garnett, Nigel Fosker, Rebekah Hall, Patrick Garner, Daniel Kelly, Christine Bird, Sophie Palmer, Ines Gehring, Andrea Berger, Christopher M. Dooley, Zu" Beyde Ersan-Urun, Cigdem Eser, Horst Geiger, Maria Geisler, Lena Karotki, Anette Kirn, Judith Konantz, Martina Konantz, Martina Oberlander, Silke Rudolph-Geiger, Mathias Teucke, Christa Lanz, Gu" Nter Raddatz, Kazutoyo Osoegawa, Baoli Zhu, Amanda Rapp, Sara Widaa, Cordelia Langford, Fengtang Yang, Stephan C. Schuster, Nigel P. Carter, Zemin Ning, Javier Herrero, Steve M. J. Searle, Anton Enright, Robert Geisler, Ronald H. A. Plasterk, Charles Lee, Monte Westerfield, Pieter J. De Jong, Leonard I. Zon, John H. Postlethwait, Christiane Nu" Sslein-Volhard, Tim J. P. Hubbard, Hugues Roest Crollius, Jane Rogers & Derek L. Stemple 2013. The zebrafish reference genome sequence and its relationship to the human genome. *Nature*, 496, 498-503.
- Huang, L., Maaswinkel, H. & Li, L. 2005. Olfactory retinal centrifugal input modulates zebrafish retinal ganglion cell activity: a possible role for dopamine-mediated Ca²⁺ signalling pathways. *Journal of Physiology*, 569, 939-948.
- Jafari, S. & Alenius, M. 2021. Odor response adaptation in *Drosophila*—a continuous individualization process. *Cell Tissue Res.*, 383, 143-148.
- Jaffe, Johnston, Lasser-Ross, Lisman, Miyakawa & Ross 1992. The spread of Na⁺ spikes determines the pattern of dendritic Ca²⁺ entry into hippocampal neurons. *Nature*, 357, 244-246.
- Jesuthasan, S. 2018. The Vertebrate Habenula. *Seminars in Cell and Developmental Biology*, 78.
- Jesuthasan, S., Krishnan, S., Cheng, R.-K. & Mathuru, A. 2020. Larval zebrafish respond to the alarm pheromone Schreckstoff by immobility and a change in brain state. *BioRxiv*.
- Jia, H., Rochefort, N., Chen, X. & Konnerth, A. 2011. In vivo two-photon imaging of sensory-evoked dendritic calcium signals in cortical neurons. *Nature Protocols*, 6.
- Johnston, J., S, S., L, D., S, R., M, O. & L, L. 2019. A Retinal Circuit Generating a Dynamic Predictive Code for Oriented Features. *Neuron*, 102, 1211-1222.
- Kaneko, A. 1970. Physiological and morphological identification of horizontal, bipolar and amacrine cells in goldfish retina. *The Journal of Physiology*, 207.

- Kastner, D. B. & Baccus, S. A. 2011. Coordinated dynamic encoding in the retina using opposing forms of plasticity *Nature Neuroscience*, 14, 1317-1322.
- Katherine Nagel & Wilson., R. 2011. Biophysical mechanisms underlying olfactory receptor neuron dynamics. *Nature Neuroscience*, 14, 208-216.
- Katzen, F. 2007. Gateway(®) recombinational cloning: a biological operating system. *Expert Opin Drug Discovery*, 2, 571-589.
- Kermen, F., Darnet, L., Wiest, C., Palumbo, F., Bechert, J., Uslu, O. & Yaksi, E. 2020. Stimulus-specific behavioral responses of zebrafish to a large range of odors exhibit individual variability. *BMC Biology*, 18.
- Kermen, F., Franco, L. M., Wyatt, C. & Yaksi, E. 2013. Neural circuits mediating olfactory-driven behavior in fish. *Front Neural Circuits*, 7, 62.
- Kim, D. H., Kim, J., Marques, J. C., Grama, A., Hildebrand, D. G. C., Gu, W., Li, J. M. & Robson, D. N. 2017. Pan-neuronal calcium imaging with cellular resolution in freely swimming zebrafish. *Nature Methods*, 14, 1107-1113.
- Kimbell, H. S., Chapman, B. B., Dobbison, K. E. & Morrell., L. J. 2019. Foraging guppies can compensate for low-light conditions, but not via a sensory switch. *Behavioural Ecology and Sociobiology*, 73.
- Kimmel, C. B., Ballard, W. W., Kimmel, S. R., Ullmann, B. & Schilling, T. F. 1995. Stages of Embryonic Development of the Zebrafish. *Developmental Dynamics*, 203.
- Koide, T., Miyasaka, N., Morimoto, K., Asakawa, K., Urasaki, A., Kawakami, K. & Yoshihara, Y. 2009. Olfactory neural circuitry for attraction to amino acids revealed by transposon-mediated gene trap approach in zebrafish. *Proceedings of the National Academy of Sciences of the United States of America.*, 106, 9884-9889.
- Koide, T., Yabuki, Y. & Yoshihara, Y. 2018. Terminal Nerve GnRH3 Neurons Mediate Slow Avoidance of Carbon Dioxide in Larval Zebrafish. *Cell Reports*, 22, 1115-1123.
- Kolb 1995. Simple Anatomy of the Retina. *Webvision: The Organization of the Retina and Visual System*.
- Koren, V. & Denève, S. 2017. Computational Account of Spontaneous Activity as a Signature of Predictive Coding. *PLoS Comput Biol*.
- Krishnan, S., Mathuru, A., Kibat, C., Rahman, M., Lupton, C., Stewart, J., Claridge-Chang, A., Yen, S.-C. & Jesuthasan, S. 2014. The right dorsal habenula limits attraction to an odor in zebrafish. *Current Biology*, 11.
- Kuang, S. & Zhang, T. 2014. Smelling directions: Olfaction modulates ambiguous visual motion perception. *Scientific Reports*, 4.
- L Busse, K C Roberts, R E Crist, Weissman, D. H. & Woldorff, A. M. G. 2005. The spread of attention across modalities and space in a multisensory object. *Proceedings of the National Academy of Sciences of the United States of America*, 102, 18751-18756.
- Laberge 1995. Attentional Processing: The Brain's Art of Mindfulness. *Cambridge, MA: Harvard University Press*.
- Lauer, J., Zhou, M., Ye, S., Menegas, W., Schneider, S., Nat, T., Rahman, M. M., Santo, V. D., Soberanes, D., Feng, G., Murthy, V. N., Lauder, G., Dulac, C., Mathis, M. W. & Mathis, A. 2022. Multi-animal pose estimation, identification and tracking with DeepLabCut . *Nature Methods*, 496-504.
- Leveteau & Macleod 1966. Olfactory discrimination in the rabbit olfactory glomerulus. *Science*, 153, 175-176.

- Li, Mack-Bucher, J. A., Souren, M., Yaksi, E., Higashijima, S.-I., Mione, M., Fetcho, J. R. & Friedrich, R. W. 2005. Early development of functional spatial maps in the zebrafish olfactory bulb. *Journal of Neuroscience*, 25, 5784-5795.
- Li, E. & Saha, M. 2021. Optimizing Calcium Detection Methods in Animal Systems: A Sandbox for Synthetic Biology. *biomolecules*, 11.
- Lindsey, S. M. & Vogt, R. G. 2004. Behavioural Responses of Newly Hatched Zebrafish to Amino Acid Chemostimulants. *Chemical Senses*, 29, 93-100.
- Lister, J. A., Robertson, C. P., Lepage, T., Johnson, S. L. & Raible, D. W. 1999. nacre encodes a zebrafish microphthalmia-related protein that regulates neural-crest-derived pigment cell fate. *Development*, 3757-67.
- Maaswinkel, H. & Li, L. 2003a. Olfactory input increases visual sensitivity in zebrafish: a possible function for the terminal nerve and dopaminergic interplexiform cells. *Journal of Exp Biol*.
- Maaswinkel, H. & Li, L. 2003b. Spatio-temporal frequency characteristics of the optomotor response in zebrafish. *Vision Research*, 43, 21-30.
- Mack-Bucher, J. A., Li, J. & Friedrich, R. W. 2007. Early functional development of interneurons in the zebrafish olfactory bulb. *European Journal of Neuroscience*, 25, 460-470.
- Masland, R. H. 2012. The Neuronal Organisation of the Retina. *Neuron*, 266-280.
- Mausfeld 2013. The Biological Function of Sensory Systems. In: GALIZIA C., L. P. (ed.) *Neurosciences - From Molecule to Behaviour: A University Textbook*. Berlin, Heidelberg.: Springer Spektrum.
- Mclaughlin, I., Dani, J. A. & Biasi, M. D. 2017. The medial habenula and interpeduncular nucleus circuitry is critical in addiction, anxiety, and mood regulation. *Journal of Neurochemistry*, 142, 130-143.
- Meier, A., Nelson, R. & Connaughton, V. 2018. Color Processing in Zebrafish Retina. *Frontiers in Cellular Neuroscience*.
- Miyasaka, N., Wanner, A. A., Li, J., Mack-Bucher, J., Genoud, C., Yoshihara, Y. & Friedrich, R. W. 2013. Functional development of the olfactory system in zebrafish. *Mech Dev*, 130, 336-46.
- Moini, J., Avgeropoulos, N. G. & Samsam, M. 2021. Chapter 1 - Anatomy and Physiology. In: PRESS, A. (ed.) *Epidemiology of Brain and Spinal Tumors*.
- Morrot, G., Brochet, F. & Dubourdiou, D. 2001. The Color of Odors. *Brain and Language*, 79, 309-320.
- Motter 1994. Neural correlates of attentive selection for color or luminance in extrastriate area V4. *Journal of Neuroscience*, 14, 2178-2189.
- Moya-Diaz, J., James, B., Esposti, F., Johnston, J. & Lagnado, L. 2022. Diurnal changes in the efficiency of information transmission at a sensory synapse. *Nature Communications*, 13.
- Mu, Y., Bennett, D., Rubinov, M., Narayan, S., Yang, C.-T., Tanimoto, M., Mensh, B., Looger, L. & Ahrens, M. 2019. Glia Accumulate Evidence that Actions Are Futile and Suppress Unsuccessful Behavior. *Cell*, 178, 27-43.
- Mu, Y., Li, X.-Q., Zhang, B. & Du, J.-L. 2012. Visual input modulates audiomotor function via hypothalamic dopaminergic through a cooperative mechanism. *Neuron*, 688-699.
- Mueller, T. 2012. What is the Thalamus in Zebrafish? *Frontiers in Neuroscience*, 6.
- Nakai, J., Ohkura, M. & Imoto, K. 2001. A high signal-to-noise ca²⁺ probe composed of a single green fluorescent protein. *Nature Biotechnology*, 19, 137-141.

- Nevin, L. M., Robles, E., Baier*, H. & Scott, A. E. K. 2010. Focusing on optic tectum circuitry through the lens of genetics. *BMC Biology*, 8.
- Nikolaev, A., Leung, K., Odermatt, B. & Lagnado, L. 2013. Synaptic mechanisms of adaptation and sensitization in the retina. *Nature Neuroscience*, 16, 934-941.
- Northcutt, R. G. & Wullimann, M. F. 1988. The Visual System in Teleost Fishes: Morphological Patterns and Trends. In: ATEMA J., F. R. R., POPPER A.N., TAVOLGA W.N (ed.) *Sensory Biology of Aquatic Animals*. New York, NY: Springer.
- Northmore, D. P. The Optic Tectum. 2009.
- Nüsslein-Volhard, C. & Dahm, R. 2002. *Zebrafish: A Practical Approach*.
- Pachitariu, M., Stringer, C., Dipoppa, M., Schröder, S., Rossi, F., Dalgleish, H., Carandini, M. & Harris, K. D. 2017. Suite2p: beyond 10,000 neurons with standard two-photon microscopy. *BioRxiv*.
- Pacholko, A., Wotton, C. & Bekar, L. 2020. Astrocytes - The ultimate effectors of long range neuromodulatory networks. *Frontiers in Cellular Neuroscience*.
- Patterson, B. W., Abraham, A. O., Maciver, M. A. & Mclean, D. 2013. Visually guided gradation of prey capture movements in larval zebrafish. *Journal of Exp Biol*.
- Patterson, S. S., Neitz, M. & Neitz, J. 2019. Reconciling Color Vision Models With Midget Ganglion Cell Receptive Fields. *Frontiers in Neuroscience*.
- Pence, T. S., Reiter, E. R., Dinardo, L. J. & Costanzo, A. R. M. 2014. Risk-Factors for Hazardous Events in Olfactory-Impaired Patients. *JAMA Otolaryngol Head Neck Surg*, 140, 951-955.
- Pezzulo, G., Zorzi, M. & Corbetta, M. 2021. The secret life of predictive brains: what's spontaneous activity for? *Trends in Cogn Sci*.
- Pichler, P. & Lagnado, L. 2019. The Transfer Characteristics of Hair Cells Encoding Mechanical Stimuli in the Lateral Line of Zebrafish. *J Neurosci*, 39, 112-124.
- Pierce, J. 2009. Generating stimuli for neuroscience using PsychoPy. *Frontiers in Neuroinformatics*, 2, 1-8.
- R O Karlstrom, T Trowe, S Klostermann, H Baier, M Brand, A D Crawford, B Grunewald, P Haffter, H Hoffman, S U Meyer, B K Müller, S Richter, F J Van Eeden, C Nüsslein-Volhard & Bonhoeffer, F. 1996. Zebrafish mutations affecting retinotectal axon pathfinding. *Development*, 123, 427-438.
- Ramón & Cajal 1893. Neue darstellung vom histologischen bau des centralnervensystem. . *Arch. Anat. Entwickl*, 319-428.
- Reiten, I., Uslu, F. E., Fore, S., Pelgrims, R., Ringers, C., Verdugo, C. D., Hoffman, M., Lal, P., Kawakami, K., Pekkan, K., Yaksi, E. & Jurisch-Yaksi, N. 2017. Motile-Cilia-Mediated Flow Improves Sensitivity and Temporal Resolution of Olfactory Computations. *Current Biology*, 27, 166-174.
- Richardson, R., Tracey-White, D., Webster, A. & Moosajee, M. 2017. The zebrafish eye-a paradigm for investigating human ocular genetics. *Eye*, 31, 68-86.
- Ripp, I., Nieden, A.-N. Z., Blankenagel, S., Franzmeier, N., Lunström, J. N. & Freiherr, J. 2018. Multisensory integration processing during olfactory-visual stimulation - An fMRI graph theoretical network analysis. *Human Brain Mapping*, 39, 3713-3727.
- Robles, E., Laurell, E. & Baier, H. 2014. The retinal projectome reveals brain-area-specific visual representations generated by ganglion cell diversity. *Current Biology*, 24, 2085-2096.
- Rolls, E. & Baylis, L. 1994. Gustatory, olfactory, and visual convergence within the primate orbitofrontal cortex. *J Neurosci*, 14, 5437-5452.

- Rolls, E., Critchley, H., Mason, R. & Wakeman, E. 1996. Orbitofrontal cortex neurons: role in olfactory and visual association learning. *Journal of Neurophysiology*.
- Rubin, A., Sheintuch, L., Brande-Eilat, N., Pinchasof, O., Rechavi, Y., Geva, N. & Ziv, Y. 2019. Revealing neural correlates of behavior without behavioral measurements. *Nature Communications*, 10.
- Ryan, B., Joilin, G. & Williams, J. M. 2015. Plasticity-related microRNA and their potential contribution to the maintenance of long-term potentiation.
- Salbreux, G., Barthel, L. K., Raymond, P. A. & Lubensky, D. K. 2012. Coupling mechanical deformations and planar cell polarity to create regular patterns in the zebrafish retina. *PLoS Comput Biol*, 8.
- Santaca, M., Dadda, M. & Bisazza, A. 2021. The role of visual and olfactory cues in social decisions of guppies and zebrafish. *BioRxiv*.
- Sarafoleanu, C., Mella, C., Georgescu, M. & Perederco, C. 2009a. The importance of the olfactory sense in the human behavior and evolution. *The Journal of Medicine and Life*, 2, 196-198.
- Sarafoleanu, C., Mella, C., Georgescu, M. & Perederco, C. 2009b. The importance of the olfactory sense in the human behavior and evolution. *J Med Life*, 2, 196-8.
- Sarafoleanu, D. 1999. *Paraclinical and functional exploration in otorhinolaryngology*, Bucharest, Didactic and Pedagogical Publishing House.
- Satou, M. 1990. Synaptic organization, local neuronal circuitry, and functional segregation of the teleost olfactory bulb. *Prog Neurobiol*, 34, 115-42.
- Seigneuric, A., Durand, K., Jiang, T., Baudouin, J.-Y. & Schaal, B. 2010a. The nose tells it to the eyes: crossmodal associations between olfaction and vision. *Perception*, 39.
- Seigneuric, A., Durand, K., Jiang, T., Baudouin, J.-Y. & Schaal, B. 2010b. The nose tells it to the eyes: crossmodal associations between olfaction and vision. *Perception*, 39.
- Semmelhack, J. L., Donovan, J. C., Thiele, T. R., Kuehn, E., Laurell, E. & Baier, H. 2014. A dedicated visual pathway for prey detection in larval zebrafish. *eLife*.
- Shapley, R. & Enroth-Cugell, C. 1984. Visual Adaptation and Retina Gain Controls. *Progr. Ret. Res.*, 3.
- Shepherd, G. M. 2004. *The Synaptic Organization of the Brain*, Oxford Scholarship Online.
- Shiple, M. & Ennis, M. 1996. Functional Organisation of Olfactory System. *Developmental Neurobiology*, 30, 123-176.
- Sliney, D. 2016. What is light? The visible spectrum and beyond. *Nature*, 222–229.
- Sonne, J., Reddy, V. & Lopez-Ojeda, W. 2017. *Neuroanatomy, Cranial Nerve 0 (Terminal Nerve)*, StatPearls.
- Steinfeld, R., Herb, J. T., Sprengel, R., Schaefer, A. T. & Fukunaga, I. 2015. Divergent Innervation of the Olfactory Bulb by Distinct Raphe Nuclei. *Journal of Comparative Neurology*, 523, 805-813.
- Stephenson, J., Whitlock, K. & Partridge, A. J. 2012. Food and Conspecific Chemical Cues Modify Visual Behavior of Zebrafish, *Danio rerio*. *Zebrafish*, 9, 68-73.
- Stickel, S., Weismann, P., Kellermann, T., Regenbogen, C., Habel, U., Greiherr, J. & Checkko, N. 2019. Audio-visual and olfactory-visual integration in healthy participants and subjects with autism spectrum disorder. *Human Brain Mapping*, 40, 4470-4486.
- Sun, S., Zhu, C., Ma, M., Ni, B., Chen, L., Zhu, H. & Zuxiang, L. 2019. A pentylenetetrazole-induced kindling zebrafish larval model for evoked recurrent seizures. *BioRxiv*.

- Tabor, R., Yaksi, E. & Friedrich, R. W. 2008. Multiple functions of GABA A and GABA B receptors during pattern processing in the zebrafish olfactory bulb. *European Journal of Neuroscience*, 28, 117-127.
- Tabor, R., Yaksi, E., Weislogel, J.-M. & Friedrich, R. W. 2004. Processing of Odor Mixtures in the Zebrafish Olfactory Bulb. *J Neurosci*.
- Takeuchi, T., Duzsikiewicz, A. J. & Morris, R. G. 2014. The synaptic plasticity and memory hypothesis: encoding, storage and persistence. *Philosophical Transactions of The Royal Society B*.
- Talsma, D. 2015. Predictive coding and multisensory integration: an attentional account of the multisensory mind. *Frontiers in Integrative Neuroscience*, 9.
- Tan, G. J. H., Chow, K. W. B., Ho, M. S. M. & Jesuthasan, S. 2021. Identification of potential astrocytes in the teleost brain. *BioRxiv*.
- Temizer, I., Donovan, J. C., Baier, H. & Semmelhack, J. L. 2015. A visual pathway for looming-evoked escape in larval zebrafish. *Current Biology*, 25, 1823-1834.
- Thévanaz, P., Ruttimann, U. & Unser, M. 1998. A Pyramid Approach to Subpixel Registration Based on Intensity. *IEEE Transactions on Image Processing*, 7, 27-41.
- Thompson, A. W., Vanwalleghem, G. C., Heap, L. A. & Scott, E. K. 2016. Functional Profiles of Visual-, Auditory-, and Water Flow-Responsive neurons in the zebrafish tectum. *Current Biology*, 26, 743-754.
- Timothy W Dunn, Y. M., Sujatha Narayan, Owen Randlett, Eva a Naumann, Chao-Tsung Yang, Alexander F Schier, Jeremy Freeman, Florian Engert, Misha B Ahrens 2016. Brain-wide mapping of neural activity controlling zebrafish exploratory locomotion. *eLife*.
- Tong, W., Meffin, H., Garrett, D. & Ibbotson, M. 2020. Stimulation Strategies for Improving the Resolution of Retinal Prostheses. *Frontiers in Neuroscience*.
- Ucl, Z. 2022. *RETINOFUGAL PROJECTIONS* [Online]. Available: <https://zebrafishucl.org/retinofugalprojections> [Accessed].
- Umatani, C., Misu, R., Oishi, S., Yamaguchi, K., Abe, H. & Oka, Y. 2015. GnRH suppresses excitability of visual processing neurons in the optic tectum. *Journal of Neurophysiology*, 114, 2775-2784.
- V Van Wassenhove, Grant, K. W. & Poeppel, A. D. 2005. Visual speech speeds up the neural processing of auditory speech. *Proceedings of the National Academy of Sciences of the United States of America*, 102, 1181-1186.
- Vanwalleghem, G., Heap, L. A., Favre-Bulle, I., Schuster, K., Thompson, A. & Scott, E. K. 2015. Sensory integration in the Zebrafish brain, what are the functions of the thalamus and the cerebellum? *Frontiers*
- Vitebsky, A., Reyes, R., Mj Sanderson, Michel, W. & Whitlock, K. 2005. Isolation and charecterisation of the laure olfactory behavioural mutant in the zebrafish, *Danio rerio*. *Developmental Dynamics*, 234, 229-242.
- Vrapciu, A. D. & Popescu, M. V. 2016. The cranial nerve zero – mini review. *Romanian Journal of Rhinology*, 6.
- Vucinic, D., Cohen, L. B. & Kosmidis, E. K. 2006. Interglomerular center-surround inhibition shapes odorant-evoked input to the mouse olfactory bulbs in vivo. *Journal of Neurophysiology*, 95, 1881-1887.
- Wahis, J. & Holt, M. 2021. Astrocytes, Noradrenaline, α 1-Adrenoreceptors, and Neuromodulation: Evidence and Unanswered Questions. *Frontiers in Cellular Neuroscience*.

- Wallenberg 1898. Das mediale Opticusbündel der Taube. *Neurol Zbl.*, 17, 532-537.
- Wan, J. & Goldman, D. 2016. Retina regeneration in zebrafish. *Current Opinion in Genetic Development*, 40, 41-47.
- Weiss, O. & Meyer, D. 1988. Odor stimuli modulate retinal excitability in fish. *Neuroscience Letters*.
- Whitlock, K. E. & Palominos, M. F. 2022. The Olfactory Tract: Basis for Future Evolution in Response to Rapidly Changing Ecological Niches. *Frontiers in Neuroanatomy*.
- Wilson, M. & Lindstrom, A. S. H. 2011. What the bird's brain tells the bird's eye: the function of descending input to the avian retina. *Visual Neuroscience*, 28, 337-350.
- Woodson, W., Reiner, A., Anderson, K. & Karten, H. 1991. Distribution, laminar location, and morphology of tectal neurons projecting to the isthmo-optic nucleus and the nucleus isthmi, pars parvocellularis in the pigeon (*Columba livia*) and chick (*Gallus domesticus*): a retrograde labelling study. *Journal of Comparative Neurology*, 470-488.
- Wosniack, M. E., Kirchner, J. H., Chao, L.-Y., Zabouri, N., Lohmann, C. & Gjorgjieva, J. 2021. Adaptation of spontaneous activity in the developing visual cortex. *eLife*.
- Wullimann, M. F. 1998. The central nervous system. In: EVANS, D. H. (ed.) *The Physiology of Fishes*. Boca Raton, New York: CRC Press.
- Wyatt, C., Bartoszek, E. M. & Yaksi, E. 2015. Methods for studying the zebrafish brain: past, present and future. *European Journal of Neuroscience*, 42, 1746-1763.
- Yang, S., Zhou, J. & Li, D. 2021. Functions and Diseases of the Retinal Pigment Epithelium. *Frontiers in Pharmacology*.
- Yasuda, R., Nimchinsky, E., Scheuss, V., Pologruto, T., Oertner, T. & Sabatini, B. 2004. Imaging calcium concentration dynamics in small neuronal compartments. *Sci STKE*.
- Yeomans, M. 2006. Olfactory influences on appetite and satiety in humans. *Physiology and Behaviour*, 87, 800-804.
- Yoshimatsu, T., Schröder, C., Berens, P. & Baden, T. 2019. Cellular and molecular mechanisms of photoreceptor tuning for prey capture in larval zebrafish. *BioRxiv*.
- Zhou, F.-W., Shao, Z.-Y., Shipley, M. T. & Puche, A. C. 2020. Short-term plasticity in glomerular inhibitory circuits shapes olfactory bulb output. *J Neurophysiol*.
- Zhou, G., Lane, G., Cooper, S. L., Kahnt, T. & Zelano, C. 2019. Characterizing functional pathways of the human olfactory system. *eLife*, 8.
- Zhou, W., Jiang, Y., He, S. & Chen, D. 2010. Olfaction Modulates Visual Perception in Binocular Rivalry. *Current Biology*, 20, 1356-1358.